

UC Irvine

UC Irvine Electronic Theses and Dissertations

Title

Searching for Physics Beyond the Standard Model and Beyond

Permalink

<https://escholarship.org/uc/item/72x1p5cf>

Author

Abdullah, Mohammad

Publication Date

2017

Peer reviewed|Thesis/dissertation

UNIVERSITY OF CALIFORNIA,
IRVINE

Searching for Physics Beyond the Standard Model and Beyond

DISSERTATION

submitted in partial satisfaction of the requirements
for the degree of

DOCTOR OF PHILOSOPHY

in Physics

by

Mohammad Abdullah

Dissertation Committee:
Professor Yuri Shirman, Chair
Professor Arvind Rajaraman
Professor Tim M.P. Tait

2017

Chapter 2 © 2014 American Physical Society
Chapter 3 © 2017 American Physical Society
Chapter 4 © 2015-2016 American Physical Society
Chapter 5 © 2013 SISSA
All other materials © 2017 Mohammad Abdullah

DEDICATION

To my father

TABLE OF CONTENTS

	Page
LIST OF FIGURES	vi
LIST OF TABLES	x
ACKNOWLEDGMENTS	xi
CURRICULUM VITAE	xii
ABSTRACT OF THE DISSERTATION	xv
1 Introduction	1
2 Searching for New Resonances using Topological Models	9
2.1 Topologies in $\ell^+\ell^-jj$	12
2.2 The Models	15
2.2.1 $(qq)(\ell\ell)$ Topological Model	15
2.2.2 $(qq\ell)\ell$ Topological Model	16
2.2.3 $(q\ell\ell)q$ Topological Model	18
2.3 Backgrounds to $\ell\ell jj$	18
2.4 Mass reconstruction and LHC Sensitivity	19
2.4.1 $(\ell\ell)(jj)$ topology	21
2.4.2 $\ell(\ell jj)$ topology	25
2.4.3 $j(j\ell\ell)$ topology	26
2.5 Conclusions	35
3 Searching for spin-3/2 leptons	36
3.1 Introduction	36
3.2 Theory	37
3.3 Bounds	39
3.4 Collider Phenomenology	41
3.5 Limits from LHC data	42
3.6 Conclusions	44
4 Reviving bino dark matter with vectorlike fourth generation particles	48
4.1 Introduction	48
4.2 The Model	53

4.2.1	Particle Content	53
4.2.2	Simplifying Assumptions	56
4.2.3	Existing Bounds	58
4.3	Relic Density	59
4.4	Higgs Boson Mass	64
4.5	Direct Detection of Dark Matter	66
4.5.1	Effective Neutralino–Nucleon Coupling	67
4.5.2	Spin-Independent Cross Sections	69
4.5.3	Spin-Dependent Cross Sections	72
4.6	Indirect Detection of Dark Matter	73
4.6.1	Gamma Rays	74
4.6.2	Neutrinos and Positrons	77
4.7	Collider Signals	78
4.7.1	LLCP searches	80
4.7.2	Vector-like Lepton Searches	80
4.7.3	Extra Slepton Searches	81
4.7.4	Collider Summary and Discussion	83
4.8	Conclusions	86
5	Flavored Gauge Mediation	96
5.1	Introduction	96
5.2	Models	100
5.2.1	The models and supersymmetric alignment.	100
5.2.2	A -terms and scalar masses	103
5.3	Higgs mass and superpartner masses	106
5.3.1	The Higgs and stop masses	106
5.3.2	Superpartner spectra and LHC signatures	111
5.4	Conclusions	114
6	Conclusion	118
	Bibliography	120
A	Derivation of the soft terms	136
A.1	Analytic continuation in the presence of mixing	137
A.2	slepton mass	142
A.3	Higgs mass	144
A.4	Multiple couplings	146
A.5	Soft terms in the three generation model	148
A.6	Explicit 2-loop Calculation	152
A.7	H field soft mass squared	154
A.7.1	l field mass squared	155
B	Spin-Independent Scattering Cross Section of Bino-Like Neutralinos	159

C	Monte Carlo simulation of vector-like leptons at the LHC	164
C.1	Analysis procedure	164
C.2	Results	166

LIST OF FIGURES

		Page
2.1	Diagram for $Z' \rightarrow \chi_1 \chi_2 \rightarrow \ell^+ j \ell^- j$	13
2.2	Diagram for $Z' \rightarrow \chi_1 \chi_2 \rightarrow \ell^+ \ell^- jj$	14
2.3	Diagrams for $Z' \rightarrow \ell^\mp L \rightarrow \ell^\mp (\ell^\pm jj)$ (right)	14
2.4	Diagram for $Z' \rightarrow jQ \rightarrow j (\ell^+ \ell^- j)$	14
2.5	Cross section for Z' production at $\sqrt{s} = 14$ TeV, including all decay modes. .	17
2.6	Distribution of $m_{\ell+\ell^-}$ in simulated events for background process contributing to the $\ell\ell jj$ final state in pp collisions at $\sqrt{s} = 14$ TeV with $\mathcal{L} = 300 \text{ fb}^{-1}$, after preselection requirements.	20
2.7	In simulated $Z' \rightarrow \chi_1 \chi_2 \rightarrow \ell\ell jj$ events, the distribution of reconstructed invariant $\ell\ell$, jj and $\ell\ell jj$ masses for several values of $m_{Z'}$, m_{χ_1} and m_{χ_2} . The normalization is arbitrary. The shoulder in m_{jj} is due to imperfect selection of the jet pair.	22
2.8	In the $(\ell\ell)(jj)$ topology, distribution of $m_{\ell\ell jj}$ in simulated signal and background events for two example mass points, after requirements on $m_{\ell\ell}$ and m_{jj} in pp collisions at $\sqrt{s} = 14$ TeV with $\mathcal{L} = 300 \text{ fb}^{-1}$. Top shows the case of $m_{Z'} = 250$ GeV, $m_{\chi_1, \chi_2} = 100$ GeV; bottom shows the case of $m_{Z'} = 500$ GeV, $m_{\chi_1, \chi_2} = 100$ GeV. In both cases, an arbitrary value of $\sigma(pp \rightarrow Z' \rightarrow \chi_1 \chi_2 \rightarrow \ell\ell jj)$ is assumed.	23
2.9	In the $(\ell\ell)(jj)$ topology, selection efficiency and expected cross-section upper limits versus m_{χ_1} and m_{χ_2} for several choices of $m_{Z'}$ at $\sqrt{s} = 14$ TeV with $\mathcal{L} = 300 \text{ fb}^{-1}$. For small values of m_{χ_2} , the efficiency is small due to jet p_T requirements and jet resolution effects. For values of m_{χ_1} near m_Z , the larger backgrounds lead to weakened limits.	24
2.10	In the $(\ell\ell)(jj)$ topology, expected upper limits on the cross section $\sigma(pp \rightarrow Z' \rightarrow \chi_1 \chi_2 \rightarrow \ell\ell jj)$ at 95% CL versus $m_{Z'}$ for several choices of m_{χ_1} and m_{χ_2} in pp collisions at $\sqrt{s} = 14$ TeV with $\mathcal{L} = 300 \text{ fb}^{-1}$. The $m_{\chi_{1,2}} = 200, 100$ GeV (red) and $m_{\chi_{1,2}} = 100, 200$ curves have different dependences on $m_{Z'}$ due to the asymmetry in the lepton and jet efficiencies for large values of p_T^X	25
2.11	Limits on coupling $g_{Z'qq}$ for two choices of $\text{BF}(Z' \rightarrow \chi_1 \chi_2)$. The shaded region shows the current limits on the coupling from other topologies (see text) where the width of the band reflects the variation with assumed m_{χ_1} and m_{χ_2} in pp collisions at $\sqrt{s} = 14$ TeV with $\mathcal{L} = 300 \text{ fb}^{-1}$	26

2.12	In simulated $Z' \rightarrow \ell L \rightarrow \ell l j j$ events, distribution of reconstructed invariant $\ell j j$ and $\ell l j j$ masses for several values of $m_{Z'}$ and m_L . Normalization is arbitrary.	27
2.13	In the $\ell(\ell j j)$ topology, the distribution of $m_{\ell l j j}$ in signal and background events for two example mass points, after requirements on $m_{\ell j j}$ and $m_{\ell \ell}$ in pp collisions at $\sqrt{s} = 14$ TeV with $\mathcal{L} = 300 \text{ fb}^{-1}$. Left shows the case of $m_{Z'} = 250$ GeV, $m_L = 100$ GeV; right shows the case of $m_{Z'} = 500$ GeV, $m_L = 200$ GeV.	29
2.14	In the $\ell(\ell j j)$ topology, selection efficiency and expected cross-section upper limits versus $m_{Z'}$ and m_L at $\sqrt{s} = 14$ TeV with $\mathcal{L} = 300 \text{ fb}^{-1}$. For large $m_{Z'} - m_L$, the efficiency drops due to large transverse momentum of the L , which leads to small opening angles of the L decay products.	29
2.15	In the $\ell(\ell j j)$ topology, expected upper limits on the coupling $g_{Z'gg}$ versus $m_{Z'}$ and m_L for two choices of $BF(Z' \rightarrow \ell L)$ at $\sqrt{s} = 14$ TeV with $\mathcal{L} = 300 \text{ fb}^{-1}$. The shaded region shows the current limits on the coupling from other topologies (see text) where the width of the band reflects the variation with assumed m_L	30
2.16	In the $j(j \ell \ell)$ topology, distribution of reconstructed invariant $j \ell \ell$ and $\ell l j j$ masses for several values of $m_{Z'}$ and m_Q . Normalization is arbitrary.	31
2.17	In the $j(j \ell \ell)$ topology, distribution of $m_{\ell l j j}$ in signal and background events for two example mass points, after requirements on $m_{j \ell \ell}$ and $m_{\ell \ell}$ at $\sqrt{s} = 14$ TeV with $\mathcal{L} = 300 \text{ fb}^{-1}$. Left shows the case of $m_{Z'} = 250$ GeV, $m_Q = 200$ GeV; right shows the case of $m_{Z'} = 600$ GeV, $m_Q = 200$ GeV. In both cases, an arbitrary value of $\sigma(pp \rightarrow Z' \rightarrow qQ \rightarrow j j \ell \ell)$ is assumed.	32
2.18	In the $j(j \ell \ell)$ topology, selection efficiency (top) and expected cross-section upper limits (bottom) versus $m_{Z'}$ and m_Q at $\sqrt{s} = 14$ TeV with $\mathcal{L} = 300 \text{ fb}^{-1}$. For large $m_{Z'} - m_Q$, the efficiency drops due to large transverse momentum of the Q , which leads to small opening angles of the Q decay products.	33
2.19	Expected upper limits on the coupling $g_{Z'gg}$ versus $m_{Z'}$ and m_Q for two choices of $BF(Z' \rightarrow qQ)$ at $\sqrt{s} = 14$ TeV with $\mathcal{L} = 300 \text{ fb}^{-1}$. The shaded region shows the current limits on the coupling from other topologies (see text) where the width of the band reflects the variation with assumed m_Q	34
3.1	Production modes of the spin-3/2 leptons via standard model electroweak bosons.	41
3.2	Distribution of H_T^{leptons} for simulated spin-3/2 lepton samples; the selection required $H_T^{\text{leptons}} > 500$ GeV. The left pane shows the case where only electrons are considered; the right pane shows the case where electrons and muons are considered.	43
3.3	Overall efficiency of the selection defined in Ref. [21] which requires $H_T^{\text{leptons}} > 500$ GeV for OSSF off- Z , as a function of the spin-3/2 lepton mass. The left pane shows the case where only electrons are considered; the right pane shows the case where electrons and muons are considered.	45
3.4	Observed and expected limits as a function of ℓ^* and ν^* mass, in the case of $\ell^* = e^*$, $\nu^* = \nu_e^*$	46

3.5	Observed and expected limits as a function of ℓ^* and ν^* mass, in the case of $\ell^* = e^*, \mu^*, \nu^* = \nu_e^*, \nu_\mu^*$	47
4.1	Cosmologically preferred regions in the $(m_{\tilde{\ell}_4}, m_{\tilde{B}})$ plane for the QUE (left) and QDEE (right) models. In each shaded region, the relic density is in the preferred range $\Omega_{\tilde{B}} h^2 = 0.12 \pm 0.012$ for the value of m_{ℓ_4} indicated.	63
4.2	Contours of constant relic density $\Omega_{\tilde{B}} h^2$ for the QUE (left) and QDEE (right) models in the $(m_{\tilde{\ell}_4}, m_{\ell_4})$ plane with fixed $m_{\tilde{B}} = 1.2 m_{\ell_4}$. Between the dashed lines $\Omega_{\tilde{B}} h^2 = 0.12 \pm 0.012$	64
4.3	Contours of constant Higgs boson mass (in GeV) in the $(m_{\tilde{q}_4}, m_{\tilde{t}})$ plane, assuming no left-right squark mixings, for fixed $m_{t_4} = 1$ TeV.	67
4.4	Left: For MSSM4G models, the correlation of the neutralino dark matter's \tilde{W} , \tilde{H}_d , and \tilde{H}_u fractions with the SI proton scattering cross section $\sigma_{\text{SI}}^{(p)}$. Right: For MSSM4G models, the correlation of the neutralino dark matter's \tilde{H}_u fraction with $\sigma_{\text{SI}}^{(p)}$, color-coded by the value of $ \mu $ for each model point. The dashed line represents the analytic approximation for the cross section given in Eq. (4.40). In both panels, points in each scatter plot represent QUE and QDEE MSSM4G models that have 125 GeV Higgs bosons, are consistent with all collider bounds, and have the thermal relic density $\Omega_{\text{DM}} h^2 = 0.12 \pm 0.012$	71
4.5	Scatter plot of theoretical predictions for MSSM4G models in the $(m_\chi, \sigma_{\text{SI}}^{(p)})$ plane. The points represent QUE and QDEE MSSM4G models that have 125 GeV Higgs bosons, are consistent with all collider bounds, and have the correct thermal relic density. QUE models populate the mass range $200 \text{ GeV} \lesssim m_\chi \lesssim 540 \text{ GeV}$, and QDEE models populate the full range $200 \text{ GeV} \lesssim m_\chi \lesssim 700 \text{ GeV}$. The points are color-coded by the value of $ \mu $ in each model point. The upper shaded region is excluded by the current bound from LUX [22], and the dashed contours indicate the projected future sensitivities for DEAP3600 [23], Xenon 1T [24], DarkSide G2 [25], LZ [26], and Darwin [27]. In the lower shaded region, coherent neutrino scattering is a background.	91
4.6	Left: Predictions for the neutron SD cross section in MSSM4G models, along with experimental bounds. The shaded regions show the excluded parameter space from Xenon 100 [28] and LUX [29], and the projected sensitivities of LZ [29], Xenon1T and DARWIN [30] are given by dashed lines. Right: Predictions of the proton SD cross section in MSSM4G models, along with existing bounds from PICO-60 [31] and IceCube [32] and the projected sensitivities of LZ and DARWIN. The IceCube bounds assume dark matter pair annihilates to W^+W^- or $\tau^+\tau^-$, as indicated.	92

4.7	Theoretical predictions for, and current and future experimental sensitivities to, the annihilation cross sections to W^+W^- (left) and $\tau^+\tau^-$ (right) final states in the QUE (top) and QDEE (bottom) MSSM4G models as functions of the dark matter mass (top axis) and average energy $\bar{E} = m_{\tilde{B}}/2$ of the annihilation products (bottom axis). The green-shaded regions are the theoretical predictions for models with thermal relic density in the range $\Omega_{\text{DM}}h^2 = 0.12 \pm 0.012$; decays to 3rd-generation leptons are assumed for the $\tau^+\tau^-$ panels. The dashed blue lines are the existing dwarf bounds from the combined MAGIC and Fermi-LAT data, and the dashed red lines are the CTA projections for Galactic Center sensitivities assuming 500 hours of observation time and an Einasto dark matter profile.	93
4.8	Current bounds and LHC Run 2 discovery prospects for searches for extra sleptons $\tilde{\tau}_{4(5)}$ in MSSM4G models with e -mixed or μ -mixed extra lepton generations. For the QUE (QDEE) model, the dark-gray (light-gray) region is excluded by 8 TeV searches [33], and the solid (dashed) contours outline the expected exclusion sensitivities of the 14 TeV LHC with integrated luminosities of 300, 1000, and 3000 fb^{-1} , from left to right. The small dots show the parameter points we simulated to determine the Run 2 prospects.	94
4.9	The cosmologically preferred parameter space of QUE (left) and QDEE (right) MSSM4G models, and the exclusion sensitivity of LHC searches in the e -mixing case. The μ -mixing case results in almost identical sensitivity, while the LHC is expected to be insensitive to the τ -mixing case. In both panels, the unified mass relations are assumed and we consider $m_{\ell_4} > 200$ GeV. In the shaded regions, m_{ℓ_4} is can be tuned so that the model has $\Omega_{\text{DM}}h^2 = 0.12$; contours of constant m_{ℓ_4} are shown in gray. Outside the shaded regions, the model cannot satisfy $\Omega_{\text{DM}}h^2 = 0.12$ with $m_{\ell_4} > 200$ GeV. The black lines are the expected exclusion limits at the 14 TeV LHC. Those parallel to the m_{ℓ_4} -contours are from extra lepton searches. The other lines are from extra slepton searches; they are not limited to the color-filled region because they are independent of m_{ℓ_4} . For both searches, dotted, dashed, and solid lines are for an integrated luminosities of $\int \mathcal{L} = 300, 1000, \text{ and } 3000 \text{ fb}^{-1}$, respectively. On the red contour in the right plot, the masses satisfy the relation $m_{\ell_4} + m_{\tilde{B}} = m_{\tilde{\ell}_4}$	95
5.1	The Higgs and stop masses for $N = 1$, $M = 900$ TeV, $\tan\beta = 10$. Fig. 5.1a shows the Higgs mass for a wide range of y_t . The predictions of minimal gauge mediation can be read off from the line $y_t = 0$. The white region is excluded because it leads to tachyonic stops (see text). In Fig. 5.1b, we show Higgs mass (solid), heavy stop mass (dotted) and light stop mass (dashed) contour lines in a smaller region of y_t . In Fig. 5.1c we show Higgs (solid), μ (dashed) and $x_t = X_t/M_S $ (dotted) contour lines in the same region.	107
5.2	Same plots as in Fig 5.1a and 5.1b with $M = 400$ TeV and $\tan\beta = 10$	109
5.3	Same plots as in Fig 5.1a and 5.1b with $M = 10^{12}$ GeV and $\tan\beta = 10$	110
5.4	Same plots as in Fig 5.1a and and 5.1b with $M = 10^8$ GeV, $\tan\beta = 20$	111
5.5	Higgs mass contours in the $y_t - y_b$ plane with $M = 10^8$ GeV, $\Lambda = 230$ TeV, and $\tan\beta = 10$	117

LIST OF TABLES

	Page	
2.1	Expected yield from background processes at $\sqrt{s} = 14$ TeV with $\mathcal{L} = 300 \text{ fb}^{-1}$ after preselection requirements. Uncertainties are dominated by theoretical cross section uncertainties.	19
3.1	Allowed decay modes for spin-3/2 leptons ℓ^* and ν^*	41
3.2	The ratios of g_W and g_B and the main decay feature of each benchmark point	42
4.1	List of relevant parameters to the direct detection cross section, and the ranges used for our MICROMEGAS calculation.	70
4.2	Future prospects for searches for vector-like leptons at the 14 TeV LHC for three values of integrated luminosity. The first table is for the QUE models, and the second for the QDEE models. We consider vector-like leptons with a mass $m_{\ell_4} \geq 200$ GeV; the expressions 0^{+250} GeV etc. show that the central value of exclusion or discovery limit is below our model points and we may achieve the limit of 250 GeV with 1σ statistical fluctuation. In the dashed entries the upper limit is less than 200 GeV even with 1σ statistical fluctuation. The CL_s method is used for statistical treatment, where the statistical uncertainty and a 20% systematic uncertainty for the background contribution are taken into account, while the theoretical uncertainty on the signal cross section as well as the NLO correction are not considered. See Appendix C for further details.	82
5.1	R-parity and Z_3 charges.	102
5.2	Model parameters, and resulting Higgs parameters and spectra for eight sample models. All mass parameters are given in GeV.	112

ACKNOWLEDGMENTS

I cannot possibly do justice to everyone who contributed in one way or another to either my passion for science, which lead me towards a career in physics, my success in education which carried me through, or my well-being without which I would have failed nonetheless, be it friends, family members, or colleagues.

It's only pertinent to begin with special thanks to my dissertation committee members, Prof. Arvind Rajaraman and Prof. Tim Tait, and particularly to the head of committee and thesis advisor Prof. Yuri Shirman for his availability, guidance, and care during my time at UCI, not to mention his spirited embrace of the pleasure I took in mocking his constantly disorganized office.

A very honorable mention is due to the mentorship, expertise, and cynicism relief of Prof. Jonathan Feng who I had the pleasure of working with. I have also enjoyed and learned much from collaborations with Prof. Daniel Whiteson whose pragmatism is a fine benchmark for one to live up to. I would also like to recognize Prof. Mohammad Abdulkarim and Prof. Edward Davis who went far out of their way in both teaching and guidance during my undergraduate studies.

Throughout the 10 or so years of physics education I have had countless collaborations and interesting discussions with more colleagues than I can list in this page, among which are Anthony Difranzo, Patrick Fox, Iftah Galon, Jesi Goodman, Sho Iwamoto, Ben Lillard, Hamid Rasheed, Yael Shadmi, Chase Shimmin, Jordan Smolinsky, Flip Tanedo, Reiko Toriumi, and Alex Wijangco.

I'd like to allocate extra credit to Nic Canac, Anthony Difranzo, Hamid Rasheed, Alex Wijangco and, in particular, Chase Shimmin, for their friendship has been the source of much needed joy and personal fulfillment.

Last but not least, I would not have made it to this stage without the pouring support from my family. I would like to thank my mom for her care and nurture, and for putting up with my spoiled, grumpy behavior for all those years. I would like to thank, with utmost gratitude, my dad for teaching me most of what I'm proud of today. He taught me about science, research, character, communication, and leadership, just to name a few. He supported me both emotionally and financially during my graduate education and stood by every decision I made, assuring me that a PhD is too low of a bar for me to fail.

My research has been fully funded by the Kuwait University Scholarship.

CURRICULUM VITAE

Mohammad Abdullah

EDUCATION

Doctor of Philosophy in Physics

University California, Irvine

Advisor: Prof. Yuri Shirman

2017

Irvine, California

Master of Science in Physics

University California, Irvine

2012

Irvine, California

Bachelor of Science in Physics with Minor in Mathematics

Kuwait University

2010

Kuwait

Graduated with honors

RESEARCH EXPERIENCE

Graduate Research Assistant

University of California, Irvine

2012–2017

Irvine, California

TEACHING EXPERIENCE

Teaching Assistant

University of California, Irvine

Summer 2012

Irvine, California

SELECTED HONORS AND AWARDS

Kuwait University Scholarship

2011-2017

REFEREED JOURNAL PUBLICATIONS

- Searching for spin-3/2 leptons** **2017**
with Kevin Bauer, Luis Gutierrez, John Sandy, and Daniel Whiteson, Phys. Rev. D 95, 035008, arXiv:1609.05251
- Heavy bino dark matter and collider signals in the MSSM with vectorlike fourth-generation particles** **2016**
with Jonathan L. Feng, Sho Iwamoto, and Benjamin Lillard, Phys. Rev. D 94, 095018, arXiv:1608.00283
- Reviving bino dark matter with vectorlike fourth generation particles** **2015**
with Jonathan L. Feng, Phys. Rev. D 93, 015006, arXiv:1510.06089
- Hidden On-Shell Mediators for the Galactic Center Gamma-Ray Excess** **2014**
with Mohammad Abdullah, Arvind Rajaraman, Tim M. P. Tait, Philip Tanedo, and Alexander M. Wijangco, Phys. Rev. D 90, 035004 (2014), arXiv:1404.6528
- Systematically Searching for New Resonances at the Energy Frontier using Topological Models** **2014**
with Mohammad Abdullah, Eric Albin, Meghan Frate, Craig Pitcher, Chase Shimmin, Suneet Upadhyay, James Walker, Pierce Weatherly, Patrick J. Fox, and Daniel Whiteson, Phys. Rev. D 89, 095002 (2014), arXiv:1401.1462
- Flavored Gauge Mediation, A Heavy Higgs, and Supersymmetric Alignment** **2013**
with Iftah Galon, Yael Shadmi, and Yuri Shirman, J. High Energ. Phys. (2013) 2013: 57, arXiv:1209.4904

PRESENTATIONS

- Dark Matter at the LHC 2017 Poster Session** **April 2017**
Heavy bino dark matter and collider signals in the MSSM with vectorlike fourth-generation particles
- SLAC Seminar Talk** **November 2016**
Reviving bino dark matter with vectorlike fourth generation particles
- UC Berkeley Seminar Talk** **November 2016**
Reviving bino dark matter with vectorlike fourth generation particles
- Cornell Seminar Talk** **October 2016**
Reviving bino dark matter with vectorlike fourth generation particles
- University of Syracuse Seminar Talk** **October 2016**
Reviving bino dark matter with vectorlike fourth generation particles

Phenomenology 2016 Symposium **May 2016**
Reviving bino dark matter with vectorlike fourth generation particles

Phenomenology 2015 Symposium **May 2015**
Searching for new collider resonances through topological models

TASI Student Talk **June 2013**
Flavored Gauge Mediation of Supersymmetry Breaking

SCHOOLS

TASI 2013, CU Boulder **June 2013**

ABSTRACT OF THE DISSERTATION

Searching for Physics Beyond the Standard Model and Beyond

By

Mohammad Abdullah

Doctor of Philosophy in Physics

University of California, Irvine, 2017

Professor Yuri Shirman, Chair

The hierarchy problem, convolved with the various known puzzles in particle physics, grants us a great outlook of new physics soon to be discovered. We present multiple approaches to searching for physics beyond the standard model. First, two models with a minimal amount of theoretical guidance are analyzed using existing or simulated LHC data. Then, an extension of the Minimal Supersymmetric Standard Model (MSSM) is studied with an emphasis on the cosmological implications as well as the current and future sensitivity of colliders, direct detection and indirect detection experiments. Finally, a more complete model of the MSSM is presented through which we attempt to resolve tension with observations within the context of gauge mediated supersymmetry breaking.

Chapter 1

Introduction

As it stands today, the standard model of particle physics is the most precisely tested theory we know of. The particle content and properties as well as the underlying Poincarè and gauge symmetries, which serve as fundamental cornerstones to its formulation, has been thoroughly examined by numerous high precision experiments and observations [1]. Yet, we have great confidence that it is not the whole picture and that some new physics, likely manifest in the form of yet to be discovered particles, is lurking right around the corner. The two questions we want to address are: why do we expect to find new physics around the TeV scale? and how to go about looking for such physics?

Let us turn back in time to the 4th of July, 2012, when the ATLAS [2] and CMS [3] collaborations at the Large Hadron Collider (LHC) announced at the 5σ level an observation of a new field consistent with the Standard Model Higgs boson predicted more than 40 years earlier [4–9]. Since then the significance of the conclusion has only improved, and pending a measurement of the Higgs coupling with light fermions, we have great confidence that the final puzzle piece of the standard model has now been found.

With this discovery, however, a well known and dreaded problem has been solidified, the

so-called *Hierarchy Problem* [10, 11]. In the simplest of terms, it is the question of why the electroweak scale, characterized by the Higgs mass of 125 GeV, is so different from the only fundamental scale of a theory with only gravitational interactions, namely the unique combination of the Planck constant \hbar , the speed of light c , and Newton's gravitational constant $G = 6.70861(31) \times 10^{-39} \hbar c (\text{GeV}/c^2)^{-2}$ which, in units where $\hbar = c = 1$, results in a unit of energy known as the Planck energy or Planck mass $M_P = \sqrt{\frac{\hbar c}{8\pi G}} \simeq 2.4 \times 10^{18} \text{ GeV}$ [1].

To quantify the problem more, we begin with the observation that the Higgs is, by default, assumed to be a fundamental scalar, and is the only occurrence found in nature thus far. This means that there is, in general, no symmetry protecting it's mass from quantum corrections. Sure enough, the Higgs receives quadratically divergent mass corrections from various fields, the largest of which is via it's coupling with the top quark. A common way of regulating this divergence is by cutting off the energy integral at the scale beyond which our theory ceases to be valid which, is taken to be the Planck scale. The Higgs mass we observe is smaller by about 16 orders of magnitude.

These corrections can, of course, be "swept under the rug" through mass renormalization where a new term (the counterterm) is introduced in the Lagrangian to absorb the quadratic correction. The new mass parameter, then, is what we interpret as the observable measured in our experiments. In other words, we postulate a contribution to the mass term similar in magnitude to the quadratic corrections in order for our theory to be consistent with observation. For that to work, though, we would need to fine-tune the counterterm to a level of roughly one part in 10^{32} , a level that is often described as *unnatural*. If we demand that our theory is natural, then we would expect new physics to appear at about the TeV scale to cancel the mass corrections or otherwise invalidate our computation.

One can, however, dismiss the previous argument on the basis that it relies on how we regulate the divergence and the interpretation thereof. For instance, one can utilize dimensional regularization in which case the offending quadratic sensitivity does not seem to be present.

Even then, there is a potential source of quadratic mass corrections. It has been demonstrated that a heavy field that communicates with the Higgs can generate, depending on the nature of the interaction, sizable mass corrections to the Higgs [12]. Since we do not observe such corrections, we expect either that the new physics has to appear at a lower scale or that some extra physics appears at a lower scale to invalidate our calculation. The question, then, remains of whether or not such new physics exist. This is an open question which might lead one to declare the hierarchy problem as being circular; new physics is implied from the assumption of new physics. Fortunately, there is a strong case to be made for the expectation of new phenomena at some high, possibly untestable, scale of which we will now mention a few primary examples.

But before we do that we would like to restate our premise for extra clarity. From a purest's perspective, the Higgs mass is considered to be unnatural due to virtual quadratic sensitivity to the Planck scale which motivates the expectation of new physics to appear at the TeV scale. From a more pragmatic stand point, the presence of certain classes of new physics at a high scale would lead to sizable physical corrections to the Higgs mass which, in the absence of physics at the TeV scale, would require fine tuned cancelations among such corrections. We will go through a few examples of particle physics puzzles that qualify as stand-alone motivations for new physics. The solutions to those puzzles will, to varying degrees, lead to the (fortunate?) corrections to the Higgs mass which then motivates us to look for such physics at around the TeV scale.

Among the popular examples of new physics is the dark matter hypothesis. A large body of cosmological evidence, ranging from galactic rotation curves to anisotropies in the Cosmic Microwave Background, consistently suggests that about 27% [13] of the matter-energy content of the universe consist of a new form of massive, non-luminous matter (see Ref. [1] for a quick up-to-date review of experimental status or [14] for a historical introduction).

At first, dark matter seems disconnected from the hierarchy problem since there is no a priori

a reason to assume that dark matter interacts with the standard model in any way besides gravity. But such an assumption is nonetheless reasonable and necessary for experimental investigation of dark matter and so, from a practical sense, a link between dark matter and the Higgs mass could very well exist.

Another cosmological problem is baryogenesis, the process that generated the asymmetry between the matter and anti-matter content of the universe. Sakharov derived three conditions required to generate this asymmetry: 1. Out-of-equilibrium dynamics, 2. Baryon number violation, and 3. CP and C violation [15]. The last condition is the only one that cannot be accommodated within the standard model and calls for new physics to be added. One example would be adding extra vector-like generations of standard model fermions [16]. The extra fermions can result in a strong first order phase transition and even provide extra CP violation through Yukawa couplings with the Higgs which could lead to the unwanted mass corrections.

A more compelling case arises from what is, arguably, the strongest indicator of new physics, namely the fact that neutrinos have mass [1]. This has been overwhelmingly verified by the observation of neutrino flavor oscillations. By comparing the flavors of neutrinos originating from the Sun, cosmic rays, particle accelerators or nuclear reactors to the flavors measured at neutrino detectors, it was found that neutrinos can alternate between the three flavors. Such oscillations are predicted to only occur if the neutrinos have different masses, which implies that at least two of them are massive.

Neutrino can be given a mass term if they are assumed to be Majorana in nature, that is, the left handed and right handed fields are identical. But, if we insist on gauge invariance then this term will necessarily have dimensions larger than four. Such terms are nonrenormalizable, indicating the existence of heavier degrees of freedom that have been integrated out of the theory in order to generate those terms. A simple and widely popular example is the type-I seesaw mechanism [17] where a heavy right handed, and therefore gauge singlet (or

sterile), neutrino is introduced to generate the neutrino masses. In this and similar models, the hierarchy problem is potentially present.

Interestingly, models of neutrino masses can be used to generate a matter-anti-matter asymmetry in the lepton sector (leptogenesis) which could be transferred over to the baryonic sector hence providing a mechanism for baryogenesis [18].

It is quite possible that the origin of neutrino masses is a seemingly unexciting Dirac mass term generated by a Yukawa coupling between the Higgs, the lepton doublet and a sterile neutrino. When matched with the observed limits on neutrino masses, though, these Yukawa couplings would be required to be significantly smaller than any standard model counterpart. But one can then wonder why such a hierarchy exists. In fact, this would fall under a larger question addressing the observed mass hierarchy between fermions of different flavors.

A popular class of models in which the flavor structure is explained is the Froggatt-Nielsen mechanism [19]. In such models, an underlying symmetry is used to forbid the mass terms to different degrees through a judicious choice of charges which, after the spontaneous breaking of that symmetry, would lead to a proportionally different masses. Since the terms generated from such models are Higgs Yukawa interactions, there will, in general, be a connection between this new physics and the Higgs sector thus leading, once again, to the risk of a hierarchy problem.

A somewhat related idea is Grand Unified Theories, or GUTs, which are hinted at by the observation that the standard model gauge couplings get suggestively close at around 10^{16} GeV [1]. Depending on how this unification is implemented, we expect that new fields exist at about the same scale which are charged under the standard model gauge groups. It is worth pointing out that in some of those models the way the observable matter is embedded in the unifying group results, at low energy, in a sterile neutrino [20]!

We should reemphasize that non of the above would, by itself, compellingly lead to the

conclusion that new physics exists at the TeV scale. Rather, when one is confronted with an overabundance of known and unknown possibilities and the urgency to decide which ones to pursue, an overarching principle is desirable, and it is through the totality of the various lines of experimentally motivated and intuition based evidence combined with the observed Higgs mass that such a seemingly optimistic expectation is reached.

We now turn briefly to the second question: how to go about looking for such new physics? Once the likelihood of new phenomena has been motivated, an ideal approach would be to look for such phenomena in as model-independent a way as possible. The difficulty with this approach is that particle physics is generally a large data field with too many observables to choose from where new physics might hide.

The other extreme would be to concoct a complete model with very concrete predictions. Given the limitless possibilities of new fields and interactions to introduce, it pays to set a standard of theoretical motivation and demand that a new model would address one or more of the known puzzles with little or no contrived assumptions. The down side, obviously, is that the experimental effort of testing the associated predictions will be harder to carry over to other theories.

In the remainder of this thesis we will study several examples that fall somewhere on the spectrum spanning those two extremes. We will begin, in Ch. 2, with a somewhat agnostic search strategy for new physics at the LHC. We will choose a given final state topology, namely two leptons and two hadronic jets, and systematically construct all possible ways to produce such a final state that also leads to a resonance. As it turns out, we could fill in some of the gaps left by the standard LHC searches.

In Ch. 3, we will take more liberty in borrowing from theoretical frameworks to look for new physics at the LHC. We will study a model of spin-3/2 vector-like leptons with a set of effective operators used to induce decays. In models where the known fermions are composite,

it is possible that excited states of higher spins are allowed. Yet, such fermions are not well studied due to how rarely they appear in the particle physics literature. Note that while we opt to highlight the theoretical motivations of our model, this is merely for completeness, and the spirit of our search does not impose such a constraining demand.

In Ch. 4 we will build on the existing lore of supersymmetry, which is one of the leading candidates to address the hierarchy problem. In this theory, an additional symmetry of space-time is assumed that interchanges fermions and bosons. As a result, every known degree of freedom must have an associated degree of freedom with the same mass and charges but opposite Fermi-Bose statistics. With such a symmetry, all corrections to the Higgs mass automatically cancel each other out. Additionally, supersymmetry generically improves the quality of gauge coupling unification and, when supplemented with an additional discrete symmetry, can provide several attractive dark matter candidates.

Supersymmetry has already been ruled out unless it is spontaneously broken, and the degree of this breaking, which is typically manifest in the mass scales of the new fields, determines how fine-tuned the Higgs mass is. Ironically, a common problem with supersymmetry is that the Higgs mass is too light, requiring either extra assumptions or an increase of mass correction from the *superpartners* which generally reintroduces some amount of fine-tuning back into the theory and renders the new fields too heavy to be discovered in the foreseeable future.

One idea that has been in the literature for a while is to add an extra generation of vector-like fermions which can be used to induce mass corrections to the Higgs without the need of too much fine-tuning. It has also been shown that only two unique combinations of such fields can be added in order to preserve perturbative gauge coupling unification. We show that, in addition, we can significantly increase the mass parameter space of one of the dark matter candidates, the so-called bino.

We will follow up with a comprehensive discussion of the experimental signature of this model from particle colliders, direct detection, and indirect detection experiments, and the complementarity of how those experiments probe the parameter space is demonstrated.

A large number of parameters are introduced in supersymmetry, and since fine-tuning is a key motivation behind its assumption, one has to demand that the choice of such parameters is not itself a form of fine-tuning. To address this, a more complete picture of how supersymmetry is broken needs to be included. In Ch. 5, we move further into the liberal end of the model building spectrum and present an extension to previous work in which supersymmetry is broken in a secluded sector and the breaking is communicated via the standard model gauge bosons. The original model has been faced with the difficulty of raising the Higgs mass to its observed value without increasing the supersymmetry scale and keeping the new fields beyond the reach of the LHC. By coupling the Higgs more directly to the supersymmetry breaking sector, we show that a realistic Higgs mass is possible with light particle spectra, albeit with some drawbacks to be discussed.

Finally, we present our conclusions in Ch. 6.

Chapter 2

Systematically Searching for New Resonances at the Energy Frontier using Topological Models

Based on arXiv:1401.1462 [37]

Collisions of particles at the energy frontier offer enormous potential for the discovery of new particles or interactions. To date, no evidence for physics beyond the standard model has been reported. However, the current program consists overwhelmingly of searches for specific theoretical models, and the possibility remains of a theoretically unanticipated discovery.

Searches for new particles without the guidance of a specific theory model face daunting challenges, the most prominent being the enormous space of signatures in which to search. An examination of every possible observable in every final state configuration suffers from an enormous trials factor, such that discovery is nearly impossible unless the signal is enormous. Previous approaches [38–40] have been to consider only the total yields in a large set of final states – which significantly reduces the discovery sensitivity, or to search for excesses in

high- p_T tails of many distributions in many final states – which suffer from poor statistics and large systematic uncertainties.

In this chapter, we propose a new approach which focusses on exploring the complete set of models which have identifiable resonant features: for each final state, systematically construct all possible topologies which would give resonant features, seen as peaks in reconstructed invariant mass distributions¹. This reasonable experimental requirement constrains the space of discoverable models dramatically without being dominated by theoretical prejudice, and guides the analysis strategy: to search for the resonant features of each specifically constructed topological model. This does not completely evade the trials factor, which is unavoidable if one examines many final states, but is an experimentally motivated strategy for reducing the number of observables in a given final state. Limits or discoveries may be reported in terms of cross sections in the space of particle masses. Perhaps most importantly, the topological model strategy emphasizes *completeness*, where theoretical motivations may not have inspired us to examine specific topologies. For example, we describe below how topological models motivate a search for $Z' \rightarrow \chi_1\chi_2 \rightarrow \ell^+\ell^-jj$ which features resonances in $m_{\ell\ell}$, m_{jj} and $m_{\ell\ell jj}$; this is similar to existing searches for new resonances decaying to $WZ \rightarrow \ell^+\ell^-jj$ but without the constraint that $m_{\ell\ell} \approx m_Z$ and $m_{jj} \approx m_W$. In this way, it points to new directions where discovery potential is untapped in the current data.

This approach shares a motivational principle with the simplified model approach [34], in that it seeks to characterize our knowledge in terms of particle masses rather than theoretical parameters, giving limits on cross sections for given decay modes rather than on theoretical parameters for full theories. However, while simplified models reduce the complexity of a set of full models by specifying the minimal particle content of a topology, the topological model strategy aims to cover the complete experimental space of a particular final state or set of final states.

¹There are some cases in which resonances may not be reconstructable, such as compressed mass spectra where the decay products are too soft to be observed, or resonances with invisible decay products.

This topological model approach is best considered as an extension of the effective field theory strategy, where the new particles are considered to be too heavy to be directly observed as resonances and the interactions they mediate are replaced by effective operators which integrate out the details of the complete theory. Typically, exhaustive lists of possible operators are formed, giving a completeness to the analysis. In the same way, the topological model approach we describe here seeks to compile the list of potentially discoverable new physics topologies, but where the new particles are light enough to be directly seen as resonances.

The completeness of a survey of topological models in a final state gives more weight to a negative result: if nothing is seen in the data we can say with some confidence that no new observable resonances exist. In addition, another strength is it helps to organize the experimental results, which are currently presented in the context of searches for specific theories.

The number of topologies grows quickly with the number of final state objects. For concreteness, we choose a final state with a reasonable but non-trivial number of objects: $\ell^+\ell^-jj$. Note that in the examples below we have focused on $\ell = e, \mu$, quark-originated jets, and that in the event selection we allow more than two jets in order to improve the probability to locate the two jets of interest among those generated by radiation. Additionally, one could consider further categorization by jet flavor.

Though we examine a single final state here, one important advantage of this approach is that it allows the coherent consideration of multiple final states. For example, one could consider 4ℓ or $4j$ modes of $Z' \rightarrow \chi_1\chi_2$ decay. By contrast, a similar interpretation of multiple final-state-specific simplified-model results is not possible, as the results are reported per final-state and the necessary correlational information needed to combine final states is not typically reported.

In the following sections, we construct the list of topological models for $\ell^+\ell^-jj$, detail theoretical models built to describe the phenomenology of those topologies, and present LHC sensitivity studies for each topology.

2.1 Topologies in $\ell^+\ell^-jj$

In the $\ell^+\ell^-jj$ final state, resonant features can be seen in several distinct topological arrangements; there can be two-, three-, or four-body resonances present. Since it will allow for the largest production cross section, we always consider the case of a 4-body $\ell^+\ell^-jj$ resonance. From a $q\bar{q}$ initial state this first resonance must be either a color singlet or octet, Lorentz vector or scalar, and we focus here on the simple case of color-singlet vector boson, a Z' boson. In this case the intermediate 2- (3-) body resonances are scalars (fermions). In particular, the topologies which arise are:

- $Z' \rightarrow \chi_1\chi_2 \rightarrow (\ell^+j)(\ell^-j)$ see Fig. 2.1
- $Z' \rightarrow \chi_1\chi_2 \rightarrow (\ell^+\ell^-)(jj)$ see Fig. 2.2
- $Z' \rightarrow \ell^\pm L \rightarrow \ell^\pm(\ell^\mp jj)$ see Fig. 2.3
- $Z' \rightarrow jQ \rightarrow j(\ell^+\ell^-j)$ see Fig. 2.4

The first topology (see Fig. 2.1) describes resonant production of new particles, each of which decays to a lepton and a jet. This is essentially a lepto-quark model [41], and territory which is well-explored experimentally and will not be discussed further here.

The second topology (see Fig. 2.2) describes production of new particles χ_1 and χ_2 which decay to lepton pairs or quark pairs. This is similar to searches for heavy resonances which decay to ZZ with one hadronically and one leptonically decaying Z boson, or decays to WZ

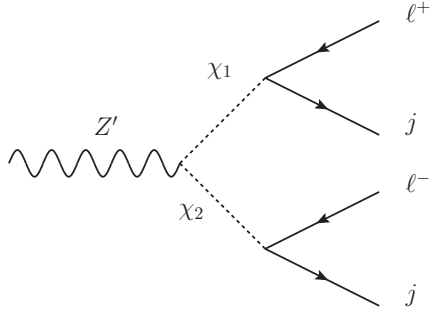


Figure 2.1: Diagram for $Z' \rightarrow \chi_1 \chi_2 \rightarrow \ell^+ j \ell^- j$

with hadronic W -boson and leptonic Z -boson decays. This is well-explored territory, but only for the cases where χ_1 and χ_2 have masses close to $m_{W,Z}$. In the case when these intermediate particles are heavier, *the experimental data have not been examined, and discovery potential remains*. This topological approach therefore provides a useful and natural generalization of an existing effort.

The final two topologies (see Figs. 2.3 and 2.4) include decays $Q \rightarrow \ell^+ \ell^- j$ or $L \rightarrow \ell^\pm j j$. These arise from a higher dimension four-fermion contact operator, representing the mediation of this interaction via some new heavy particle which is integrated out. To be perfectly exhaustive, one should consider the case where the mediator is light enough to be produced on-shell, giving, for example $Q \rightarrow X j \rightarrow \ell^+ \ell^- j$.

Note that we do not discuss in detail $Z' \rightarrow (\ell^+ \ell^- j j)$ through an effective five-point interaction, because this topology provides no further intermediate resonances to guide the search beyond $m_{\ell j j}$.

In the next sections, we construct example models which give these topologies, propose techniques for experimental analysis, and estimate the sensitivity of the LHC at $\sqrt{s} = 14$ TeV, with $\mathcal{L} = 300 \text{ fb}^{-1}$.

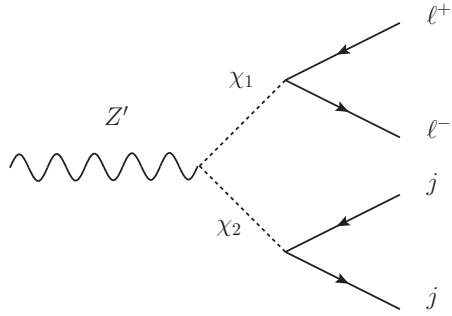


Figure 2.2: Diagram for $Z' \rightarrow \chi_1 \chi_2 \rightarrow \ell^+ \ell^- jj$

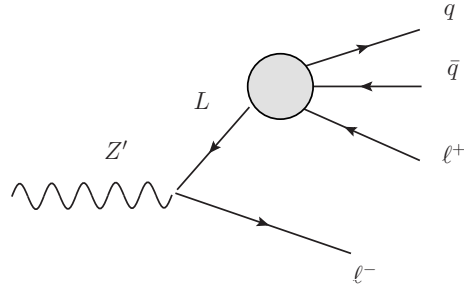


Figure 2.3: Diagrams for $Z' \rightarrow \ell^\mp L \rightarrow \ell^\mp (\ell^\pm jj)$ (right)

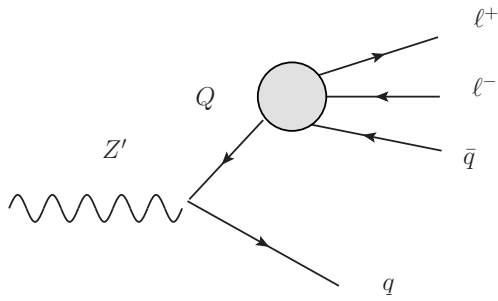


Figure 2.4: Diagram for $Z' \rightarrow jQ \rightarrow j (\ell^+ \ell^- j)$

2.2 The Models

In order to allow simulation of these topologies, toy models were built in FeynRules [42] for MadGraph [43]. To allow production, the Z' resonance must couple to some of the SM quarks. This may occur either through charging some of the quarks under the $U(1)'$, or through a higher dimension operator as an “effective Z' ” [44]. The former requires the addition of new heavy fermions to cancel gauge anomalies, these can always be vector-like under the SM and chiral under the $U(1)'$ [45], and alters the structure of the SM Yukawa couplings. With some SM quarks charged under the $U(1)'$ the Yukawa couplings must either become higher dimension operators, or the leptons will also carry a $U(1)'$ charge, leading to strong constraints. The latter approach requires heavy fermions that mix with SM fermions, these can be vector-like under both the SM and the $U(1)'$ but does not alter the rest of the SM Lagrangian in anyway. For simplicity, we consider a flavor independent coupling of the RH quarks to the Z' , although other choices are also possible. Since it does not affect the physics we are interested in, our toy models are not complete and do not contain either sets of heavy fermions necessary to make the models consistent. Nor do we attempt a complete description of the flavor structure of the SM fermions. Furthermore, we assume the Higgs field that is responsible for breaking the $U(1)'$ is sufficiently massive that it does not play a role in the following. How the Z' decays determines the final state topology; each case is discussed below.

2.2.1 $(qq)(\ell\ell)$ Topological Model

This toy model contains two new scalars ϕ_1 and ϕ_2 , that are charged under the Z' . These ϕ fields are not the mass eigenstates, instead they mix with one another to give the mass eigenstates χ_1 and χ_2 . In general there will be decays of Z' to all open channels *i.e.* $\chi_1\chi_1$, $\chi_1\chi_2$, and $\chi_2\chi_2$. However, by judicious choice of the scalar charges and mixing angles, it is

possible to build a toy model in which the Z' decays are restricted to jj along with $\chi_1\chi_2$ only, or $\chi_1\chi_2$ and one of $\chi_1\chi_1$ or $\chi_2\chi_2$.

To allow the scalars to decay we turn on some higher dimension operators of the form $\lambda_{ij}^k \frac{\phi_k X^n}{\Lambda^{1+n}} \ell_i H e_j^c$ where n is chosen to make the operator $U(1)'$ invariant and $\langle X \rangle \neq 0$. The λ coefficients are a new source of flavor changing processes mediated by the ϕ 's, for which there are strong constraints. If the λ are taken proportional to the SM Yukawa matrices then the couplings of ϕ will be diagonal in the quark/lepton mass basis, which then means the χ 's preferentially decay to heavy flavor. However, since we do not take advantage of flavor tagging in this analysis, we make a simplifying assumption that instead the couplings of χ are flavor universal in the quark and lepton mass bases.

Cross section for Z' production in pp collisions at $\sqrt{s} = 14$ TeV is given in Fig 2.5.

2.2.2 $(qq\ell)\ell$ Topological Model

A model to describe this resonant structure begins with a new Z' boson, as above. In addition, we include heavy vector-like pairs of leptons (L, L^c) that will mix with the right-handed standard model leptons. L^c has the quantum numbers of the RH leptons under the SM, *i.e.* $Y = 1$, and is charge 1 under the $U(1)'$, the L is the opposite under both. This mixing is induced through operators involving the field, X , responsible for the Z' mass, $\lambda X L_i e_i^c$. To avoid lepton flavor constraints we have included three generations of heavy vector-like leptons and they mix with the SM RH leptons in a flavor universal fashion. However, when investigating the reach at the LHC in this final state we will focus exclusively on $\ell = e$. This mixing term also allows the heavy leptons to decay, through an off shell X field. We introduce higher dimension couplings of X to (down-type) quarks of the form $\lambda'_{ij} \frac{X}{\Lambda} q_i H d_j^c$, so that $L \rightarrow \ell \bar{q} q$ and, as before, we take this coupling to be universal in the mass basis of the quarks. Thus, the toy model under investigation is one in which the possible final states

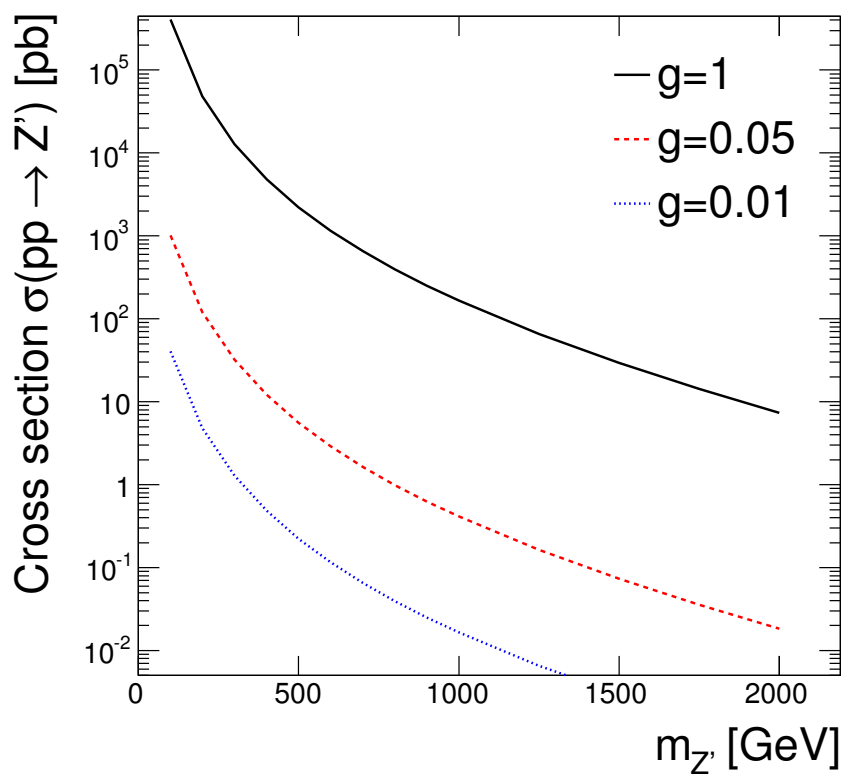


Figure 2.5: Cross section for Z' production at $\sqrt{s} = 14$ TeV, including all decay modes.

of the Z' are dijets, L^+L^- , $L^\pm e^\mp$, and e^+e^- , with the heavy leptons decaying as $L^\pm \rightarrow e^\pm q\bar{q}$. For small mixing, ϵ , the couplings of these last three states are in the ratio $1 : \epsilon : \epsilon^2$, so the strongly constrained dilepton rate can be made parametrically small whilst maintaining an interesting rate in $L^\pm e^\mp$.

2.2.3 $(q\ell\ell)q$ Topological Model

A model describing the resonant structure $(q\ell\ell)q$ begins as well with a new Z' boson and is very similar to the model for $(q\bar{q}\ell)\ell$, but the heavy lepton L is replaced by a heavy quark, Q , taken to have the SM quantum numbers of the d_R , and X decays to leptons, Fig. 2.4. The final states of the Z' are dijet, $Q\bar{q}$, and $Q\bar{Q}$ if it is kinematically accessible. Thus, in addition to the final state we are interested in there will be constraints from dijet resonance searches as well as strong constraints from multilepton searches. Searches for a heavy quark decaying as $Q \rightarrow qZ$ can also be recast [46] to place bounds on this model.

2.3 Backgrounds to $\ell\ell jj$

In pp collisions, the dominant background in the $\ell\ell jj$ final state to any of these new models is $Z/\gamma \rightarrow \ell^+\ell^-$ in association with jets. Secondary backgrounds include diboson production ($WZ \rightarrow q\bar{q}'\ell^+\ell^-$ and $ZZ \rightarrow q\bar{q}'\ell^+\ell^-$) and top-quark pair production ($t\bar{t} \rightarrow W^+bW^-\bar{b} \rightarrow \ell^+\nu b\ell^-\nu\bar{b}$). Other sources, such as $W \rightarrow \ell^\pm\nu$ in association with jets where one jet is misidentified as a lepton, are minor in comparison and neglected here.

Events are simulated with MADGRAPH5 [43] with PYTHIA [47] for showering and hadronization and DELPHES [48] for detector simulation. Table 2.1 and Fig. 2.6 shows the expected background yields at this stage. Next-to-leading order cross sections are used in each case [49–51]. Throughout, limits are calculated using a frequentist asymptotic calcula-

Table 2.1: Expected yield from background processes at $\sqrt{s} = 14$ TeV with $\mathcal{L} = 300 \text{ fb}^{-1}$ after preselection requirements. Uncertainties are dominated by theoretical cross section uncertainties.

Process	$\ell\ell+\text{jj}$	$\mu\mu+\text{jj}$	$ee+\text{jj}$
$Z+\text{jets}$	$(2.35 \pm 0.1) \cdot 10^7$	$(1.3 \pm 0.1) \cdot 10^7$	$(1.0 \pm 0.1) \cdot 10^7$
ZZ	$(5.77 \pm 0.3) \cdot 10^4$	$(3.1 \pm 0.2) \cdot 10^4$	$(2.6 \pm 0.1) \cdot 10^4$
WZ	$(8.68 \pm 0.4) \cdot 10^4$	$(4.6 \pm 0.2) \cdot 10^4$	$(4.0 \pm 0.2) \cdot 10^4$
$t\bar{t}$	$(1.24 \pm 0.1) \cdot 10^5$	$(6.6 \pm 0.4) \cdot 10^4$	$(5.9 \pm 0.3) \cdot 10^4$
Total	$(2.37 \pm 0.1) \cdot 10^7$	$(1.3 \pm 0.1) \cdot 10^7$	$(1.0 \pm 0.1) \cdot 10^7$

tion [52, 53].

We select events which satisfy the basic event topology:

- exactly two electrons or two muons, both with $p_T > 20$ GeV and $|\eta| < 2.5$
- at least two jets, each with $p_T > 25$ GeV and $|\eta| < 2.5$

In addition, we require $\cancel{E}_T < 100$ GeV to partially suppress the $t\bar{t}$ background at little cost to the signal efficiency. This basic selection we refer to as our *preselection*. For each signal hypothesis, we make further requirements on the reconstructed invariant masses. Note that though the masses of the new particles are not specified, we can treat each potential set of mass values as a distinct model with fixed mass parameters and optimize the selection to those parameters. This raster scan approach is possible without look-elsewhere penalties in the case of limit-setting; in the event of an excess in data, the calculation of its significance would require accounting for the number of mass hypotheses considered.

2.4 Mass reconstruction and LHC Sensitivity

In each topology, there are combinatorial ambiguities in the assignment of reconstructed jets to colored partons [54]. In the heavy lepton model, there is an additional ambiguity regarding

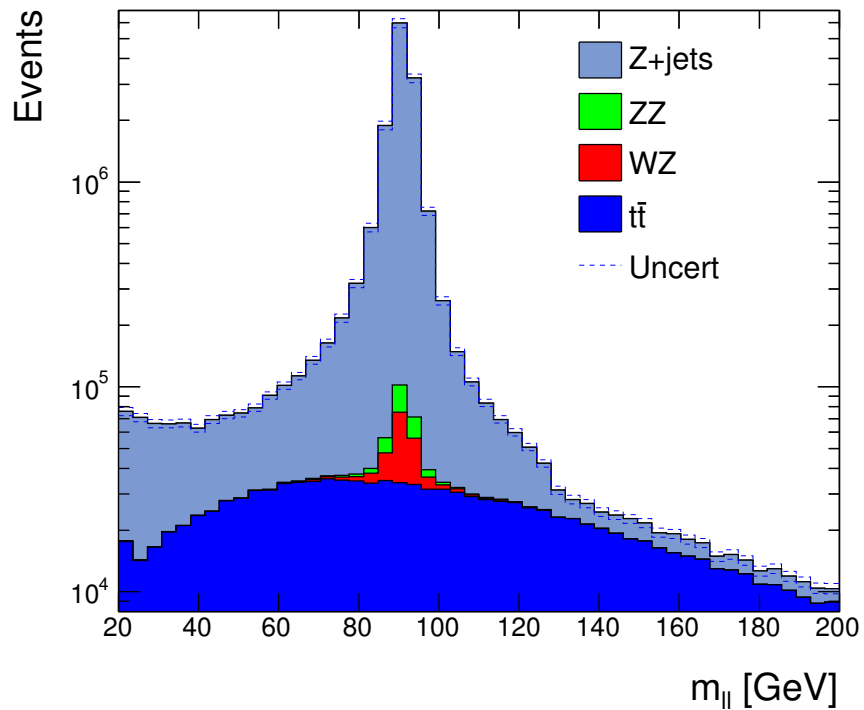


Figure 2.6: Distribution of $m_{\ell\ell}$ in simulated events for background process contributing to the $\ell\ell jj$ final state in pp collisions at $\sqrt{s} = 14$ TeV with $\mathcal{L} = 300 \text{ fb}^{-1}$, after preselection requirements.

which charged lepton is assigned to the decay of the heavy lepton, see Fig 2.3. To resolve ambiguities, we use the separation $\Delta R = \sqrt{\Delta\phi^2 + \Delta\eta^2}$ to either select decay products with the smallest or largest opening angle depending on the kinematic configuration. Details are given below in each case.

2.4.1 $(\ell\ell)(jj)$ topology

In the $(\ell\ell)(jj)$ topology, there are no lepton ambiguities, so the $(\ell\ell)$ system is well-defined. In the case of the jets, if more than two jets are found there are several possibilities for the (jj) system. The (jj) pair momentum balances the momentum of the $(\ell\ell)$ pair, and we choose the pair of jets with largest $\Delta R(\ell\ell, jj)$. Examples of reconstructed masses are shown in Fig 2.7.

In addition to the preselection requirements above, we select events with reconstructed mass values close to the true values, $m_{\ell\ell} \in [m_{\chi_1} - 25, m_{\chi_1} + 25]$, $m_{jj} \in [m_{\chi_2} - 100, m_{\chi_2} + 50]$, and $m_{lljj} \in [m_{Z'} - 250, m_{Z'} + 100]$ GeV. Example distributions after m_{ll} and m_{jj} requirements can be seen for two examples in Fig 2.8. Efficiency of the final selection and expected upper limits on $\sigma(pp \rightarrow Z' \rightarrow \chi_1\chi_2 \rightarrow \ell\ell jj)$ can be seen in Fig 2.9.

Limits on cross section are shown in Fig 2.10 and converted into limits on the coupling $g_{Z'qq}$ versus $m_{Z'}$ in Fig 2.11 for two choices of $\text{BF}(Z' \rightarrow \chi_1\chi_2)$. The model as constructed would give a signature in $\ell\ell jj$, but the new particles and interactions introduced would yield signatures in other channels, where existing limits may also constrain the parameters of this model. Specifically, $Z' \rightarrow \chi_1\bar{\chi}_1$ gives a $llll$ final state, while $Z' \rightarrow \chi_2\bar{\chi}_2$ gives a $jjjj$ final state and $Z' \rightarrow jj$ gives a di-jet final state.

Both CMS [55] and ATLAS [56] have SUSY-motivated searches for four leptons and with and without missing energy using the full dataset. These results place strong constraint on

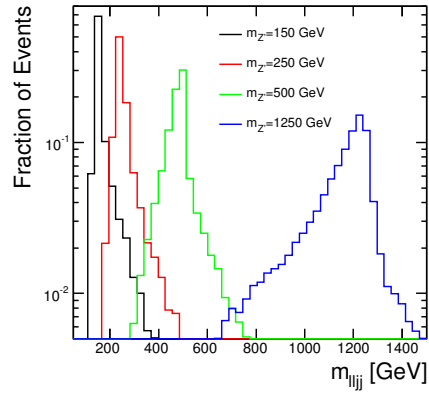
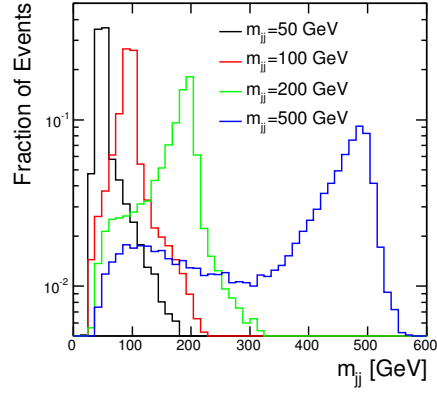
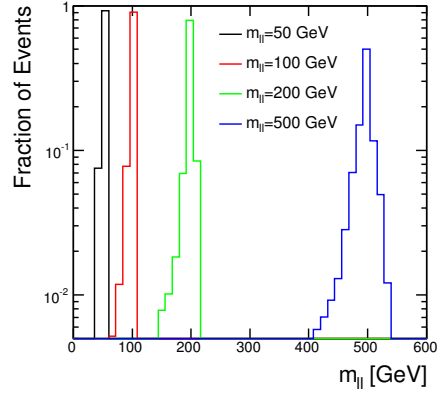


Figure 2.7: In simulated $Z' \rightarrow \chi_1 \chi_2 \rightarrow \ell \ell j j$ events, the distribution of reconstructed invariant $\ell\ell$, jj and $\ell\ell jj$ masses for several values of $m_{Z'}$, m_{χ_1} and m_{χ_2} . The normalization is arbitrary. The shoulder in m_{jj} is due to imperfect selection of the jet pair.

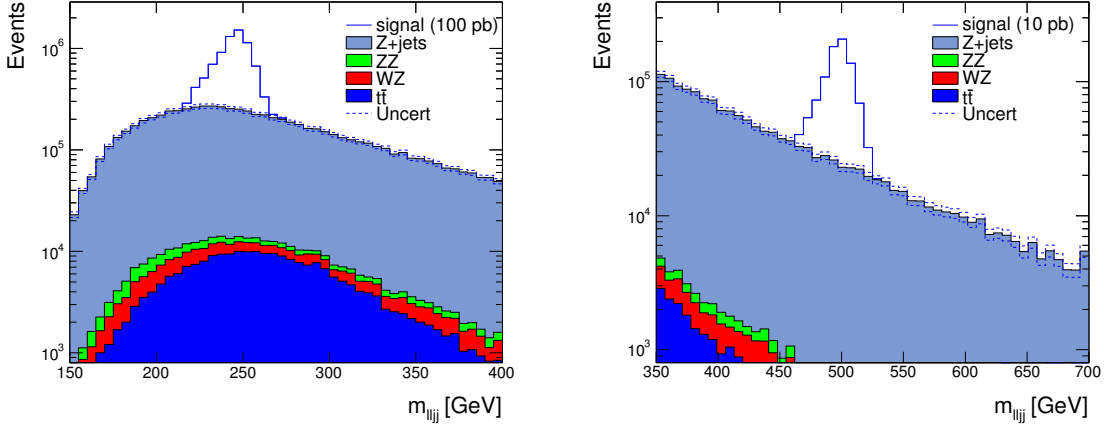


Figure 2.8: In the $(\ell\ell)(jj)$ topology, distribution of $m_{\ell\ell jj}$ in simulated signal and background events for two example mass points, after requirements on $m_{\ell\ell}$ and m_{jj} in pp collisions at $\sqrt{s} = 14$ TeV with $\mathcal{L} = 300 \text{ fb}^{-1}$. Top shows the case of $m_{Z'} = 250$ GeV, $m_{\chi_1, \chi_2} = 100$ GeV; bottom shows the case of $m_{Z'} = 500$ GeV, $m_{\chi_1, \chi_2} = 100$ GeV. In both cases, an arbitrary value of $\sigma(pp \rightarrow Z' \rightarrow \chi_1 \chi_2 \rightarrow \ell\ell jj)$ is assumed.

our 4ℓ final state that contains no intrinsic missing energy. This constraint is stronger than those coming from any other channel. However, as discussed earlier, it is possible that the mixings of the scalars are such that $Z' \rightarrow \chi_1 \bar{\chi}_1$ is forbidden and this strong constraint is avoided; we focus on this possibility here. Both the Tevatron and LHC have searched for $4j$ final states [57–59]. These coloron searches can be recast in terms of our model. Finally, there are bounds on dijet resonances [61–63], though exactly which analysis is strongest depends sensitively on the mass of the Z' boson [36]. Using the constraints on a vector boson of a gauged baryon number, g_B , presented in Ref. [36] our coupling is bounded by $g_{Z'qq} \lesssim g_B/6\sqrt{BF(jj)}$.

In order to compare the limits from all these searches we must assume something about the branching ratios of the Z' . As described earlier, the Z' must minimally decay to $\chi_1 \chi_2$ and jj . Since the 4ℓ mode is so constraining we consider the situation where this mode is forbidden at tree level and further we make the simplifying assumption that branching fractions to $\chi_1 \chi_2$ and $\chi_2 \chi_2$ are equal, with the remaining decay mode being back to dijets. The constraints from the other modes, along with the results of our analysis, on the common

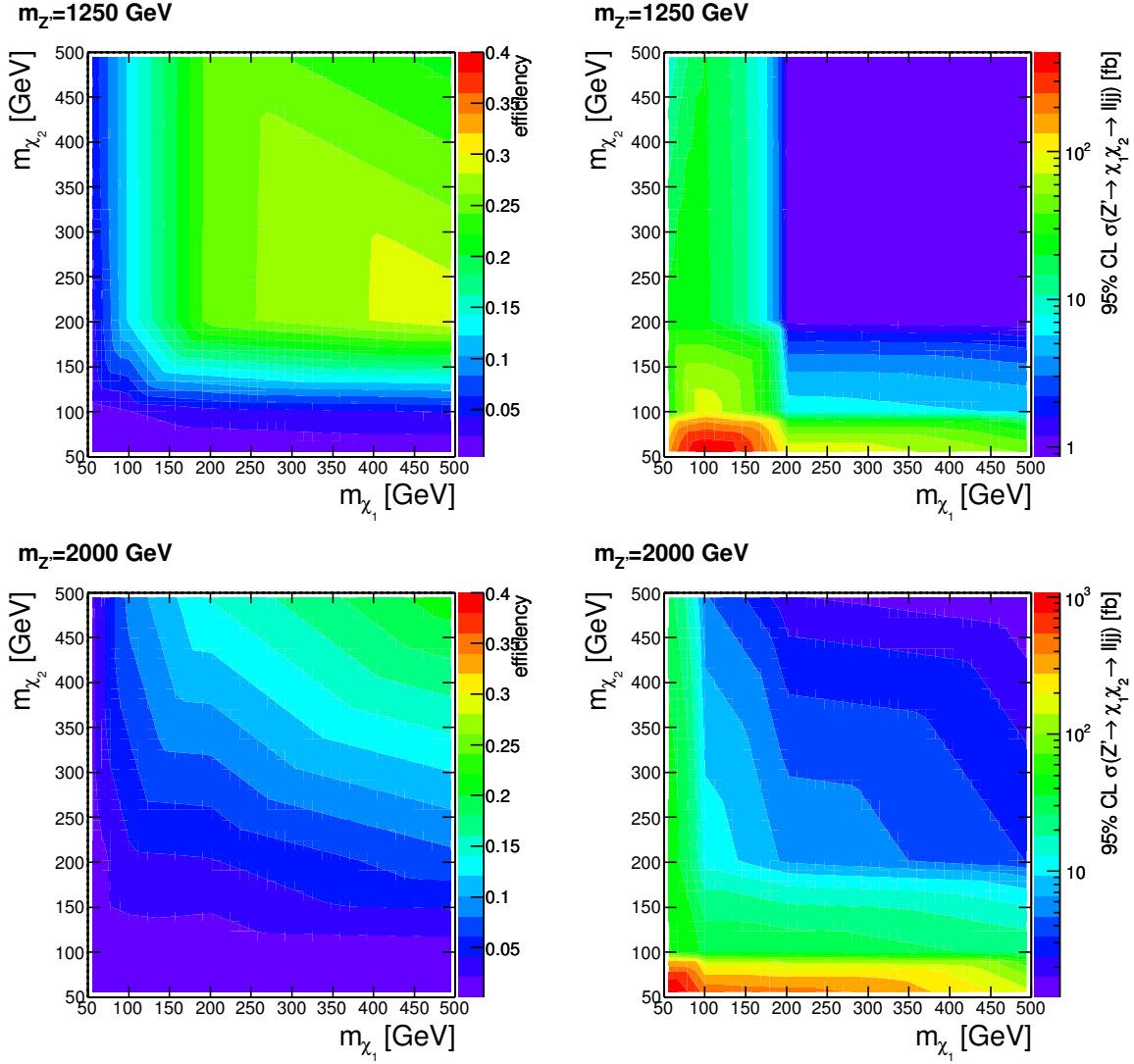


Figure 2.9: In the $(\ell\ell)(jj)$ topology, selection efficiency and expected cross-section upper limits versus m_{χ_1} and m_{χ_2} for several choices of $m_{Z'}$ at $\sqrt{s} = 14$ TeV with $\mathcal{L} = 300 \text{ fb}^{-1}$. For small values of m_{χ_2} , the efficiency is small due to jet p_T requirements and jet resolution effects. For values of m_{χ_1} near $m_{Z'}$, the larger backgrounds lead to weakened limits.

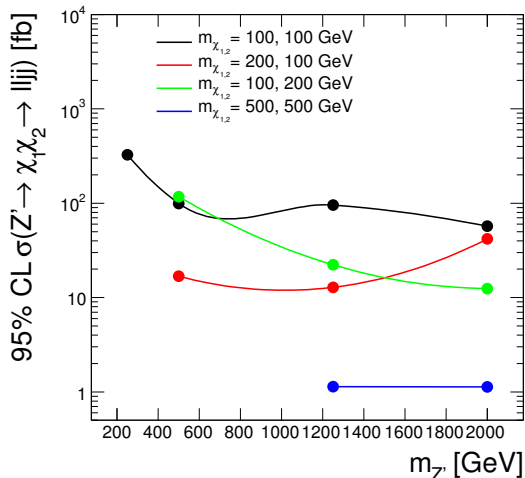


Figure 2.10: In the $(\ell\ell)(jj)$ topology, expected upper limits on the cross section $\sigma(pp \rightarrow Z' \rightarrow \chi_1\chi_2 \rightarrow \ell\ell jj)$ at 95% CL versus $m_{Z'}$ for several choices of m_{χ_1} and m_{χ_2} in pp collisions at $\sqrt{s} = 14$ TeV with $\mathcal{L} = 300 \text{ fb}^{-1}$. The $m_{\chi_{1,2}} = 200, 100$ GeV (red) and $m_{\chi_{1,2}} = 100, 200$ GeV curves have different dependences on $m_{Z'}$ due to the asymmetry in the lepton and jet efficiencies for large values of p_T^χ .

coupling of $g_{Z'}$ are shown in Fig. 2.11 for two different choices of branching fraction.

2.4.2 $\ell(\ell jj)$ topology

Resonance reconstruction in the $\ell(\ell jj)$ topology begins with the identification of the two jets produced in $L \rightarrow \ell jj$ decay. If more than two jets are found in the event, the pair with smallest $\Delta R(j, j)$ are chosen. The lepton with smaller $\Delta R(\ell, jj)$ is chosen to form $m_L = m_{\ell jj}$. The second lepton then completes the system. Examples of reconstructed masses are shown in Fig 2.12.

In addition to the preselection requirements above, we select events with reconstructed mass values close to the true values, $m_{\ell\ell j} \in [m_L - 100, m_L + 50]$, and $m_{\ell jj} \in [m_{Z'} - 250, m_{Z'} + 100]$. The requirement that $m_{\ell\ell} > 120$ GeV suppresses the Z -boson+jets background. Example distributions after $m_{\ell jj}$ and $m_{\ell\ell}$ requirements can be seen for two examples in Fig 2.13. Note that the dominant background, $t\bar{t} \rightarrow \ell\ell jj$ can be controlled by the mixed-flavor $e\mu jj$ final

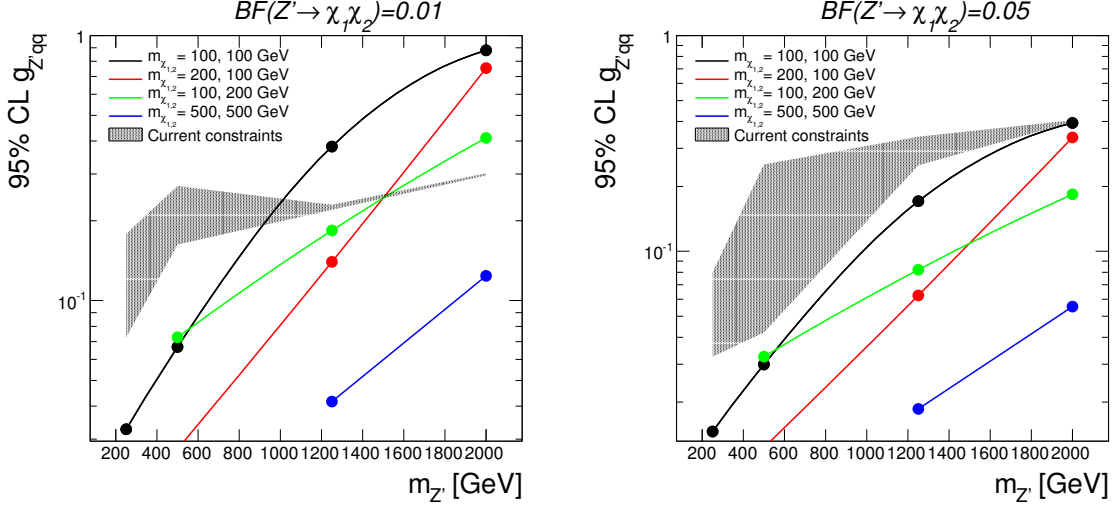


Figure 2.11: Limits on coupling $g_{Z'qq}$ for two choices of $\text{BF}(Z' \rightarrow \chi_1 \chi_2)$. The shaded region shows the current limits on the coupling from other topologies (see text) where the width of the band reflects the variation with assumed m_{χ_1} and m_{χ_2} in pp collisions at $\sqrt{s} = 14$ TeV with $\mathcal{L} = 300 \text{ fb}^{-1}$.

state, or could be further suppressed by the application of a b -jet veto.

Efficiency of the final selection and expected upper limits on $\sigma(pp \rightarrow Z' \rightarrow \ell L \rightarrow \ell(\ell jj))$ can be seen in Fig 2.14.

As mentioned earlier, there are additional constraints coming from both dijet and dilepton decays of the Z' . We use the ATLAS search for a dileptonic resonance, using 20 fb^{-1} of data [60]. The relevant dijet resonance search [61–63] depends upon the mass [36]. All of these constraints are shown together in Fig 2.15, over most of the parameter space considered the analysis outlined above provides the strongest constraint.

2.4.3 $j(j\ell\ell)$ topology

Resonance reconstruction in the $j(j\ell\ell)$ topology begins with the identification of the two leptons produced in $Q \rightarrow j\ell\ell$ decay, for which there are no ambiguities. The jet with smallest $\Delta R(j, \ell\ell)$ is chosen to form $m_Q = m_{j\ell\ell}$, and the jet with largest $\Delta R(j, j\ell\ell)$ is chosen

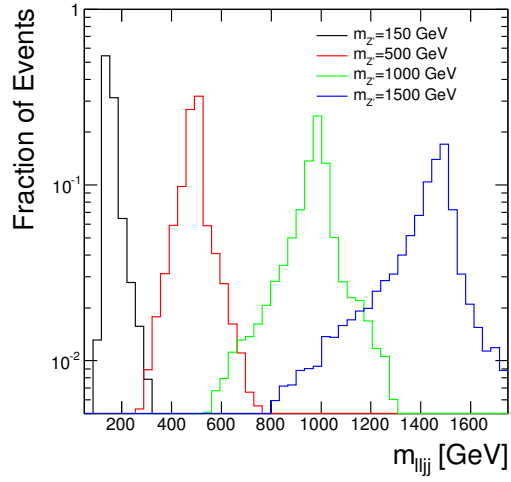
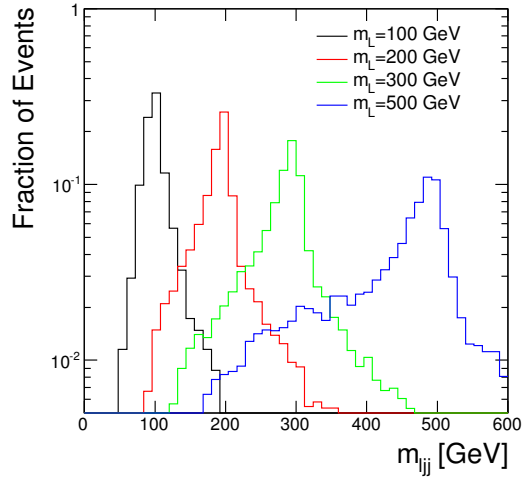


Figure 2.12: In simulated $Z' \rightarrow \ell L \rightarrow \ell l j j$ events, distribution of reconstructed invariant $l j j$ and $\ell l j j$ masses for several values of $m_{Z'}$ and m_L . Normalization is arbitrary.

to form $m_{Z'} = m_{\ell\ell jj}$. Examples of reconstructed masses are shown in Fig 2.16.

In addition to the preselection requirements above, we select events with reconstructed mass values close to the true values, $m_{\ell jj} \in [m_Q - 100, m_Q + 50]$, and $m_{\ell jj} \in [m_{Z'} - 250, m_{Z'} + 100]$. Again, a requirement of $m_{\ell\ell} > 120$ GeV suppresses the Z -boson+jets background. Example distributions after $m_{\ell\ell j}$ and $m_{\ell\ell}$ requirements can be seen for two examples in Fig 2.17. As with the $\ell(\ell jj)$ topology, the dominant background of $t\bar{t}$ could be suppressed further using a b -jet veto and calibrated in data using the $e\mu jj$ sample. The efficiency of the final selection and expected upper limits on $\sigma(pp \rightarrow Z' \rightarrow jQ \rightarrow j(j\ell\ell))$ can be seen in Fig 2.18.

As before there are other search modes for this model in related final states that place constraints on the same couplings. There are constraints coming from dijet decays of the Z' [61–63]. There is a constraint from an ATLAS search for a heavy quark [64], using 1.04 fb^{-1} of 7 TeV data, where the singly produced heavy quark decays to a light quark and a leptonic Z . Finally, there is a very strong constraint from LHC multilepton searches [55, 56] on the pair production of Q where each Q decays to a jet and two leptons. For the points in parameter space where the decay of $Z' \rightarrow Q\bar{Q}$ is kinematically accessible this is the strongest constraint, but if $M_Q > M_{Z'}/2$ the multilepton final state is suppressed by three body phase space and the mode searched for in this study becomes an important constraint. In Fig 2.19 we show the limit on the coupling $g_{Z'qq}$ coming from $j(j\ell\ell)$ as well as the strongest, over all M_Q at each $M_{Z'}$, of these other constraints. Over all of the parameter space considered the heavy quark constraints are weakest, and the analysis described above is stronger than the dijet constraints for much, but not all, of the parameter space. Although the multilepton constraint appears to be the strongest for every Z' mass, it actually only applies for those parameter points where $M_Q < M_{Z'}/2$.

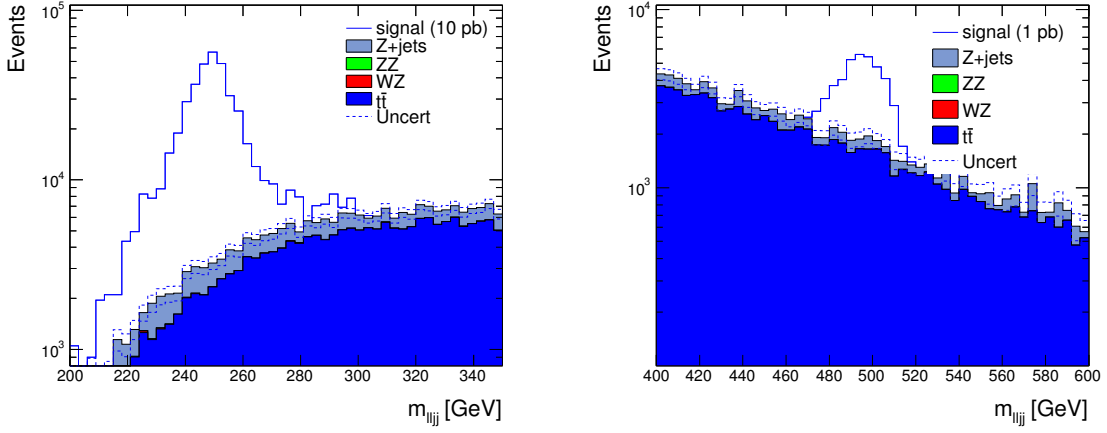


Figure 2.13: In the $\ell(\ell jj)$ topology, the distribution of $m_{\ell\ell jj}$ in signal and background events for two example mass points, after requirements on $m_{\ell jj}$ and $m_{\ell\ell}$ in pp collisions at $\sqrt{s} = 14$ TeV with $\mathcal{L} = 300 \text{ fb}^{-1}$. Left shows the case of $m_{Z'} = 250$ GeV, $m_L = 100$ GeV; right shows the case of $m_{Z'} = 500$ GeV, $m_L = 200$ GeV.

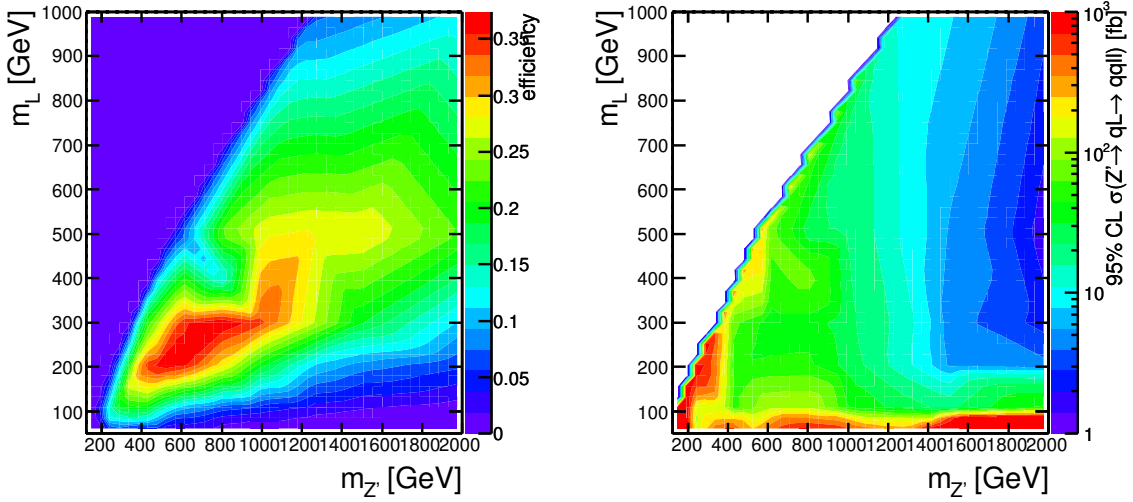


Figure 2.14: In the $\ell(\ell jj)$ topology, selection efficiency and expected cross-section upper limits versus $m_{Z'}$ and m_L at $\sqrt{s} = 14$ TeV with $\mathcal{L} = 300 \text{ fb}^{-1}$. For large $m_{Z'} - m_L$, the efficiency drops due to large transverse momentum of the L , which leads to small opening angles of the L decay products.

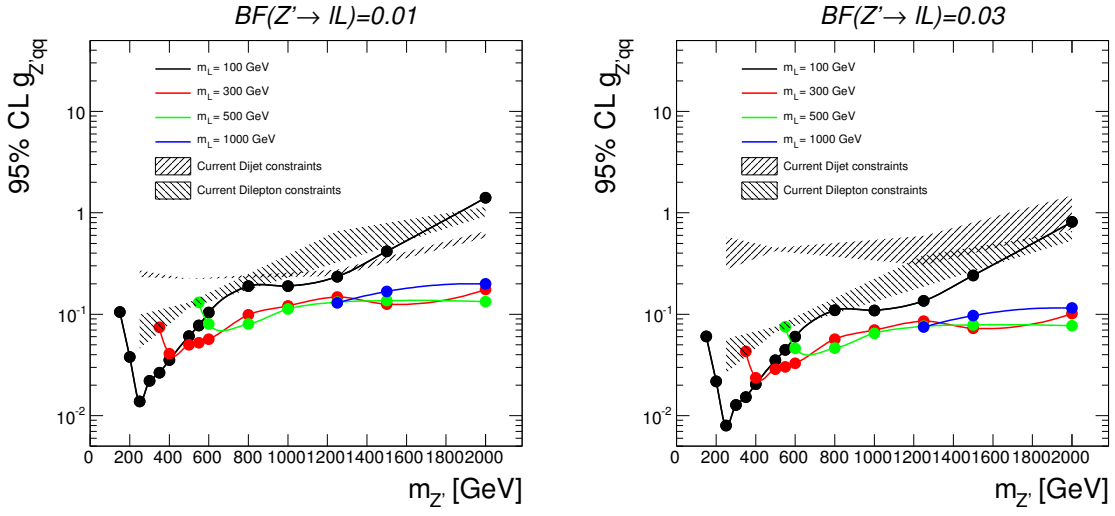


Figure 2.15: In the $\ell(\ell jj)$ topology, expected upper limits on the coupling $g_{Z'gg}$ versus $m_{Z'}$ and m_L for two choices of $BF(Z' \rightarrow \ell L)$ at $\sqrt{s} = 14 \text{ TeV}$ with $\mathcal{L} = 300 \text{ fb}^{-1}$. The shaded region shows the current limits on the coupling from other topologies (see text) where the width of the band reflects the variation with assumed m_L .

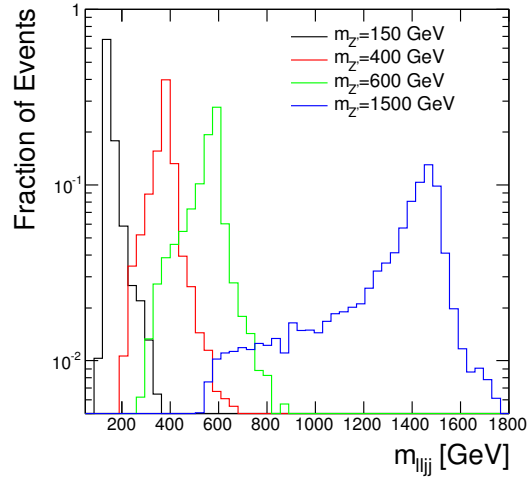
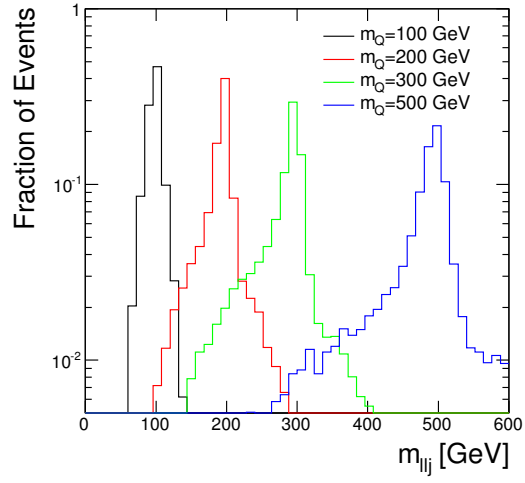


Figure 2.16: In the $j(j\ell\ell)$ topology, distribution of reconstructed invariant $j\ell\ell$ and $\ell\ell jj$ masses for several values of $m_{Z'}$ and m_Q . Normalization is arbitrary.

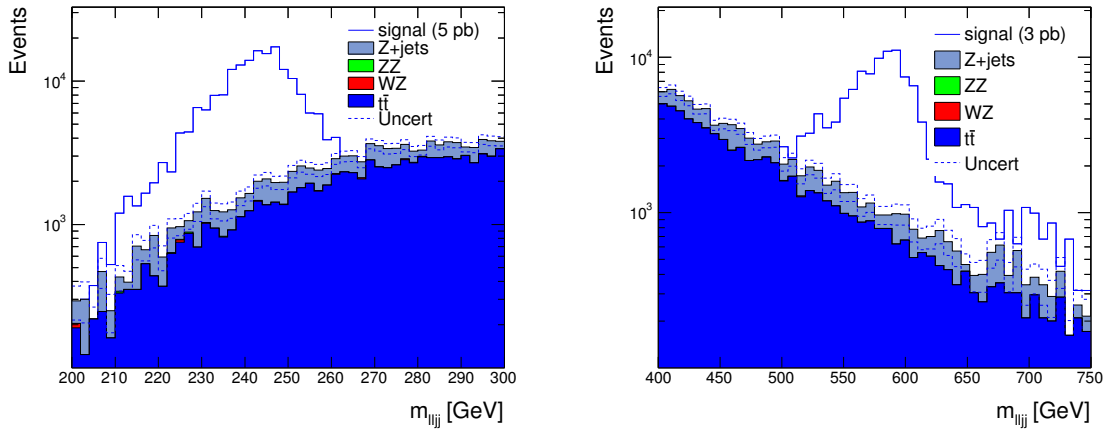


Figure 2.17: In the $j(j\ell\ell)$ topology, distribution of $m_{\ell\ell jj}$ in signal and background events for two example mass points, after requirements on $m_{j\ell\ell}$ and $m_{\ell\ell}$ at $\sqrt{s} = 14$ TeV with $\mathcal{L} = 300 \text{ fb}^{-1}$. Left shows the case of $m_{Z'} = 250$ GeV, $m_Q = 200$ GeV; right shows the case of $m_{Z'} = 600$ GeV, $m_Q = 200$ GeV. In both cases, an arbitrary value of $\sigma(pp \rightarrow Z' \rightarrow qQ \rightarrow jj\ell\ell)$ is assumed.

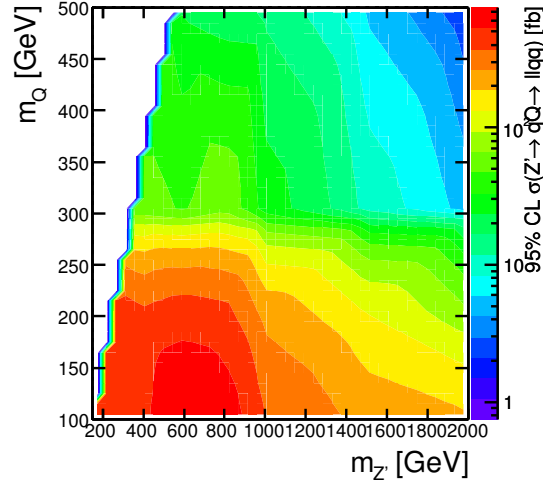
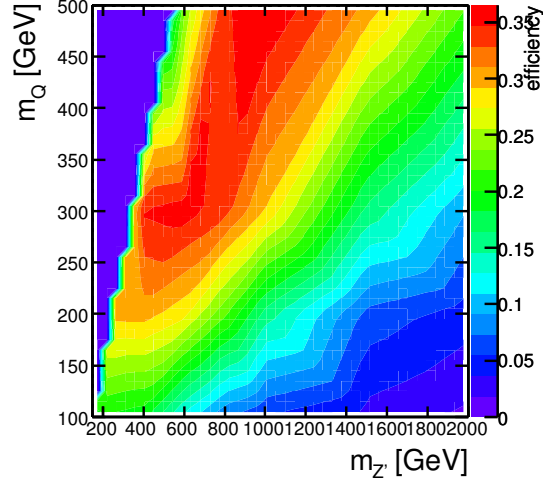


Figure 2.18: In the $j(j\ell\ell)$ topology, selection efficiency (top) and expected cross-section upper limits (bottom) versus $m_{Z'}$ and m_Q at $\sqrt{s} = 14$ TeV with $\mathcal{L} = 300 \text{ fb}^{-1}$. For large $m_{Z'} - m_Q$, the efficiency drops due to large transverse momentum of the Q , which leads to small opening angles of the Q decay products.

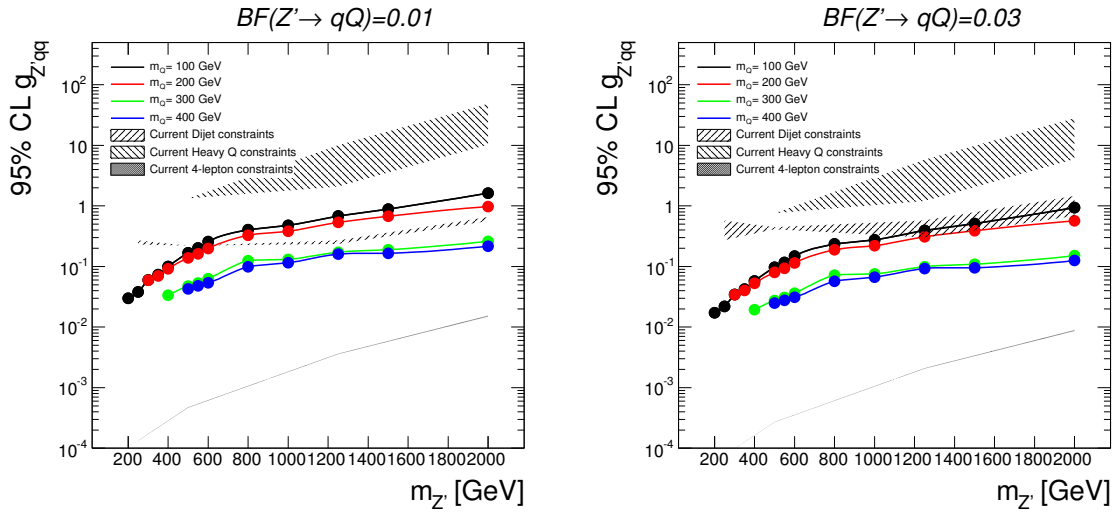


Figure 2.19: Expected upper limits on the coupling $g_{Z'gg}$ versus $m_{Z'}$ and m_Q for two choices of $BF(Z' \rightarrow qQ)$ at $\sqrt{s} = 14 \text{ TeV}$ with $\mathcal{L} = 300 \text{ fb}^{-1}$. The shaded region shows the current limits on the coupling from other topologies (see text) where the width of the band reflects the variation with assumed m_Q .

2.5 Conclusions

We have introduced a new approach, topological models, to systematically search for new physics, which, in the absence of the discovery of a theoretically predicted new particle, can point to new experimental search directions. Like the simplified model approach, we advocate for minimal model descriptions to aid in the search for new phenomena. However, rather than one or two simple models for a given final state, the topological models approach aims to cover the complete space of topologies for a particular final state. By investigating all possible kinematic combinations of final state particles, whether they be motivated by existing models or not, additional discovery potential is unearthed. In addition to the completeness of this approach, the characterization by final state resonance structure helps organize the presentation of experimental results.

As an example, we consider the final state of $\ell\ell jj$. Some of the topologies that have been previously studied have only been analyzed under restrictive assumptions about the resonance masses, we generalize this. Furthermore, we study those topologies, of the five possible, that have not been studied before. We propose analysis techniques and study sensitivity for a 14 TeV LHC with $\mathcal{L} = 300 \text{ fb}^{-1}$. Both this generalization of existing searches and the addition of new topologies, fill in gaps in experimental analyses where there exists potential for discovery. Repeating this procedure on actual LHC data and in more final states can potentially lead to untapped discoveries.

Chapter 3

Searching for spin-3/2 leptons

Based on arXiv:1609.05251 [67]

3.1 Introduction

A major open question in modern particle physics is whether the standard model fermions are fundamental particles, or whether they are composite, such as stable states of more fundamental particles [68] [69] [70] [71] [72].

Such compositeness could be identified by the observation of excited states, which has been studied in depth [73]. Here, we propose an alternative possibility, the existence of vector-like spin-3/2 copies of the standard model fermions, in which the left- and right-handed fermions have identical charges.

In this chapter, we propose such a model, discuss the potential signals at the Large Hadron Collider (LHC) and apply existing LHC data to calculate constraints on the mass of spin-3/2 leptons.

3.2 Theory

We assume that the new spin-3/2 lepton fields are charged identically to the standard model leptons but are vector-like; specifically, the right- and left-handed fields couple identically, for otherwise the model would be heavily constrained by a combination of constraints from electroweak precision data and Higgs boson observables [74]. This still leaves two options: the leptons can be $SU(2)$ doublets, which means they will couple to all electroweak bosons, or $SU(2)$ singlets, which means they will only couple to photons and Z bosons. The doublet model will be the focus of this study due to its richer structure; we will supplement it with effective operators that allow for decays.

The Lagrangian for such a model can be written as:

$$\mathcal{L} = \mathcal{L}_{\text{free}} + \mathcal{L}_{\text{gauge}} + \mathcal{L}_{\text{vector}} \quad (3.1)$$

The first two terms contain the mass and kinetic terms and are given by

$$\mathcal{L}_{\text{free}} + \mathcal{L}_{\text{gauge}} = \epsilon^{\mu\nu\rho\sigma} \bar{L}_\mu^* \gamma_5 \gamma_\sigma D_\nu L_\rho^* + im_L \bar{L}_\mu^* \gamma^{\mu\nu} L_\nu^* \quad (3.2)$$

where D is the covariant derivative, $\gamma^{\mu\nu} \equiv \frac{i}{2}[\gamma^\mu, \gamma^\nu]$, ℓ can be either e , μ , or τ and the $*$ denotes the spin-3/2 leptons. If we expand the derivative term, the free part of the Lagrangian will be

$$\begin{aligned} \mathcal{L}_{\text{free}} = & \epsilon^{\mu\nu\rho\sigma} (\ell_\mu^{*+} \gamma_5 \gamma_\sigma \partial_\nu \ell_\rho^{*-} + \bar{\nu}_{\ell\mu}^* \gamma_5 \gamma_\sigma \partial_\nu \nu_{\ell\rho}^*) \\ & + im_L \ell_\mu^{*+} \gamma^{\mu\nu} \ell_\nu^{*-} + im_L \bar{\nu}_{\ell\mu}^* \gamma^{\mu\nu} \nu_{\ell\nu}^* \end{aligned} \quad (3.3)$$

Note that the charged and neutral components have the same mass (m_L) due to $SU(2)$ gauge invariance. Expanding the covariant derivative we get the interactions with the standard model vector bosons which, after electroweak symmetry breaking, look like

$$\begin{aligned}
\mathcal{L}_{\text{gauge}} &= \epsilon^{\mu\nu\rho\sigma} [2ie_W (W_\nu^+ \bar{\nu}_{\ell\mu}^* \gamma_5 \gamma_\sigma \ell_\rho^{*-} + W_\nu^- \ell_\mu^{*+} \gamma_5 \gamma_\sigma \nu_{\ell\rho}^*) \\
&+ \frac{ie(-\frac{1}{2} + s_W^2)}{s_W c_W} Z_\nu \ell_\mu^{*+} \gamma_5 \gamma_\sigma \ell_\rho^{*-} \\
&+ \frac{ie}{2s_W c_W} Z_\nu \bar{\nu}_{\ell\mu}^* \gamma_5 \gamma_\sigma \nu_{\ell\rho}^* \\
&+ -ieA_\nu \ell_\mu^{*+} \gamma_5 \gamma_\sigma \ell_\rho^{*-}] \tag{3.4}
\end{aligned}$$

where all couplings are well measured electroweak parameters given approximately by

$$\begin{aligned}
e &= \sqrt{4\pi\alpha} \simeq 0.3 \\
e_W &\equiv \frac{e}{s_W 2\sqrt{2}} \simeq 0.2 \\
s_W &\equiv \sin\theta_W \simeq 0.5 \\
c_W &\equiv \cos\theta_W \simeq 0.9
\end{aligned}$$

Next, we move to the effective operators without which the new fields would be stable; note that the charged and neutral components of the new leptons have identical masses. Since the compositeness scale is higher than the electroweak scale, it makes more sense to write down operators that respect the underlying $SU(2)$ symmetry of the theory which reduces the number of allowed terms and parameters. For concreteness and simplicity we will assume only the following effective operators

$$\begin{aligned}
\mathcal{L}_{\text{vector}} &= -\frac{i}{2} \frac{1}{\Lambda_B} B^{\mu\nu} (\bar{L}_\mu^* \gamma_\nu L + \bar{L} \gamma_\nu L_\mu^*) \\
&+ \frac{i}{2} \frac{1}{\Lambda_W} W^{\mu\nu a} (\bar{L}_\mu^* \sigma_a \gamma_\nu L + \bar{L} \sigma_a \gamma_\nu L_\mu^*) \\
&\equiv -\frac{i}{2} g_B B^{\mu\nu} (\bar{L}_\mu^* \gamma_\nu L + \bar{L} \gamma_\nu L_\mu^*) \\
&+ \frac{i}{2} g_W W^{\mu\nu a} (\bar{L}_\mu^* \sigma_a \gamma_\nu L + \bar{L} \sigma_a \gamma_\nu L_\mu^*) \tag{3.5}
\end{aligned}$$

where Λ_B and Λ_W are scales generated by some UV physics to which we are oblivious. Note that we assume a field definition where the off-shell parameters have already been absorbed [75].

Other operators that we could have considered are 4-fermion operators involving both new and standard model fields, in which case the final state leptons are direct decay products of the spin-3/2 fields rather than secondary particles making them easier to detect. Alternatively we could have chosen electroweak symmetry breaking operators that lead to mass splitting between the neutral and charged fields allowing one to decay to the other. We leave an exploration of such possibilities for future work.

3.3 Bounds

Since the new fields are vector-like and do not couple to the Higgs at tree level, their electroweak charge causes no conflict with measurement of S, T, U parameters [76] [77] (or, effectively, the electroweak bosons' self-energy). The effective operators are, in principle, constrained by measurements of the anomalous magnetic moment of charged leptons, especially that of the muon [1]. Such constraints can easily be avoided if the couplings g_B and g_W are sufficiently small. Ensuring that these couplings are small also ensures that the

effective operators do not compete with the gauge interactions in the production of the new fermions. On the other hand, if the couplings are too small the new fields would correspond to particles with long lifetimes and would be severely constrained by long-lived charged particle searches [78] [79] [80]. The range $10^{-9} \text{ GeV}^{-1} < g_B, g_W < 10^{-4} \text{ GeV}^{-1}$ satisfies these requirements and we will assume such values for the remainder of the chapter. We emphasize that the exact values are, for a given ratio of g_B and g_W , unimportant since they modify neither the branching ratios nor the production rate.

Collider bounds on spin-1/2 vector-like leptons are potentially applicable, but the degree to which this statement is true depends heavily on the production and decay modes. For instance, if the production of the new fields is through novel operators [81] then the limits are difficult to recast into our model where we rely on Standard-Model-like electroweak production. We are also not interested in searches for long-lived leptons [78] since we will always assume our fields to decay promptly.

There have been searches for models with production channels identical to ours and with overlapping final states [82] [83]. Such searches could be recast as limits on certain decay channels in our model. However, these particular decay channels may be small depending on our choice of effective couplings, and even in the most ideal scenarios the results could be improved by taking advantage of the additional channels that exist in our model. Moreover, it is possible that the difference in kinematics due to the higher spin are significant enough to alter the limits, so it is worthwhile to study this particular case as an addition to what has already been done in the literature.

3.4 Collider Phenomenology

The production of the new fields is predominantly through Drell-Yan pair production with electroweak gauge bosons as mediators (see Fig. 3.1), and the cross sections are fixed by standard model couplings for a given mass. As explained earlier, the couplings of the effective operators are chosen to be small enough to contribute sub-dominantly to production even at the highest mass considered.

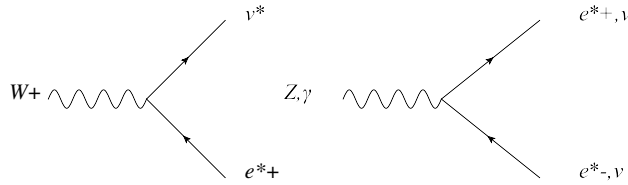


Figure 3.1: Production modes of the spin-3/2 leptons via standard model electroweak bosons.

The pairs that can be produced are $l^{*+}l^{*-}$, $\bar{\nu}_l^* \nu_l^*$, $l^{*+} \nu_l^*$, and $l^{*-} \bar{\nu}_l^*$, with the last two being the most common since W production at the LHC is the larger of the three bosons. As for decays, the effective operators open up a variety of channels. The allowed decays are shown in the table below.

Table 3.1: Allowed decay modes for spin-3/2 leptons ℓ^* and ν^* .

ℓ^{*-}	$Z\ell^-$	$\gamma\ell^-$	$W^-\nu_\ell$	$W^-Z\nu_\ell$	$W^-\gamma\nu_\ell$	$W^+W^-\ell^-$
ν_ℓ^*	$Z\nu_\ell$	$\gamma\nu_\ell$	$W^+\ell^-$	$W^+Z\ell^-$	$W^+\gamma\ell^-$	$W^+W^-\nu_\ell$

By contrived choices of g_W and g_B we can turn off one of the decays in the first two columns. All the other columns depend only on g_W and can only be turned off by setting it to zero, in which case the decays in the first two columns must either be all on or all off. One good feature of this set of decays is that there will always be some visible decay products, even if we produce a pair of spin-3/2 neutrinos.

In this work will limit ourselves to 2-body decays including electron and muons, which results

in promising signals; we leave the photon channels for a future work. We will place the limits on the benchmark points listed in Table 3.2 where the forbidden decay channel is indicated in each case.

Benchmark Point	g_W :	g_B	Forbidden Channels
1	1	1	None
2	c_W	s_W	$\nu^* \rightarrow \gamma\nu$
3	c_W	$-s_W$	$e^* \rightarrow \gamma e$
4	s_W	c_W	$e^* \rightarrow Z\nu$
5	s_W	$-c_W$	$\nu^* \rightarrow Z\nu$
6	0	1	All decays including W's

Table 3.2: The ratios of g_W and g_B and the main decay feature of each benchmark point

3.5 Limits from LHC data

Assuming production via an intermediate electroweak boson and the decays given in Table 3.1, there are ten distinct production modes for the LHC:

$$W \rightarrow \ell^* \nu^* \rightarrow Z\ell Z\nu, W\nu Z\nu, W\nu W\ell, Z\ell W\ell$$

$$Z \rightarrow \ell^* \ell^* \rightarrow Z\ell Z\ell, W\nu W\nu, Z\ell W\nu$$

$$Z \rightarrow \nu^* \nu^* \rightarrow Z\nu Z\nu, Z\nu W\ell, W\ell W\nu$$

which generate final states including many charged leptons, which offer low background rates at the LHC.

We apply selections from the same-sign 2ℓ [84] and 3ℓ [21] searches at ATLAS. We provide a brief summary below of the signal regions considered.

For the 2ℓ search, the final states $e^\pm e^\pm$, $e^\pm \mu^\pm$ and $\mu^\pm \mu^\pm$ are considered in categories defined

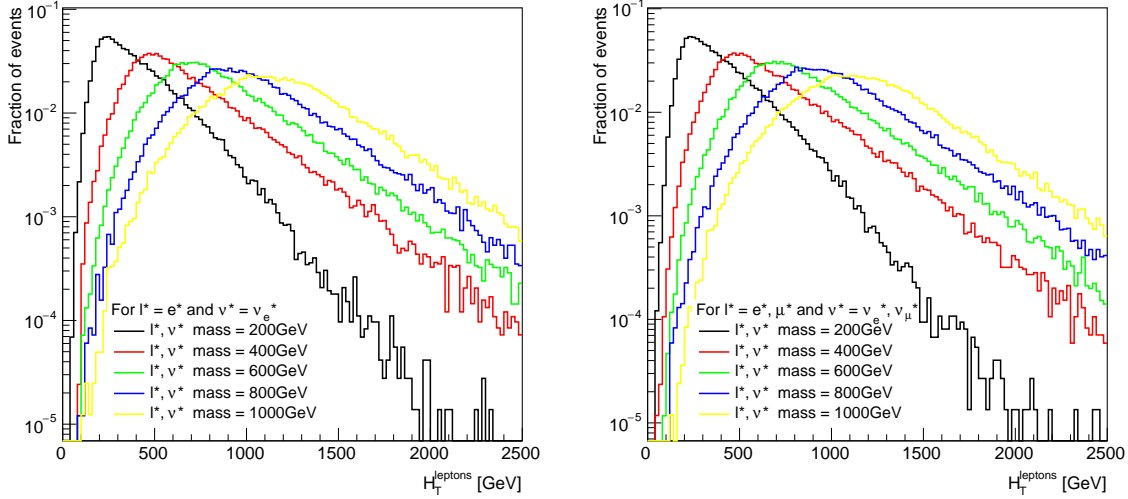


Figure 3.2: Distribution of H_T^{leptons} for simulated spin-3/2 lepton samples; the selection required $H_T^{\text{leptons}} > 500$ GeV. The left pane shows the case where only electrons are considered; the right pane shows the case where electrons and muons are considered.

by the dilepton invariant mass.

For the 3ℓ search, events are classified using the three highest- p_T selected leptons, distinguishing between those that do not contain an opposite-sign same-flavour pair (denoted no-OSSF) and those that do contain an OSSF pair, which are further subdivided into on- Z and off- Z based on the dilepton and three highest- p_T selected leptons invariant mass. For each category, there are several signal regions used to characterize events based on the quantities: H_T^{leptons} , the scalar sum of the transverse momentum p_T of the three leptons used to categorize the event; $p_T^{\ell, \text{min}}$, the minimum transverse momentum p_T of the three leptons used to categorize the event; E_T^{miss} , the missing transverse momentum; m_{eff} , the scalar sum of E_T^{miss} , H_T^{jets} , and the p_T of all identified leptons in the event; and $m_T^W = \sqrt{2p_T^{\ell} E_T^{\text{miss}} (1 - \cos(\Delta\phi))}$, defined only for on- Z events. For the transverse mass, p_T^{ℓ} corresponds to the transverse momentum of the highest- p_T lepton not associated to a Z boson candidate and $\Delta\phi$ is the azimuthal angle between the highest- p_T lepton not associated to a Z boson candidate and the missing transverse momentum E_T^{miss} .

Simulated samples of spin-3/2 leptons were generated with MADGRAPH5 [85] [86] using model files generated through FeynRules [42], and the decays were performed through PYTHIA [87] for a variety of ℓ^* and ν^* masses under two scenarios. First, we consider the simple case in which $\ell^* = e^*$ and $\nu^* = \nu_e^*$; second, we extend to the second generation and allow $\ell^* = e^*, \mu^*$, $\nu^* = \nu_e^*, \nu_\mu^*$. For both, we set $m_{e^*} = m_{\nu_e^*} = m_{\mu^*} = m_{\nu_\mu^*}$. We generated samples of production cross sections and decay widths for a range of masses and combined them according to each of the six coupling benchmarks described in Table 3.2.

From among the signal regions in the two ATLAS searches described above, we choose the SR which gives the most powerful expected limits: $H_T^{\text{leptons}} > 500$ GeV for OSSF off- Z . Distributions of H_T^{leptons} in simulated samples after all selection requirements are made are shown in Fig. 3.2.

According to Ref. [21], the expected backgrounds are 3.7 ± 0.9 events, with one event observed in data. These give expected (observed) limits of 0.26 (0.18) fb on the visible cross section, at 95% confidence level. To calculate limits on the total cross section, we follow the prescription provided in Ref. [21], dividing by the total efficiency as shown Fig. 3.3. Observed and expected limits are shown in Fig. 3.4 and Fig. 3.5, respectively.

3.6 Conclusions

We investigated the sensitivity of existing LHC data to a model of spin-3/2 leptons. Such fields are possible within the context of fermion compositeness which is well studied in the literature. We focused on a scenario where the new fields are dominantly produced by Drell-Yan processes through electroweak bosons and promptly decay through effective operators to electroweak bosons and standard model leptons of the same flavor as the new fields.

We looked at final states resulting in same-sign 2ℓ or 3ℓ and found comparable limits for

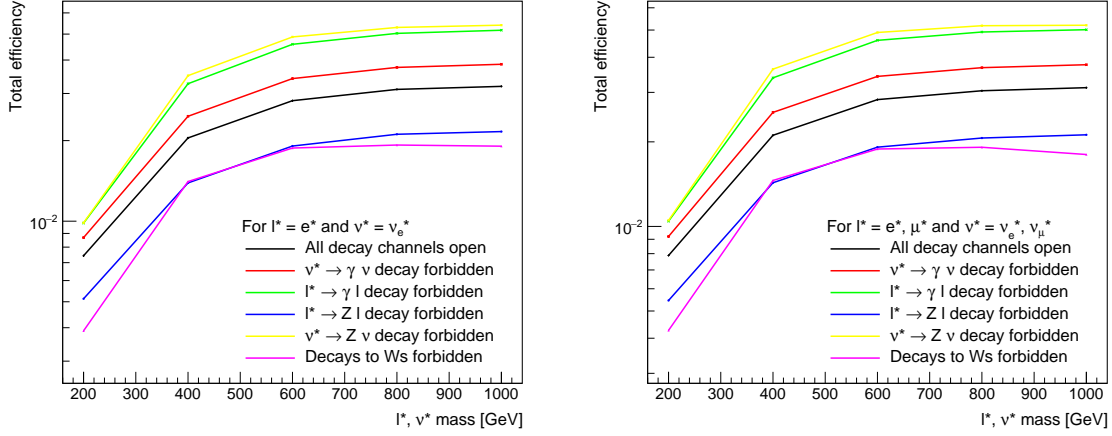


Figure 3.3: Overall efficiency of the selection defined in Ref. [21] which requires $H_T^{\text{leptons}} > 500$ GeV for OSSF off- Z , as a function of the spin-3/2 lepton mass. The left pane shows the case where only electrons are considered; the right pane shows the case where electrons and muons are considered.

each. The new fields are ruled out at the 95% confidence level for masses up to about 560 GeV for one new field with electron flavor, and up to about 620 GeV for two new, mass degenerate fields, one with electron flavor and one with muon flavor. We expect to get more stringent limits if we include the photon channel.

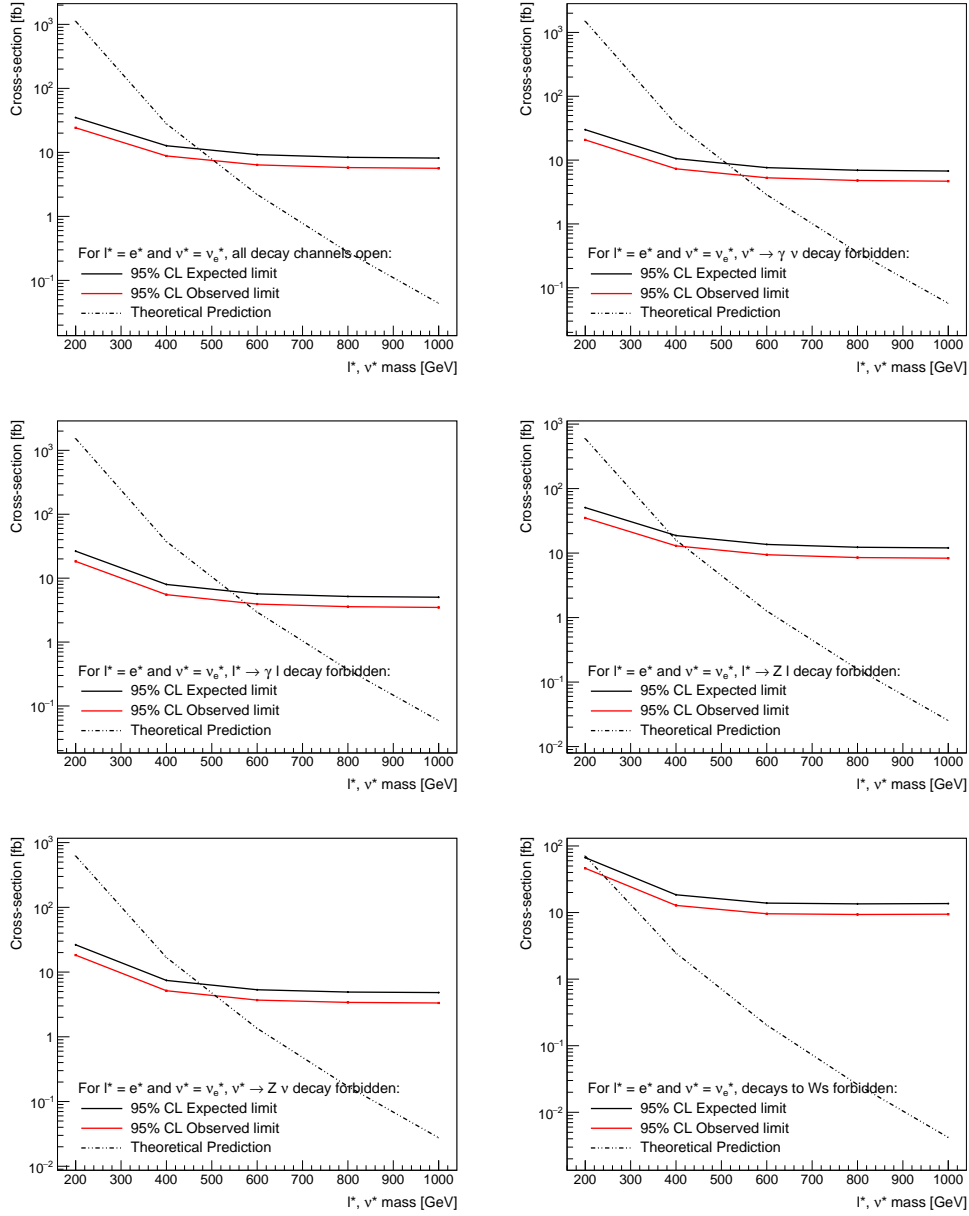


Figure 3.4: Observed and expected limits as a function of ℓ^* and ν^* mass, in the case of $\ell^* = e^*$, $\nu^* = \nu_e^*$

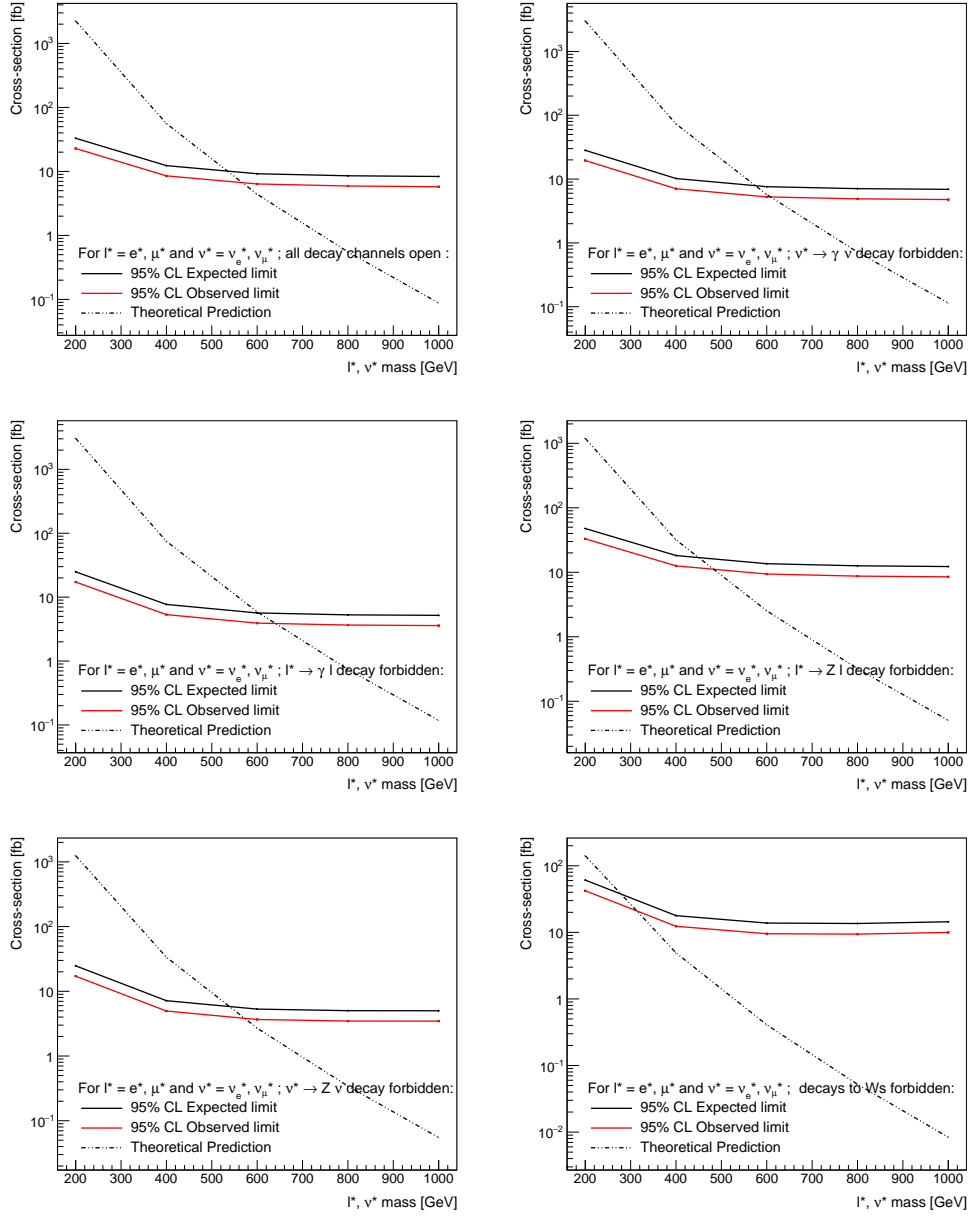


Figure 3.5: Observed and expected limits as a function of ℓ^* and ν^* mass, in the case of $\ell^* = e^*, \mu^*, \nu^* = \nu_e^*, \nu_\mu^*$

Chapter 4

Reviving bino dark matter with vectorlike fourth generation particles

Based on arXiv:1510.06089 [88] and arXiv:1608.00283 [89]

4.1 Introduction

Supersymmetric extensions of the standard model are well-motivated by three promising features that were first identified over three decades ago. First, supersymmetry (SUSY) softens the quadratically-divergent contributions to the Higgs boson mass, reducing the fine-tuning needed to explain the difference between the electroweak scale and the Planck scale [90–93]. Second, the minimal supersymmetric standard model (MSSM) provides the required new field content to improve the unification of gauge couplings [94–97]. And third, with the addition of R -parity, supersymmetric extensions contain stable neutralinos, which are natural candidates for weakly-interacting massive particle (WIMP) dark matter [98,99].

The lack of direct evidence for supersymmetry, particularly after Run I of the LHC, has excluded some supersymmetric models, but not others [100,101], and it remains important

to develop supersymmetric models that continue to have the potential to realize the original motivating promises. In this study, we consider MSSM4G models in which the MSSM is extended to include vector-like copies of standard model particles. These models have been considered previously for their promise of raising the Higgs boson mass to the observed value without extremely heavy superpartners. We will show that these models also restore Bino-like neutralinos as excellent dark matter candidates in a broad range of parameter space that simultaneously preserves gauge coupling unification and satisfies all constraints from new physics searches and Higgs, electroweak, and flavor physics.

In the non-supersymmetric context, the possibility of a 4th generation of fermions has been considered at least since the 3rd generation was discovered. The multiple deaths and rebirths of this idea are nicely summarized in Ref. [74]. Briefly, in the 1990's a 4th generation of *chiral*, or sequential, fermions was severely constrained by precision electroweak measurements at LEP, as parametrized, for example, by the S , T , and U parameters of Peskin and Takeuchi [77, 102]. These constraints excluded degenerate chiral fermions, which have vanishing contributions to T [103], but non-degenerate chiral fermions that contribute to both S and T in a correlated way remained viable [104]. The status of chiral 4th generation fermions changed once again, however, with the advent of Higgs physics at the LHC. Since chiral fermions must get their mass from interactions with the Higgs boson, they contribute to Higgs production through gluon fusion if they are colored and to Higgs diphoton decay if they are electrically charged. These contributions are famously non-decoupling, and current constraints exclude chiral 4th generation fermions up to perturbative values of the Yukawa couplings. Although loopholes still exist, for example, in models with extended Higgs sectors [105], even these possibilities are now severely constrained by the rapid improvements in precision Higgs measurements, and chiral 4th generation fermions are now essentially excluded.

The situation is completely different, however, for *vector-like* 4th generation fermions. They

can be added in any combination, as vector-like fermions do not contribute to anomalies, and they may get masses without coupling to the Higgs boson, so their contributions to Higgs production and decay do decouple, and they may rather easily satisfy bounds from precision Higgs measurements. This also means that they do not contribute to electroweak symmetry breaking effects at leading order, which keeps them safe from precision electroweak constraints. Models with vector-like 4th generation fermions therefore remain viable, and such models have been studied for a variety of reasons [106].

In the context of supersymmetry, the possibility of vector-like 4th generation particles takes on added significance. As is well-known, the measured Higgs boson mass, $m_h = 125.09 \pm 0.21 \pm 0.11$ GeV [107], implies there must be large radiative corrections [108–110]. In the MSSM, this typically requires heavy squarks, which, barring some explanation, strain naturalness. But 4th generation fermions and their scalar superpartners also contribute radiatively to the Higgs boson mass, reducing the need for very heavy superpartners. This was first noted long ago [111, 112] and has gained increasing attention through the years as the lower bound on the Higgs boson mass has grown [113–132]. At the same time, in supersymmetry, 4th generation extensions are highly constrained if one requires that they preserve gauge coupling unification and raise the Higgs mass significantly. These aspects have been discussed at length, for example, in Ref. [115], where the different possibilities for vector-like fermions were explored exhaustively with respect to their ability to increase the Higgs mass, while maintaining gauge coupling unification and avoiding bounds from electroweak precision data.

In this study, we show that, in supersymmetry, vector-like 4th generation particles are also motivated cosmologically. In many well-motivated supersymmetric models, renormalization group evolution or other effects imply that the Bino is the lightest gaugino, and so it is the lightest neutralino in “half” of parameter space (with the Higgsino being the lightest in the rest of parameter space). Pure Bininos do not annihilate to W or Z bosons, and

they annihilate to standard model fermions only through t -channel sfermions. For these annihilation channels to be sufficiently efficient that Binos do not overclose the Universe, Binos must be lighter than about 300 GeV [133, 134]. Such light Binos are now excluded in many cases by results from the LHC. For example, searches for gluino pair production, followed by decays to neutralinos, exclude neutralino masses below 300 GeV, provided the gluinos are lighter than 1.4 TeV and not highly degenerate with the neutralinos [135, 136]. Light neutralinos produced in squark decays are similarly excluded [135, 136]. These bounds have loopholes. For example, if neutralinos are degenerate with staus to within 5%, they co-annihilate in the early Universe and may be as heavy as 600 GeV without overclosing the Universe [137, 138]. Such possibilities are currently viable, and will be probed completely in the upcoming LHC run [139–141]. However, barring such degeneracies and other accidental mass arrangements, Bino dark matter in the MSSM is now significantly constrained.

Here we will show that vector-like copies of 4th (and 5th) generation fermions open up new annihilation channels for the Bino, reducing its thermal relic density to the measured value or below. These new channels are extremely efficient, with even a single 4th generation lepton channel dominating over all MSSM channels combined. Binos are therefore restored as excellent dark matter candidates in regions of parameter space where naturalness is improved, gauge coupling unification is preserved, and all constraints are satisfied. Dark matter in 4th generation supersymmetry models has been discussed previously. In Refs. [16, 142], for instance, 4th generation neutrinos were considered as dark matter candidates. In Refs. [120, 121], neutralinos were shown to be viable dark matter candidates when highly degenerate with co-annihilating sleptons. To our knowledge (and surprise), there are no discussions in the literature of the effects of vector-like 4th generation particles on the thermal relic density of Binos in the generic, non-co-annihilating case, which is the focus of this study.

In the final part of this chapter, we determine the prospects for discovering MSSM4G models at dark matter and collider experiments. The possibility of heavy Binos with the correct

thermal relic density is not realized in the MSSM, and so is not very well studied. As we will see, for direct detection, the scattering of Binors is highly suppressed, first by Yukawa couplings, as is typical of “Higgs-mediated” dark matter candidates, but, second, also by the smallness of the Higgsino component of the dark matter. The predicted cross sections are typically below current bounds, but are above the neutrino floor, making MSSM4G dark matter ideal targets for future searches. In short, direct detection eliminated “ Z models” long ago, are currently exploring “Higgs models,” and will soon probe these “Bino models” on their way to the neutrino floor.

For indirect detection, MSSM4G dark matter annihilates to 4th-generation leptons, which then decay to W , Z , and h bosons and SM leptons. We examine the prospects for detecting these decays through charged particles, neutrinos, and gamma rays, and find particularly promising prospects for future gamma-ray experiments, such as the Cherenkov Telescope Array (CTA), when the 4th-generation leptons are heavy or when they decay to taus.

Last, we examine the prospects for colliders. In contrast to the conclusions for CTA, the LHC is most promising when the 4th-generation leptons are light and decay either to electrons only or muons only. When they are heavy or decay to taus, even the high luminosity LHC with 3 ab^{-1} cannot discover new particles in the parameter region favored by thermal relic density constraints [143]. The LHC and CTA regions of sensitivity are therefore highly complementary. We also consider the prospects for TeV-scale lepton colliders, such as the International Linear Collider (ILC).

The chapter is organized as follows. In Sec. 4.2 we present the particle content, simplifying assumptions, and existing bounds for the 4th generation models we will study. Simply requiring that the vector-like 4th generation particles preserve gauge coupling unification and contribute significantly to the Higgs boson mass reduces the number of models to consider to essentially two. We then examine these two models in detail in Secs. 4.3 and 4.4, where we present our results for the relic density and Higgs mass, respectively. We then consider

discovery signals in direct detection, indirect detection, and colliders in Secs. 4.5, 4.6, and 4.7, respectively, and present our conclusions in 4.8.

4.2 The Model

4.2.1 Particle Content

The standard model, supplemented by right-handed neutrinos, includes quark isodoublets (doublets under the weak isospin $SU(2)$ gauge group) Q , up-type quark isosinglets U , down-type quark isosinglets D , lepton isodoublets L , charged lepton isosinglets E , and neutrino isosinglets N . Beginning with the MSSM, we add vector-like copies of these fermions (and their superpartners). By this we mean adding both left- and right-handed versions of fermions whose $SU(2) \times U(1)_Y$ charges are identical to one of the standard model fermions. As we are only considering vector-like extensions here, as a shorthand, we will list only one of the chiral fields, with the chiral partner implicitly included. Thus, for example, a model with an extra Q (or $\mathbf{5}$) multiplet implicitly also includes its chiral partner \bar{Q} (or $\bar{\mathbf{5}}$).

Gauge anomalies cancel within each vector-like pair, so there is no need to add a full generation at once. This would seem to lead to a Pandora's box of possibilities. However, the number of models to consider may be greatly reduced simply by requiring that the new particles preserve gauge coupling unification and contribute significantly to raising the Higgs boson mass.

To preserve gauge coupling unification, we begin by considering only full $SU(5)$ multiplets, that is, $\mathbf{1}$, $\mathbf{5}$, and $\mathbf{10}$ multiplets. Using 1-loop renormalization group equations (RGEs), the gauge couplings remain perturbative up to the GUT scale with a full vector-like generation of $\mathbf{5} + \mathbf{10}$, but this is not true when 3-loop RGEs are used [115]. Thus, gauge coupling

unification reduces the remaining possibilities to either one **10** multiplet or one, two, or three **5** multiplets (plus any number of singlets).

The **5** multiplets contain D and E fields. To raise the Higgs boson mass, these fields must couple to the Higgs field. The D field would require a Q field, which would bring in an entire **10**, ruining gauge coupling unification. The E field requires only an N , which is consistent with gauge coupling unification. However, as shown in Ref. [115], perturbativity up to the GUT scale requires that lepton Yukawa couplings be at most $h = 0.75$. The contribution of $N_g = 3$ extra generations of leptons/sleptons to the Higgs boson mass scales as $N_g h^4 \lesssim 1$; this is to be compared with the contribution from $N_c = 3$ colors of top quarks/squarks in the MSSM, which scales as $N_c y_t^4 \approx 3$. Extra lepton generations can therefore help raise the Higgs mass to its measured value only if the sleptons have extremely large masses, leading to extra fine-tuning, which defeats one of the primary purposes of adding a 4th generation [115]. This leaves us with only one possibility, adding a **10** and any number of **1s**. The singlets do not impact gauge coupling unification, cannot interact through Yukawa couplings with the Higgs boson in this model, and do not couple to Bino dark matter, and so have no effect; we will therefore omit them. The resulting model, known as the QUE model, is consistent with perturbative gauge coupling unification and can raise the Higgs boson mass through the $H_u Q U$ interaction with a significant Yukawa coupling.

The additional particles in the QUE model are

$$\text{Dirac fermions: } T_4, B_4, t_4, \tau_4 \tag{4.1}$$

$$\text{Complex scalars: } \tilde{T}_{4L}, \tilde{T}_{4R}, \tilde{B}_{4L}, \tilde{B}_{4R}, \tilde{t}_{4L}, \tilde{t}_{4R}, \tilde{\tau}_{4L}, \tilde{\tau}_{4R} , \tag{4.2}$$

where the subscripts 4 denote 4th generation particles, upper- and lower-case letters denote isodoublets and isosinglets, respectively, and L and R denote scalar partners of left- and right-handed fermions, respectively. The SUSY-preserving interactions are specified by the

superpotential

$$W_{\text{QUE}} = M_{Q_4} \hat{Q}_4 \hat{Q}_4 + M_{t_4} \hat{t}_4 \hat{t}_4 + M_{\tau_4} \hat{\tau}_4 \hat{\tau}_4 + k \hat{H}_u \hat{Q}_4 \hat{t}_4 - h \hat{H}_d \hat{Q}_4 \hat{t}_4 , \quad (4.3)$$

where the carets denote superfields, $\hat{Q}_4 = (\hat{T}_4, \hat{B}_4)$ is the quark isodoublet, \hat{t}_4 and $\hat{\tau}_4$ are the quark and lepton isosinglets, and the vector-like masses M_{Q_4} , M_{t_4} , and M_{τ_4} and the Yukawa couplings k and h are all free parameters. We also assume small but non-vanishing mixings of these fields with, say, 3rd generation fields, so that the 4th generation fermions decay and are not cosmologically troublesome. These have relevance for collider physics, but are not significant for the topics discussed here and so are not displayed. Finally, there are the soft SUSY-breaking terms

$$\begin{aligned} \mathcal{L}_{\text{QUE}} = & -m_{\tilde{Q}_4}^2 |\tilde{Q}_4|^2 - m_{\tilde{\bar{Q}}_4}^2 |\tilde{\bar{Q}}_4|^2 - m_{\tilde{t}_4}^2 |\tilde{t}_4|^2 - m_{\tilde{\bar{t}}_4}^2 |\tilde{\bar{t}}_4|^2 - m_{\tilde{\tau}_4}^2 |\tilde{\tau}_4|^2 - m_{\tilde{\bar{\tau}}_4}^2 |\tilde{\bar{\tau}}_4|^2 \\ & - A_{t_4} H_u \tilde{Q}_4 \tilde{t}_4 - A_{b_4} H_d \tilde{\bar{Q}}_4 \tilde{\bar{t}}_4 - B_{Q_4} \tilde{Q}_4 \tilde{\bar{Q}}_4 - B_{t_4} \tilde{t}_4 \tilde{\bar{t}}_4 - B_{\tau_4} \tilde{\tau}_4 \tilde{\bar{\tau}}_4 , \end{aligned} \quad (4.4)$$

where all the coefficients are free, independent parameters.

If one drops the GUT multiplet requirement, there is another possibility consistent with perturbative gauge coupling unification [115]: the QDEE model, with the U of the **10** replaced by a D , and an additional (5th generation) E . This model also (accidentally) preserves gauge coupling unification and raises the Higgs mass through the $H_d Q D$ interaction, and we will include it in our analysis.

With notation similar to that above, the QDEE model has the extra particles

$$\text{Dirac fermions: } T_4, B_4, b_4, \tau_4, \tau_5 \quad (4.5)$$

$$\text{Complex scalars: } \tilde{T}_{4L}, \tilde{T}_{4R}, \tilde{B}_{4L}, \tilde{B}_{4R}, \tilde{b}_{4L}, \tilde{b}_{4R}, \tilde{\tau}_{4L}, \tilde{\tau}_{4R}, \tilde{\tau}_{5L}, \tilde{\tau}_{5R} . \quad (4.6)$$

The superpotential is

$$W_{\text{QDEE}} = M_{Q_4} \hat{Q}_4 \hat{\bar{Q}}_4 + M_{b_4} \hat{b}_4 \hat{\bar{b}}_4 + M_{\tau_4} \hat{\tau}_4 \hat{\bar{\tau}}_4 + M_{\tau_5} \hat{\tau}_5 \hat{\bar{\tau}}_5 + k \hat{H}_u \hat{Q}_4 \hat{\bar{b}}_4 - h \hat{H}_d \hat{Q}_4 \hat{\bar{b}}_4, \quad (4.7)$$

and the soft SUSY-breaking terms are

$$\begin{aligned} \mathcal{L}_{\text{QDEE}} = & -m_{\hat{Q}_4}^2 |\tilde{Q}_4|^2 - m_{\tilde{\bar{Q}}_4}^2 |\tilde{\bar{Q}}_4|^2 - m_{\tilde{b}_4}^2 |\tilde{b}_4|^2 - m_{\tilde{\bar{b}}_4}^2 |\tilde{\bar{b}}_4|^2 - m_{\tilde{\tau}_4}^2 |\tilde{\tau}_4|^2 - m_{\tilde{\bar{\tau}}_4}^2 |\tilde{\bar{\tau}}_4|^2 - m_{\tilde{\tau}_5}^2 |\tilde{\tau}_5|^2 - m_{\tilde{\bar{\tau}}_5}^2 |\tilde{\bar{\tau}}_5|^2 \\ & - A_{t_4} H_u \tilde{Q}_4 \tilde{\bar{b}}_4 - A_{b_4} H_d \tilde{\bar{Q}}_4 \tilde{b}_4 - B_{Q_4} \tilde{Q}_4 \tilde{\bar{Q}}_4 - B_{b_4} \tilde{b}_4 \tilde{\bar{b}}_4 - B_{\tau_4} \tilde{\tau}_4 \tilde{\bar{\tau}}_4 - B_{\tau_5} \tilde{\tau}_5 \tilde{\bar{\tau}}_5. \end{aligned} \quad (4.8)$$

4.2.2 Simplifying Assumptions

Although we have reduced the number of models we consider to two fairly minimal ones, in each model there are still a large number of new parameters. To make progress and present our results, we make a number of simplifying assumptions about the weak-scale values of these parameters.

For both models, we choose the ratio of Higgs vacuum expectation values to be $\tan \beta = 10$, a moderate value that makes the tree-level Higgs mass near its maximal value. To maximize the radiative corrections from the 4th generation quark sector, we fix the up-type Yukawa couplings to be at their quasi-fixed point values: $k = 1.05$ in the QUE model and 1.047 in the QDEE model [115]. The down-type Yukawa couplings h have lower quasi-fixed point values. They can boost the Higgs boson mass if $h < 0$, but their effects are suppressed by $\tan \beta$ and so typically quite subdominant; for simplicity, we set $h = 0$. We also assume $|\mu|$ is sufficiently large that the lightest neutralino is the Bino \tilde{B} . Finally, we choose A -parameters such that there is no left-right squark mixing, that is, $A_{t_4} - \mu \tan \beta = 0$ and $A_{b_4} - \mu \cot \beta = 0$, and assume the 4th generation B -parameters are negligible.

For the QUE model, we assume spectra of the extra fermions and sfermions that can be

specified by 4 parameters: the unified (weak-scale) squark, slepton, quark, and lepton masses

$$m_{\tilde{q}_4} \equiv m_{\tilde{T}_{4L}} = m_{\tilde{T}_{4R}} = m_{\tilde{B}_{4L}} = m_{\tilde{B}_{4R}} = m_{\tilde{t}_{4L}} = m_{\tilde{t}_{4R}} \quad (4.9)$$

$$m_{\tilde{\ell}_4} \equiv m_{\tilde{\tau}_{4L}} = m_{\tilde{\tau}_{4R}} \quad (4.10)$$

$$m_{q_4} \equiv m_{T_4} = m_{B_4} = m_{t_4} \quad (4.11)$$

$$m_{\ell_4} \equiv m_{\tau_4} . \quad (4.12)$$

Strictly speaking, some of these relations cannot be satisfied exactly, as quarks (squarks) that are in the same isodoublet have SU(2)-preserving masses specified by the same parameters, and their physical masses are then split by electroweak symmetry breaking. However, these splittings are small compared to the masses we will consider and so ignoring them will have little impact on our relic density results.

For the QDEE model, we also assume 4 unifying masses

$$m_{\tilde{q}_4} \equiv m_{\tilde{T}_{4L}} = m_{\tilde{T}_{4R}} = m_{\tilde{B}_{4L}} = m_{\tilde{B}_{4R}} = m_{\tilde{b}_{4L}} = m_{\tilde{b}_{4R}} \quad (4.13)$$

$$m_{\tilde{\ell}_4} \equiv m_{\tilde{\tau}_{4L}} = m_{\tilde{\tau}_{4R}} = m_{\tilde{\tau}_{5L}} = m_{\tilde{\tau}_{5R}} \quad (4.14)$$

$$m_{q_4} \equiv m_{T_4} = m_{B_4} = m_{b_4} \quad (4.15)$$

$$m_{\ell_4} \equiv m_{\tau_4} = m_{\tau_5} . \quad (4.16)$$

Finally, for both models, we assume that the Bino is lighter than all squarks and sleptons so that it is the lightest supersymmetric particle (LSP), but heavier than at least some fermions, so that it can annihilate to them and reduce its thermal relic density. For simplicity, we assume the mass ordering

$$m_{\tilde{q}_4}, m_{\tilde{\ell}_4}, m_{q_4} > m_{\tilde{B}} > m_{\ell_4} , \quad (4.17)$$

so that Bininos annihilate to 4th generation leptons, but not 4th generation quarks. As we will see, the addition of the 4th generation lepton channels is enough to reduce the Bino relic

density to allowed levels. This ordering also allows the colored new particles to be heavy enough to avoid LHC bounds.

4.2.3 Existing Bounds

We have included a Higgs-Yukawa term for the vector-like up-type quarks, even though these already have vector-like masses. The motivation, of course, is to induce corrections to the Higgs boson mass. One has to worry, though, that such couplings could violate electroweak constraints. In Ref. [115], however, it is shown that already for 350 GeV vector-like up-type quarks, the contributions to the STU parameters are within the 1σ exclusion contours, and the contributions are even smaller for the heavier masses that yield the correct relic density.

Another reason one might worry about the Higgs terms is constraints from Higgs physics, namely Higgs production and decay through triangle diagrams with fermions in the loop. As mentioned in the introduction, for chiral fermions, the linear relation between the fermion mass and the Higgs Yukawa slows down the decoupling of those triangle diagrams as the fermion mass is increased so that, by the time the experimental constraints are satisfied, the Yukawa coupling are non-perturbative [106]. Adding a vector-like mass makes these triangle diagrams decouple more quickly. However, there are still some limits from the LHC Higgs data, which we take from Ref. [106]. According to their analysis, vector-like quarks of about 1 TeV are (barely) safe from experimental limits. Note however that their fit is based on a model with both up- and down-type isosinglets, so their limits will be weaker when applied to our models, where either the down-type or up-type isosinglet is missing. The authors also perform a fit to the STU parameters that confirms our conclusions based on Ref. [115] that our model is safe.

Last, as noted above, to allow the 4th generation fermions to decay and so satisfy cosmological bounds, we assume that they mix with MSSM fields. In general, the 4th generation fields may

then induce magnetic or electric dipole moments or mediate flavor-violating observables for fermions in the first 3 generations. We will assume that these mixings are minute, however, and dominantly with the 3rd generation, where bounds are weak and easily consistent with the lifetime requirement from cosmology.

4.3 Relic Density

With the assumptions of Sec. 4.2.2, there are now new dark matter annihilation processes: $\tilde{B}\tilde{B} \rightarrow \tau_i^+\tau_i^-$, mediated by t - and u -channel sleptons $\tilde{\tau}_{iL}$ and $\tilde{\tau}_{iR}$, where $i = 4$ for the QUE model and $i = 4, 5$ for the QDEE model. These new channels increase the thermally-averaged annihilation cross section $\langle\sigma v\rangle$, which may reduce the Bino thermal relic density $\Omega_{\tilde{B}}h^2$ to acceptable levels even for large and viable Bino masses.

For the present purposes, it suffices to calculate the relic density using the approximation [144]

$$\Omega_{\tilde{B}}h^2 = 1.07 \times 10^9 \text{ GeV}^{-1} \frac{x_f}{\sqrt{g_*} m_{\text{Pl}} a [1 + b/(2ax_F)]} \quad (4.18)$$

$$x_F = \ln r - \frac{1}{2} \ln(\ln r) + \ln(1 + b/\ln r) \quad (4.19)$$

$$r = 0.038 \frac{g}{\sqrt{g_* m_{\text{Pl}} m_\chi a}}, \quad (4.20)$$

where $x_F = m_{\tilde{B}}/T_F$, the ratio of the dark matter mass to the freezeout temperature T_F , g_* is the number of massless degrees of freedom at freezeout, $g = 2$ is the number of degrees of freedom of the Bino, $m_{\text{Pl}} \simeq 1.22 \times 10^{19}$ GeV is the Planck mass, and a and b are the S - and P -wave cross section coefficients given below. For the parameters of interest here, we find $x_F \approx 24$, and so T_F is between the W and b masses and $g_* \approx 87.25$. The current bound on the dark matter relic density is $\Omega_{\text{DM}}h^2 = 0.1199 \pm 0.0022$ [13]. Equation (4.18) is accurate to 5% [144] or better, and we will require $\Omega_{\tilde{B}}h^2 = 0.12$ to within a fractional accuracy of

10%.

The cross section for $\tilde{B}\tilde{B} \rightarrow f^+f^-$ mediated by t - and u -channel sfermions $\tilde{f}_{L,R}$ with masses $m_{L,R}$ and hypercharges $Y_{L,R}$ is

$$\left. \frac{d\sigma}{d\Omega} \right|_{\text{CM}} = \frac{1}{256\pi^2 s} \sqrt{\frac{s-4m_f^2}{s-4m_{\tilde{B}}^2}} \sum_{i,f} |\mathcal{M}|^2 \quad (4.21)$$

$$\begin{aligned} \sum_{i,f} |\mathcal{M}|^2 &= \frac{1}{4} g_Y^4 Y_L^4 \left[\frac{(m_{\tilde{B}}^2 + m_f^2 - t)^2}{(m_L^2 - t)^2} + \frac{(m_{\tilde{B}}^2 + m_f^2 - u)^2}{(m_L^2 - u)^2} - \frac{2m_{\tilde{B}}^2(s - 2m_f^2)}{(m_L^2 - t)(m_L^2 - u)} \right] \\ &+ \frac{1}{4} g_Y^4 Y_R^4 \left[\frac{(m_{\tilde{B}}^2 + m_f^2 - t)^2}{(m_R^2 - t)^2} + \frac{(m_{\tilde{B}}^2 + m_f^2 - u)^2}{(m_R^2 - u)^2} - \frac{2m_{\tilde{B}}^2(s - 2m_f^2)}{(m_R^2 - t)(m_R^2 - u)} \right] \\ &+ \frac{1}{2} g_Y^4 Y_L^2 Y_R^2 m_f^2 \left[\frac{4m_{\tilde{B}}^2}{(m_L^2 - t)(m_R^2 - t)} + \frac{4m_{\tilde{B}}^2}{(m_L^2 - u)(m_R^2 - u)} \right. \\ &\quad \left. - \frac{s - 2m_{\tilde{B}}^2}{(m_L^2 - t)(m_R^2 - u)} - \frac{s - 2m_{\tilde{B}}^2}{(m_L^2 - u)(m_R^2 - t)} \right], \end{aligned} \quad (4.22)$$

where $g_Y \simeq 0.35$ is the $U(1)_Y$ gauge coupling.

Multiplying this differential cross section by the relative velocity v , expanding in powers of v , integrating over angles, and carrying out the thermal average, we find

$$\langle \sigma v \rangle = a + b x_F^{-1} \quad (4.23)$$

$$a = \frac{g_Y^4 m_f^2}{128\pi m_{\tilde{B}}} \sqrt{m_{\tilde{B}}^2 - m_f^2} \left[\frac{Y_L^4}{\Delta_L^2} + \frac{Y_R^4}{\Delta_R^2} + \frac{2Y_L^2 Y_R^2}{\Delta_L \Delta_R} \right] \quad (4.24)$$

$$b = \frac{g_Y^4}{512\pi m_{\tilde{B}}} \frac{1}{\sqrt{m_{\tilde{B}}^2 - m_f^2}} \left[\frac{Y_L^4}{\Delta_L^4} f_{LL} + \frac{Y_R^4}{\Delta_R^4} f_{RR} + \frac{Y_L^2 Y_R^2}{\Delta_L \Delta_R} m_f^2 f_{LR} \right], \quad (4.25)$$

where

$$\begin{aligned}
f_{LL,RR} &= 13m_f^8 + m_f^6 (-26m_{L,R}^2 - 36m_{\tilde{B}}^2) + m_f^4 (70m_{L,R}^2 m_{\tilde{B}}^2 + 13m_{L,R}^4 + 49m_{\tilde{B}}^4) \\
&\quad + m_f^2 (-44m_{L,R}^2 m_{\tilde{B}}^4 - 26m_{L,R}^4 m_{\tilde{B}}^2 - 42m_{\tilde{B}}^6) + 16 (m_{L,R}^4 m_{\tilde{B}}^4 + m_{\tilde{B}}^8) \quad (4.26)
\end{aligned}$$

$$\begin{aligned}
f_{LR} &= (18m_f^2 - 12m_{\tilde{B}}^2) \\
&\quad + \frac{8(m_{\tilde{B}}^2 - m_f^2)}{\Delta_L^2 \Delta_R^2} [-3m_f^8 + m_f^6 (8m_{\tilde{B}}^2 + 6m_L^2 + 6m_R^2) \\
&\quad + m_f^4 (-6m_{\tilde{B}}^4 - 17m_L^2 m_{\tilde{B}}^2 - 3m_L^4 - 17m_R^2 m_{\tilde{B}}^2 - 3m_R^4 - 12m_L^2 m_R^2) \\
&\quad + m_f^2 (6m_L^4 m_R^2 + 7m_L^4 m_{\tilde{B}}^2 + 16m_L^2 m_{\tilde{B}}^4 \\
&\quad + 6m_R^4 m_L^2 + 7m_R^4 m_{\tilde{B}}^2 + 16m_R^2 m_{\tilde{B}}^4 + 30m_L^2 m_R^2 m_{\tilde{B}}^2) \\
&\quad + m_{\tilde{B}}^8 - 5m_L^2 m_{\tilde{B}}^6 - 4m_L^4 m_{\tilde{B}}^4 - 9m_L^2 m_R^4 m_{\tilde{B}}^2 \\
&\quad - 5m_R^2 m_{\tilde{B}}^6 - 4m_R^4 m_{\tilde{B}}^4 - 9m_R^2 m_L^4 m_{\tilde{B}}^2 - 3m_L^4 m_R^4 - 18m_L^2 m_R^2 m_{\tilde{B}}^4] , \quad (4.27)
\end{aligned}$$

and $\Delta_{L,R} = m_{\tilde{B}}^2 + m_{L,R}^2 - m_f^2$.

Equations (4.23)–(4.27) are valid for sfermions with different masses and hypercharges. For degenerate vector-like sfermions with $m_{\tilde{f}} \equiv m_L = m_R$ and $Y_V \equiv Y_L = Y_R$, the cross section coefficients simplify to

$$a = \frac{g_Y^4 Y_V^4 m_f^2}{32\pi m_{\tilde{B}}} \frac{\sqrt{m_{\tilde{B}}^2 - m_f^2}}{(m_{\tilde{B}}^2 + m_f^2 - m_f^2)^2} \quad (4.28)$$

$$\begin{aligned}
b &= \frac{g_Y^4 Y_V^4}{128\pi m_{\tilde{B}}} \frac{1}{\sqrt{m_{\tilde{B}}^2 - m_f^2} (m_{\tilde{B}}^2 + m_f^2 - m_f^2)^4} \times \\
&\quad \left[17m_f^8 - 2m_f^6 (17m_{\tilde{f}}^2 + 20m_{\tilde{B}}^2) + m_f^4 (86m_{\tilde{B}}^2 m_{\tilde{f}}^2 + 17m_{\tilde{f}}^4 + 37m_{\tilde{B}}^4) \right. \\
&\quad \left. - 2m_f^2 (26m_{\tilde{B}}^4 m_{\tilde{f}}^2 + 11m_{\tilde{B}}^2 m_{\tilde{f}}^4 + 11m_{\tilde{B}}^6) + 8m_{\tilde{B}}^4 (m_{\tilde{f}}^4 + m_{\tilde{B}}^4) \right] . \quad (4.29)
\end{aligned}$$

The expansion in v assumes that v is the only small parameter. This is not true when f and \tilde{B} become degenerate and the annihilation is near threshold. In this limit, the expressions for

b in Eqs. (4.27) and (4.29) become singular, signaling the breakdown of the expansion. The expansion is essentially an expansion in even powers of $\alpha = v/\sqrt{1 - (m_f/m_{\tilde{B}})^2}$. Requiring that the next omitted (D -wave) term be less than a 10% correction implies roughly $\alpha^4 < 0.1$. For characteristic velocities of $v \sim 0.3$ at freezeout, this implies $m_f < 0.85m_{\tilde{B}}$. The case of near-threshold annihilation was considered in Ref. [134], where it was shown in a generic setting that corrections to $\langle\sigma v\rangle$ above the few percent level may occur if $m_f > 0.95m_{\tilde{B}}$. There, alternative expressions valid in the degenerate limit were derived. Here, as we are primarily interested in the cosmologically preferred regions without accidental mass degeneracies, we will use Eqs. (4.28) and (4.29) and simply take care to avoid applying these cross section formulae to cases where the dark matter and final state fermion are in the degenerate region. We note also that an expression for $\langle\sigma v\rangle$ was presented in Ref. [133] for degenerate sfermions. The expressions there differ from our result in Eq. (4.23) with $m_L = m_R$, but the disagreement is numerically small and at most at the 5% level.

The annihilation cross section has some interesting features. First, hypercharge enters to the fourth power. Isosinglet leptons have the largest hypercharge of any MSSM fields. As we show below, the squarks need to be above a TeV to achieve the correct Higgs mass. But leptons and sleptons can be relatively light. As a result, annihilation to leptons is particularly efficient, and it is fortunate that they exist in both the QUE and QDEE models. Note also that because the fermions are vector-like, there is no chiral suppression. This differs greatly from the MSSM, where annihilations to isosinglet leptons are hypercharge-enhanced, but extremely suppressed by the chiral suppression of the S -wave cross section, since all MSSM leptons are light. In both the QUE and QDEE models, there are heavy isosinglet leptons, and annihilation to them is neither hypercharge- nor chirality-suppressed. Annihilations to 4th generation particles therefore completely dominate over MSSM channels.

In Fig. 4.1, we show regions of the $(m_{\tilde{\ell}_4}, m_{\tilde{B}})$ plane, with m_{ℓ_4} fixed to the values indicated, where Bino dark matter freezes out with a relic density within 10% of the value required to

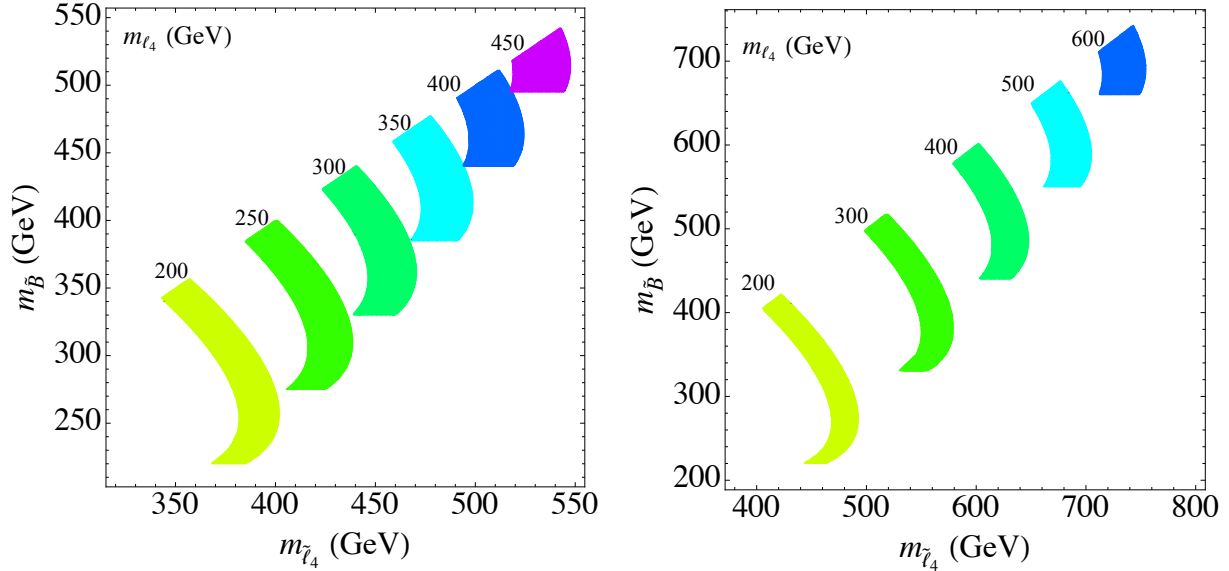


Figure 4.1: Cosmologically preferred regions in the $(m_{\tilde{\ell}_4}, m_{\tilde{B}})$ plane for the QUE (left) and QDEE (right) models. In each shaded region, the relic density is in the preferred range $\Omega_{\tilde{B}} h^2 = 0.12 \pm 0.012$ for the value of m_{ℓ_4} indicated.

be all of dark matter. These regions are bounded on all sides. We must require the mass ordering $m_{\ell_4} < m_{\tilde{B}} < m_{\tilde{\ell}_4}$ so that the Binos are the LSPs, but may pair-annihilate to 4th generation leptons. The mass of ℓ_4 is bounded from below by heavy lepton searches. As this mass is increased, the Bino and slepton masses must also increase to maintain the mass ordering. As the masses increase, however, the annihilation cross section $\langle\sigma v\rangle$ decreases, and at some point the thermal relic density of Binos is too large, providing an upper bound on all of these masses. To guarantee that the velocity expansion is reliable in the regions shown in Fig. 4.1, we have required $m_{\ell_4} < 1.1m_{\tilde{B}}$. We have not included co-annihilation, which would be important for Binos and sleptons that are degenerate to more than 5%.

Without co-annihilation, the largest possible masses are about $m_{\ell_4} = 470$ GeV in the QUE model and 670 GeV in the QDEE model. To see this upper bound more clearly, in Fig. 4.2 we plot the relic density bands in the $(m_{\tilde{\ell}_4}, m_{\ell_4})$ plane for fixed $m_{\tilde{B}} = 1.2m_{\ell_4}$. Larger masses are allowed in the QDEE model, because there are two new annihilation channels, and since $\langle\sigma v\rangle \sim m^{-2}$, the upper bound on the masses is larger by roughly a factor of $\sqrt{2}$.

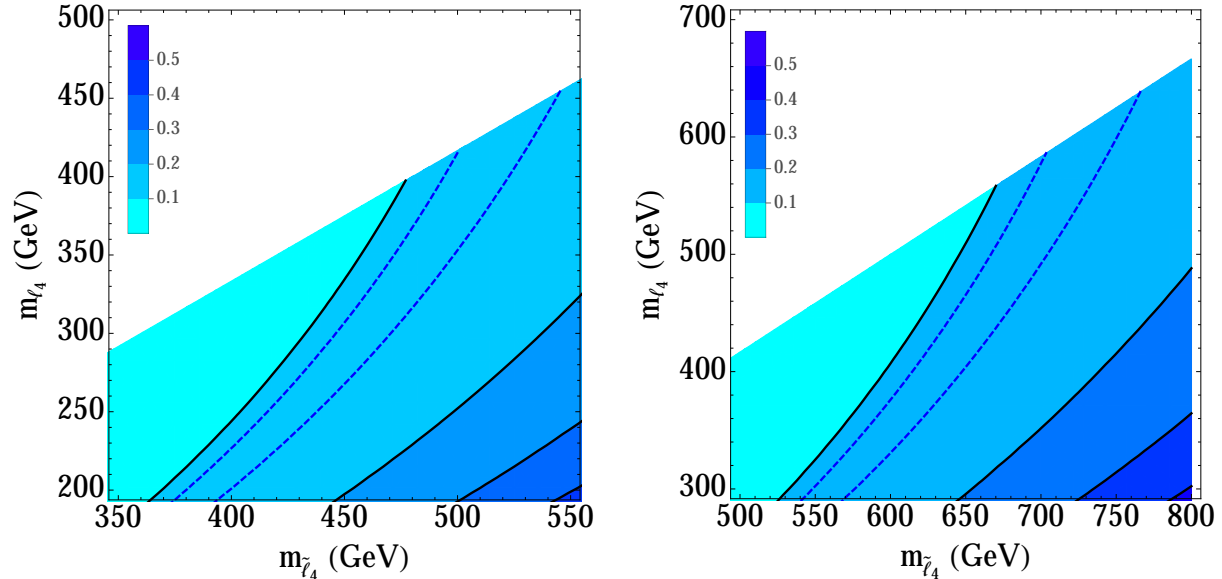


Figure 4.2: Contours of constant relic density $\Omega_{\tilde{B}} h^2$ for the QUE (left) and QDEE (right) models in the $(m_{\tilde{l}_4}, m_{\ell_4})$ plane with fixed $m_{\tilde{B}} = 1.2m_{\ell_4}$. Between the dashed lines $\Omega_{\tilde{B}} h^2 = 0.12 \pm 0.012$.

In Figs. 4.1 and 4.2 we have completely neglected the MSSM annihilation channels; including them would only move the preferred regions to slightly lower masses. For the reasons mentioned above, vector-like 4th generation particles are extremely efficient channels for annihilation and completely dominate the MSSM contributions in the case of Bino dark matter. As a result, the cosmologically-preferred Bino masses are significantly higher than in the MSSM and completely eliminate the tension between the relic density constraints and current LHC bounds on neutralino masses.

4.4 Higgs Boson Mass

In the MSSM, the Higgs boson mass is maximally the Z boson mass $M_Z = 91$ GeV at tree level, but is raised by radiative corrections, dominantly from the diagrams with top quarks and squarks in loop. Up to 2-loop corrections, assuming no left-right stop mixing, the Higgs

boson mass is [145]

$$m_h^2 = M_Z^2 \cos^2 2\beta \left(1 - \frac{3}{8\pi^2} \frac{m_t^2}{v^2} t \right) + \frac{3}{4\pi^2} \frac{m_t^4}{v^2} \left[t + \frac{1}{16\pi^2} \left(\frac{3}{2} \frac{m_t^2}{v^2} - 32\pi\alpha_3 \right) t^2 \right], \quad (4.30)$$

where

$$t = \ln \frac{M_{\tilde{t}}^2}{M_t^2} \quad (4.31)$$

$$m_t = \frac{M_t}{1 + \frac{4}{3\pi}\alpha_3(M_t)} \quad (4.32)$$

$$\alpha_3 = \frac{\alpha_3(M_Z)}{1 + \frac{b_3}{4\pi}\alpha_3(M_Z) \ln(M_t^2/M_Z^2)} \quad (4.33)$$

$$b_3 = 11 - 2N_f/3 = 7, \quad (4.34)$$

$M_t = 174$ GeV is the top quark mass, $M_{\tilde{t}}$ characterizes the masses of the left- and right-handed top squarks, $v = 174$ GeV is the Higgs vacuum expectation value, $\alpha_3(M_Z) = 0.118$ is the strong gauge coupling at the Z pole, and b_3 is the beta coefficient for the strong coupling in the MSSM without the top quark and any extra matter. For $\tan\beta = 10$, the tree-level mass is near its maximal value, but even with top squark masses $M_{\tilde{t}} = 2$ TeV, the Higgs mass is only 115 GeV, far short of the measured value of 125 GeV.

With the addition of vector-like quarks, however, this mass can be significantly increased. The contribution from a vector-like 4th generation of top quarks and squarks is [114, 115]

$$\Delta m_h^2 = \frac{N_c v^2}{4\pi^2} (k \sin\beta)^4 f(x), \quad (4.35)$$

where $N_c = 3$ is the number of colors, k is the up-type Yukawa coupling in Eqs. (4.3) and (4.7), and

$$f(x) = \ln x - \frac{1}{6} \left(5 - \frac{1}{x} \right) \left(1 - \frac{1}{x} \right) \quad (4.36)$$

$$x = \frac{m_{\tilde{q}_4}}{m_{q_4}}. \quad (4.37)$$

As a reminder, m_{q_4} and $m_{\bar{q}_4}$ are the physical masses of the 4th generation quarks and squarks, respectively, and we set k at its quasi-fixed point value $k = 1.05$ and neglect the 4th generation down-type Yukawa h . Note that we are also neglecting 2-loop contributions from vector-like matter, since those contributions are small for $m_{q_4}, m_{\bar{q}_4} \gg m_h$ [115].

We can see from Eq. (4.35) that the 4th generation contribution to the Higgs boson mass is maximal when q_4 is as light as possible. In Fig. 4.3 we show contours of the Higgs mass in the $(m_{\tilde{t}_4}, m_{\tilde{t}})$ plane for fixed $m_{t_4} = 1$ TeV. This choice of m_{t_4} is based partly on the ~ 700 GeV limit on chiral 4th generation up-type quarks [103] and partly on the STU and Higgs constraints mentioned earlier. We see that, with the addition of 4th generation tops, the correct Higgs mass can be achieved for a range of $m_{\tilde{t}_4}$ and $m_{\tilde{t}}$ where both are below 3 TeV and discoverable at future runs of the LHC. One can see from Eq. (4.35) that the corrections from the vector-like matter are functions of $x = m_{\tilde{t}_4}/m_{t_4}$. One can use this to reinterpret Fig. 4.3 as determining the required ratio x to get the correct mass. For example, for m_{t_4} between 1 and 2 TeV, the correct Higgs boson mass can be obtained as long as x is between 2.5 and 2.

4.5 Direct Detection of Dark Matter

In both the QUE and QDEE models, the lightest neutralino \tilde{B} may interact strongly enough with nuclear matter to be detected by current or future direct detection experiments. We explore this possibility for both spin-independent (SI) and spin-dependent (SD) direct detection. In Sec. 4.5.1 we discuss the qualitative behavior we expect, given an approximate analytic expression for the effective couplings between neutralinos and nucleons, which is derived in Appendix B. In Secs. 4.5.2 and 4.5.3 we use the MICROMEAS package to calculate the SI and SD cross sections for a wide range of parameter space and compare these predictions against current and future experimental sensitivities.

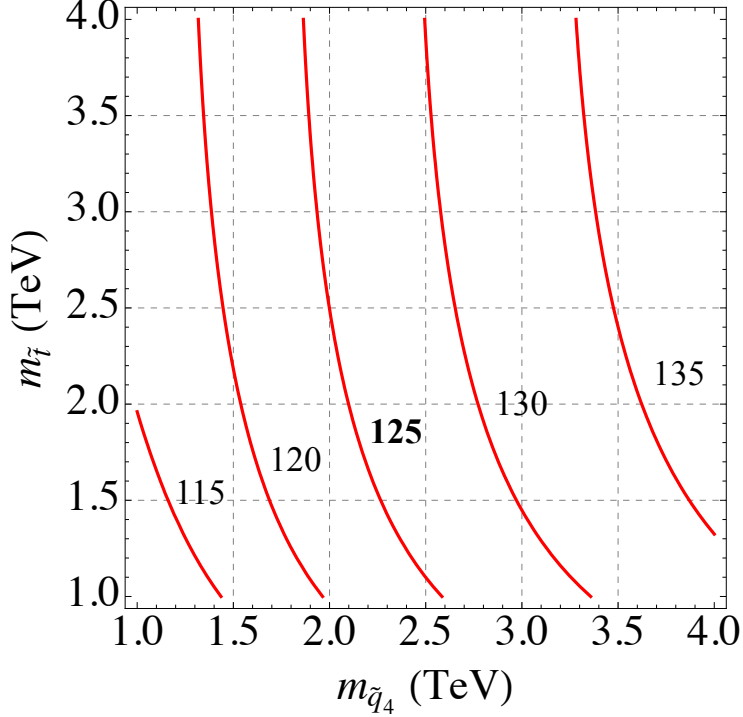


Figure 4.3: Contours of constant Higgs boson mass (in GeV) in the $(m_{\tilde{q}_4}, m_{\tilde{t}})$ plane, assuming no left-right squark mixings, for fixed $m_{t_4} = 1$ TeV.

4.5.1 Effective Neutralino–Nucleon Coupling

Interactions between Bino dark matter and the nucleons of a particle detector are primarily mediated by t -channel scalar Higgses, h^0 and H^0 , or by s -channel squarks, \tilde{q}_i . As a result, the QUE and QDEE have nearly identical direct detection prospects: the contribution from the 4th-generation quarks is limited to $\tilde{B}\tilde{B}gg$ interactions mediated by heavy squark/quark loops, which we neglect.

The non-observation of squarks at the LHC suggests that their masses are significantly larger than the Higgs mass. SI squark-mediated scattering is proportional to left–right squark mixing angles, which are highly suppressed by quark masses for the most relevant quarks, namely those of the first and second generation. For $\mathcal{O}(\text{TeV})$ squark masses we find that the SI cross section is dominated by Higgs-mediated scattering, despite the associated suppression by Yukawa couplings and the small Higgsino fraction of the neutralino. In

Appendix B we derive a simple expression for the effective neutralino–nucleon coupling for Bino-like neutralinos, in the limit of large squark masses and moderate-to-large values of $\tan\beta$ ($5 \leq \tan\beta \leq 50$). The main results are given in this section.

The differential cross section for dark matter scattering from a nucleus with mass number A and charge Z is [146]

$$\frac{d\sigma}{d|\vec{q}|^2} = \frac{1}{\pi v^2} [Z f_p + (A - Z) f_n]^2 F^2(Q) , \quad (4.38)$$

where \vec{q} is the momentum transferred in the interaction; v is the velocity of the dark matter; f_p and f_n are the effective couplings to protons and neutrons, respectively; and $F(Q)$ is the nuclear form factor, where Q is the energy transfer. In our model, f_p and f_n tend to be approximately equal.

When all the squarks and the heavy neutral Higgs boson are significantly heavier than the light Higgs boson with mass $m_h = 125$ GeV and $\tan\beta$ is moderate or large, the couplings of the dark matter are approximately

$$\frac{f_{p,n}}{m_p} \approx N_{41} [N_{21} - N_{11} \tan\theta_W] \frac{g^2}{4m_W m_h^2} \left[f_{Td} - f_{Tu} + f_{Ts} - \frac{2}{27} f_{TG} \right] , \quad (4.39)$$

where the coefficients N_{j1} are the components of the neutralino dark matter in the gauge basis $\{\tilde{B}, \tilde{W}, \tilde{H}_d, \tilde{H}_u\}$, θ_W is the weak mixing angle, and f_{Tq} and f_{TG} parameterize the quark and gluon content of the nucleon. For Bino-like dark matter, $N_{11} \sim 1$, and the other coefficients are suppressed by powers of M_1/μ . Expanding for large $|\mu|$, we find

$$\frac{f_{p,n}}{m_p} = \frac{M_1 m_Z \tan\theta_W \sin\theta_W}{\mu^2 - M_1^2 + m_Z^2 \sin^2\theta_W} \left(\frac{g^2}{4m_W m_h^2} \right) \left[f_{Td} - f_{Tu} + f_{Ts} - \frac{2}{27} f_{TG} \right] . \quad (4.40)$$

Values for f_{Tu} and f_{Td} can be obtained from pion-nucleon scattering; f_{Ts} is found more precisely from lattice calculations. The sum $f_{TG} + \sum_{u,d,s} f_{Tq} = 1$ determines f_{TG} . In

MICROMEGAS, the following values are used for f_{Tq} [147]:

$$f_{Tu}^{(p)} = 0.0153, \quad f_{Td}^{(p)} = 0.0191, \quad f_{Tu}^{(n)} = 0.011, \quad f_{Td}^{(n)} = 0.0273, \quad f_{Ts}^{(n,p)} = 0.0447. \quad (4.41)$$

The value for f_{Ts} agrees with recent lattice calculations [148], which find $f_{Ts} = 0.053 \pm 0.011 \pm 0.016$ (see also Ref. [149]). There are much larger discrepancies in the published values for f_{Tu} and f_{Td} . In Refs. [150,151], it is suggested that $f_{Tu} \approx 0.02$ and $f_{Td} \approx 0.04$. The combination that appears in the direct detection amplitude is therefore $f_{Td} - f_{Tu} + f_{Ts} - \frac{2}{27}f_{TG} \simeq -0.007$ in MICROMEGAS, but one should bear in mind that, because of large cancellations, this is subject to $\mathcal{O}(1)$ uncertainties.

Equation (4.40) displays the m_h^{-2} dependence common to all Higgs-mediated processes, which have cross sections that are currently being explored at direct detection experiments. At the same time, the $M_1 m_Z / \mu^2$ prefactor signals a further suppression from the Bino-ness of the neutralino dark matter. This implies that cross sections in this scenario are expected to be significantly smaller than in other models with Higgs-mediated interactions. It is particularly interesting to see whether these cross sections stay above the neutrino floor, and also how they depend on $|\mu|$, which is often taken as a simple indication of the naturalness of a SUSY model. To explore these issues, we now turn to a numerical analysis of the direct detection cross section.

4.5.2 Spin-Independent Cross Sections

We use the package MICROMEGAS [147, 152] to calculate the particle spectrum and to evaluate the direct detection cross sections. The 4th-generation squarks add small corrections to the MSSM cross section through box and triangle diagrams that induce couplings of the neutralinos to the gluon content of the nucleons: however, if the squark masses $m_{\tilde{q}_4}$ are sufficiently larger than $m_\chi + m_{q_4}$, where m_χ is the dark matter mass, then these correc-

Parameter	Minimum	Maximum	Parameter	Minimum	Maximum
M_1	200 GeV	700 GeV	$m_{\tilde{d}}, m_{\tilde{u}}$	1.2 TeV	4.0 TeV
μ	$M_1 + 20$ GeV	12.8 TeV	$m_{\tilde{s}}, m_{\tilde{c}}$	1.2 TeV	4.0 TeV
m_A	0.8 TeV	10 TeV	$m_{\tilde{b}}$	0.9 TeV	4.0 TeV
$\tan\beta$	5	50	$m_{\tilde{t}}$	0.9 TeV	4.0 TeV

Table 4.1: List of relevant parameters to the direct detection cross section, and the ranges used for our MICROMEAS calculation.

tions can be safely ignored. In this region of parameter space, the MSSM model used by MICROMEAS needs no alteration to accurately estimate the direct detection cross section.

We determine the SI cross section at several thousand randomly-selected points in parameter space, within the ranges shown in Table 4.1. The 3rd-generation squark mixing is turned off by fixing $A_t - \mu \cot\beta = 0$ and $A_b - \mu \tan\beta = 0$, as in the fourth generation. We fix the gaugino masses to the unification ratios $M_1 : M_2 : M_3 = 1 : 2 : 7$, and we consider the range $200 \text{ GeV} < M_1 < 700 \text{ GeV}$.

With these parameters, there is always a choice of 4th-generation parameters that can give the correct thermal relic density. Since these 4th-generation parameters do not enter the direct detection cross sections, the impact of restricting our models to those with the correct thermal relic density is simply that it restricts the mass range to $200 \text{ GeV} < M_1 < 540 \text{ GeV}$ for QUE models, while the entire range $200 \text{ GeV} < M_1 < 700 \text{ GeV}$ is accessible for QDEE models. Note that the parameter scan does include values of m_A and $\tan\beta$ for which resonance annihilation effects are important and our calculation of the relic density is not reliable. However, such points only make up a small fraction of the parameter space and we have checked that excluding them does not significantly alter the the direct detection results shown below.

In Fig. 4.4, we show the relationship between the SI cross section and the Bino, Wino, and Higgsino composition of the neutralino dark matter. The cross section predicted by Eq. (4.40) is plotted along with the MICROMEAS results; we see that the analytic approximation is

an excellent approximation for many of the models. Smaller values of $|\mu|$, when the Higgsino fractions are largest, correspond to the largest direct detection cross sections. The width of the bands in Fig. 4.4 is due to the variation of the squark and neutralino masses, and the variation in $\tan\beta$. These effects combine to change the cross section by $\mathcal{O}(1)$ factors, which are quite small compared to the five orders of magnitude explored by varying N_{41}^2 .

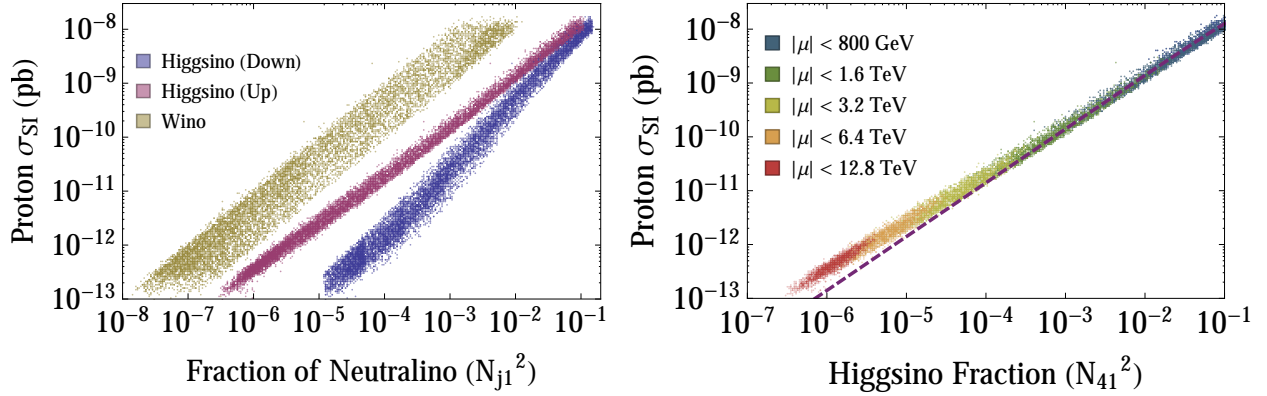


Figure 4.4: Left: For MSSM4G models, the correlation of the neutralino dark matter’s \tilde{W} , \tilde{H}_d , and \tilde{H}_u fractions with the SI proton scattering cross section $\sigma_{\text{SI}}^{(p)}$. Right: For MSSM4G models, the correlation of the neutralino dark matter’s \tilde{H}_u fraction with $\sigma_{\text{SI}}^{(p)}$, color-coded by the value of $|\mu|$ for each model point. The dashed line represents the analytic approximation for the cross section given in Eq. (4.40). In both panels, points in each scatter plot represent QUE and QDEE MSSM4G models that have 125 GeV Higgs bosons, are consistent with all collider bounds, and have the thermal relic density $\Omega_{\text{DM}}h^2 = 0.12 \pm 0.012$.

In Fig. 4.5 we compare our theoretical predictions to the current experimental bounds from LUX [22] and the projected 2 ton-year sensitivity of Xenon1T [24], as well as several other future experiments. The current LUX results exclude all of the MSSM4G models generated with $|\mu| < 500$ GeV. For heavier m_χ , models with larger values of $|\mu| \approx 700$ GeV can be ruled out. For larger $|\mu| \gtrsim 1$ TeV the cross sections are suppressed, as expected, and for $|\mu| \gtrsim 6$ TeV, the cross section drops below the floor from coherent neutrino scattering [153]. Of course, absent a quantitative theory relating the μ -parameter to the SUSY-breaking parameters, such large values of $|\mu|$ require large fine-tuning to obtain the observed weak scale and are typically judged unnatural.

To summarize, then, for extremely low or high values of $|\mu|$, direct detection cross sections are either excluded or below the neutrino floor, but for a large intermediate region with $500 \text{ GeV} < |\mu| < 6 \text{ TeV}$, MSSM4G theories with the correct thermal relic density predict SI scattering cross sections that are not yet excluded, but will be tested by future experiments as they improve their sensitivity down to the neutrino floor.

4.5.3 Spin-Dependent Cross Sections

Although the SD direct detection cross section is generally larger than the SI cross section, it is much more difficult to probe experimentally, as the SD cross section does not scale directly with the mass of the nuclei. As a result, current bounds on the neutron SD cross section are less stringent by a factor of 10^6 .

We use MICROMEGAS to predict the proton and neutron SD cross sections for the same range of models considered in Section 4.5.2. As in the SI case, the proton and neutron have similar SD cross sections. It requires different experimental techniques to measure the two cross sections, and several experiments, including PICO-2L [154], PICO-60 [31], and IceCube [32] probe only the proton SD cross section.

In Fig. 4.6, the theoretical predictions and experimental bounds are plotted together for the proton and neutron SD cross sections. The models shown in the two scatter plots are the same set shown in Fig. 4.5, although the models with $|\mu| > 6.4 \text{ TeV}$ are not shown here.

Of the existing limits from XENON 100 [28], LUX [29], PICO [31], and IceCube [32], only IceCube sets any constraint on the MSSM4G. The limits from IceCube assume that the dark matter annihilates in the Sun to produce either $\tau^+\tau^-$, W^+W^- , or $b\bar{b}$. In the QUE and QDEE models, Bino annihilation produces taus and W bosons indirectly as decay products of 4th- (or 5th-) generation leptons. As a result, the observed τ^\pm or W^\pm will carry only a

fraction of the initial energy, and IceCube becomes somewhat less sensitive to the MSSM4G. In Fig. 4.6, we make the approximation that the energy of the τ^\pm or W^\pm reconstructs only half of the Bino mass. This shifts the published limits from IceCube to higher masses by a factor of two.

Future experiments such as LZ [29], Xenon1T and DARWIN [30] are projected to probe MSSM4G models with $0.4 \text{ TeV} < |\mu| \lesssim 1 \text{ TeV}$. However, Fig. 4.5 shows that the same experiments will put much more stringent bounds on the SI cross section. Of the models that could be discovered by future SD experiments, almost all of them have already been ruled out by LUX. The SI cross section is a much more promising test of MSSM4G models.

4.6 Indirect Detection of Dark Matter

One of the primary features of MSSM4G models is that the dark matter has new annihilation channels in the early Universe. Barring the highly degenerate case where these annihilations are kinematically forbidden in the late Universe, these annihilations then contribute to indirect detection signals. Indeed, the Binos can annihilate to τ_4 pairs in the QUE model (and to both τ_4 and τ_5 pairs in the QDEE model), which then decay to SM particles.

The decays of the new leptons arise from the Yukawa mixings with their SM counterparts. These mixings imply decays to $W\nu_\ell$, $Z\ell$ or $h\ell$ where $\ell = e, \mu, \text{ or } \tau$. It is reasonable to expect that decays to one of the first three generations will dominate, and in this study, we will analyze the special cases where the mixing is purely to one of the three SM lepton generations. We will label the respective cases as “ e -mixing”, “ μ -mixing”, and “ τ -mixing”, after the SM lepton with which $\tau_{4,(5)}$ mixes.

The partial decay widths of vector-like leptons are [143]

$$\begin{aligned}
\Gamma(\tau_{4,5} \rightarrow W\nu_\ell) &= \frac{\epsilon^2}{32\pi} m_{\tau_{4,5}} r_W (1 - r_W)^2 (2 + 1/r_W) , \\
\Gamma(\tau_{4,5} \rightarrow Z\ell) &= \frac{\epsilon^2}{64\pi} m_{\tau_{4,5}} r_Z (1 - r_Z)^2 (2 + 1/r_Z) , \\
\Gamma(\tau_{4,5} \rightarrow h\ell) &= \frac{\epsilon^2}{64\pi} m_{\tau_{4,5}} (1 - r_h)^2 ,
\end{aligned}
\tag{4.42}$$

where m_W , m_Z , and m_h are the W , Z , and Higgs boson masses, respectively; $r_X = m_X^2/m_{\tau_{4,5}}^2$ for $X = W, Z, h$; $\ell = e, \mu, \tau$; and ϵ parameterizes the mixing between the SM leptons and the new leptons. Note that the ϵ dependence drops out when calculating the branching ratios. In the limit where $m_{\tau_{4,5}} \gg m_W, m_Z, m_h$, the branching ratios satisfy $B(W\nu_\ell):B(Z\ell):B(h\ell) = 50\%:25\%:25\%$, which is already almost the case for $m_{\tau_{4,5}} = 200$ GeV.

In the following subsections, we consider the prospects for the indirect detection of dark matter in MSSM4G models through gamma rays, neutrinos, and positrons.

4.6.1 Gamma Rays

Experiments such as Fermi-LAT, H.E.S.S. II, and CTA can search for high-energy photons from the dark matter annihilation in the Galactic Center or in dwarf spheroidal Milky Way satellite galaxies.

In the τ -mixing case, all the decay products (except for neutrinos) have sizable branching ratios to hadrons, resulting in π^0 decays that produce a significant excess of gamma rays that may be observed above astrophysical backgrounds. On the other hand, in the μ -mixing and e -mixing cases, although hadronic decays of the W , Z , and h bosons result in gamma rays, the μ and e lead to much weaker gamma-ray signals.

Various experimental collaborations provide current or projected sensitivities to the dark matter annihilation cross section to W^+W^- or $\tau^+\tau^-$. We have also analyzed the gamma-ray

signal from annihilation to $\mu^+\mu^-$, but the resulting bounds are very weak and we therefore omit them in this study.

In the experimental bounds it is assumed that the dark matter annihilates directly to the SM fields, and so their energies are equal to the dark matter mass. In our case the dark matter annihilates to 4th- or 5th-generation leptons, which then decay to SM fields, resulting in a distribution of final state energies. To test our model against these results we make two assumptions. First, we treat all bosons (W, Z , and h) to be the same and compare the total rate of their production to the limit on the W^+W^- channel. This is a reasonable approximation since all three have comparable masses and branching ratios to hadrons. Second, we use the average of possible final state energies to compare with the limits. To a good approximation, this average energy is simply $\bar{E} = m_{\tilde{B}}/2$. This is justified by the observation that the energy distribution of the decay products is fairly uniform for non-relativistic mother particles and the fact that the experimental sensitivities are fairly constant as functions of the dark matter mass for the range of masses we are considering. In the following we will consider the sensitivities to the W^+W^- and $\tau^+\tau^-$ channels separately. In a more thorough analysis, one would combine these results, resulting in greater sensitivity or more stringent limits.

Given the smallness of the dark matter velocity in the late Universe, the thermally-averaged cross section is dominated by the S -wave piece. The only relevant process is the annihilation to fermions through sfermion exchange which, assuming the left- and right-handed sfermions are degenerate, is given by

$$\langle\sigma v\rangle = \frac{g_Y^4 Y_L^2 Y_R^2 m_f^2}{32\pi m_{\tilde{B}}} \frac{\sqrt{m_{\tilde{B}}^2 - m_f^2}}{\left(m_{\tilde{B}}^2 + m_f^2 - m_f^2\right)^2}, \quad (4.43)$$

where $g_Y \simeq 0.35$ is the $U(1)_Y$ gauge coupling, Y_L and Y_R are the left and right hypercharges respectively (in the convention where $Q = T_3 + Y/2$), m_f is the fermion mass, $m_{\tilde{f}}$ is the

sfermion mass, and $m_{\tilde{B}}$ is the Bino mass. One can see that even the top quark contribution, enhanced by the factor m_f^2 , is suppressed compared to the $\tau_{4,5}$ contribution by a factor of $(\frac{1}{3}\frac{4}{3})^2/(2^2)^2 = 1/81$ and we therefore neglect the SM contributions.

For presentation purposes we want to reduce the number of independent masses appearing in Eq. (4.43). To maximize the Bino mass, we set $m_{\tilde{B}} = 1.2 m_{\tau_{4,5}}$ so it is close to the fermion mass, but far enough away that the velocity expansion gives accurate results. The sfermion masses $m_{\tilde{\tau}_{4,5}}$ are then constrained by the requirement of correct relic density which is measured to be $\Omega_{\text{DM}}h^2 = 0.1199 \pm 0.0022$ [13]. In the QDEE model $m_{\tau_4} = m_{\tau_5}$ and $m_{\tilde{\tau}_4} = m_{\tilde{\tau}_5}$ are assumed in this study.

The theoretical predictions are shown in Fig. 4.7 for the QUE and QDEE models along with current and future experimental sensitivities. The green strips contain the predictions for MSSM4G models with the correct thermal relic density to 10%. These strips can be extended to lower masses, although these values are less interesting in light of collider bounds on BinOs. On the other hand, extending the strip to higher masses would re-introduce the overclosure problem of Bino dark matter.

There are two things to note when comparing the theory predictions with the published experimental sensitivities. First, as mentioned above, the energy of our final state particles is roughly half of the dark matter mass, which means the experimental bounds have twice the mass reach. Second, the $\tau_{4,5}$ leptons decay to $h\tau$ and $Z\tau$ only half of the time, which reduces the annihilation cross section limit by a factor of two compared to the more common case where the dark matter annihilates directly to taus.

The strongest current limits come from a combined analysis of MAGIC and Fermi-LAT observations of dwarf spheroidal satellite galaxies [155]. The limits are barely at the threshold of probing our model and are not expected to improve much in the future. H.E.S.S. II is expected to announce limits that are slightly stronger, but still fairly weak.

CTA, on the other hand, has the ability to probe a large portion of the parameter space through the W^+W^- channel and can probe the τ -mixing scenario completely through the τ channel with 500 hours of observation of the Milky Way Galactic Center [156]. The number of years this will take depends on the fraction of arrays that go online during the first run, which is subject to funding. Optimistically the results shown should be available after less than 3 years of running. The bounds from the W^+W^- channel, although unable to probe Bino masses below around 340 GeV, are applicable to all three mixing scenarios. Therefore, in the e - and μ -mixing scenarios, this limit needs to be complemented by a different search method.

There are, however, a couple of caveats. First, the limits assume an Einasto dark matter profile; less cuspy profiles give a signal weaker by up to two orders of magnitude. This is mainly due to the uncertainty in the J -factors for Galactic Center observations [157]. We note that the corresponding uncertainty on limits from Fermi-MAGIC observations of dwarf spheroidal galaxies is not as significant [158, 159]. Second, as we approach the coannihilation domain, the Bino mass needs to be larger to retain the desired thermal relic density. Since coannihilation does not take place in the late Universe, the indirect detection signal will be weaker, according to Eq. (4.43).

4.6.2 Neutrinos and Positrons

In principle, it is possible to place limits on indirect detection from IceCube neutrino observations [160]. In these MSSM4G models, the leading signal is from the decays $\tau_{4,5} \rightarrow W\nu$, which produce the most energetic neutrinos. Softer neutrinos are also produced as secondary decay products. Unfortunately, the limits on the annihilation cross section from IceCube are larger than $10^{-24} \text{ cm}^3/\text{s}$ and are therefore far less sensitive than gamma-ray searches.

Dark matter annihilating to positrons is also an important signal, but here the prospects

are less clear. In the τ -mixing scenario, the data can be well fit by assuming dark matter annihilation to $\tau^+\tau^-$ with cross section $\langle\sigma v\rangle = 6.8_{-3.3}^{+1.4} \times 10^{-24} \text{ cm}^3/\text{s}$ [161], which is two orders of magnitude larger than one would expect from a thermal relic annihilating primarily through S -wave. The corresponding cross sections in the e - and μ -mixing scenarios are $\langle\sigma v\rangle = 5.2_{-3.8}^{+1.4} \times 10^{-27} \text{ cm}^3/\text{s}$ and $\langle\sigma v\rangle = 8.4_{-3.0}^{+7.7} \times 10^{-26} \text{ cm}^3/\text{s}$, respectively, and so much closer to those of thermal relics. Given the large uncertainties in astrophysical backgrounds, however, it appears that in MSSM4G QUE and QDEE models, the prospects for a compelling indirect detection signal are stronger in gamma rays than in positrons.

4.7 Collider Signals

Given thermal relic density constraints, the 4th- and 5th-generation leptons and sleptons in MSSM4G models cannot be arbitrarily heavy. As a result, MSSM4G models have two robust signatures at hadron colliders: one is Drell–Yan pair production of the 4th- (and 5th-) generation lepton(s) $\tau_{4(5)}$, and the other is Drell–Yan pair production of their superpartners $\tilde{\tau}_{4L,AR(5L,5R)}$, which are the next-to-lightest SUSY particles. With a large mixing parameter ϵ between the SM and extra-generation lepton(s), we also have single production of $\tau_{4(5)}$ [162].

The decays of the extra particles are controlled by the mixing parameter ϵ . The decay widths of the extra lepton(s) are summarized in Eq. (4.42). The decay length is given by

$$c\tau \approx \left(\frac{m_{\tau_{4,5}}}{16\pi}\epsilon^2\right)^{-1} = \frac{5 \times 10^{-17} \text{ m}}{\epsilon^2} \cdot \frac{200 \text{ GeV}}{m_{\tau_{4,5}}} \quad (4.44)$$

for $m_{\tau_{4,5}} \gtrsim 200 \text{ GeV}$. The extra sleptons decay through

$$\tilde{\tau}_{aM} \rightarrow \tau_a + \tilde{B} \ , \quad (4.45)$$

where $a = 4(, 5)$ and $M = L, R$, if kinematically allowed. However, as we will see in Fig. 4.9,

this channel is kinematically forbidden in a large portion of the viable parameter regions of MSSM4G obtained in Ref. [88], and it is allowed only in a small region of the QDEE models with $m_{\tilde{\tau}_{4,5}} \sim 450\text{--}500$ GeV. In the rest of the QDEE parameter space, as well as in all of the QUE parameter space, the sleptons decay through the mixing ϵ via

$$\tilde{\tau}_{aM} \rightarrow l_i + \tilde{B} , \quad (4.46)$$

where l_i is the lepton that mixes with τ_a . This channel gives exactly the same signature as the MSSM right-handed slepton that mixes with the extra sleptons.

Consequently we have three relevant searches for MSSM4G models. If the mixing is tiny, with $\epsilon \lesssim 10^{-8}$, searches for long-lived charged particles (LLCPs) are relevant. With a larger mixing, $\tau_{4(,5)}$ can be searched for by dedicated vector-like lepton searches, and the superpartners by MSSM slepton searches. With the unified-mass assumptions of Eqs. (4.12) and (4.16), the extra particles in the QUE models are thus equivalent to one vector-like lepton and two right-handed sleptons, while in QDEE models, they are equivalent to two vector-like leptons and four right-handed sleptons.¹ The discussion below assumes that the extra lepton(s) and their superpartners mix purely with either the 1st-, 2nd-, or 3rd-generation leptons and sleptons, respectively, but it can also be generalized to more complicated mixing patterns. In fact, LLCP searches are obviously independent of the mixing patterns, and sensitivities of the vector-like lepton and slepton searches would be worse in the case of multiple decay channels.

¹Note that the production cross section of $\tilde{\tau}_{aM}$ is the same as that of the MSSM right-handed sleptons, despite their being labelled with subscripts ‘ L ’ and ‘ R .’

4.7.1 LLCP searches

LLCPs are searched for by their anomalous energy loss and longer time-of-flight at the LHC. The CMS Run 1 search excluded leptons with charge $\pm e$ lighter than 574 GeV, and staus lighter than 340 GeV, assuming only Drell–Yan pair-production [78, 163], and the ATLAS Collaboration provided similar exclusion limits [79].

Interpreting this bound under the unified-mass assumptions, one finds that the QUE models with $m_{\ell_4} < 574$ GeV or $m_{\tilde{\ell}_4} < 410$ GeV are excluded, while in the QDEE model the regions with $m_{\ell_4} < 650$ GeV or $m_{\tilde{\ell}_4} < 470$ GeV are excluded, if the relevant particles are effectively stable in collider detectors. Therefore, all the parameter regions of the QUE models, and most of them of the QDEE models, which is summarized in Ref. [88] (see also Fig. 4.9), are already excluded if $\epsilon \lesssim 10^{-8}$. The remaining region of the QDEE models with $650 \text{ GeV} < m_{\ell_4} \lesssim 700 \text{ GeV}$ is expected to be covered soon at Run 2 of the LHC [141].

For slightly larger ϵ , the leptons $\tau_{4(5)}$ have an intermediate decay length $1 \text{ mm} \lesssim c\tau \lesssim 1 \text{ m}$ and their superpartners remain effectively stable at colliders, or both leptons and sleptons can have intermediate decay lengths. Charged particles with intermediate decay lengths are searched for at the LHC but constrained less severely [80], while stable $\tilde{\tau}_{aM}$'s lighter than ~ 800 GeV may be discovered at LHC Run 2 with 300 fb^{-1} of data [141].

4.7.2 Vector-like Lepton Searches

LHC searches for vector-like leptons are performed under the assumption that they mix only with electrons or with muons, which partially excludes the region with $m < 200$ GeV [82] (see also Refs. [164–166]). Constraints on vector-like leptons mixed with taus are obtained at LEP, which excluded them with masses less than 101 GeV [167].

The Run 2 prospects for τ -mixed vector-like leptons are studied in Ref. [143]. Interpreting

their results in our scenarios, we find that the 13 TeV LHC with 3000 fb⁻¹ of data may exclude $\tau_{4(5)}$ leptons lighter than 234 GeV (264 GeV) in the QUE (QDEE) model with a very optimistic background estimation. Consequently, e^+e^- colliders are essential to search for τ -mixed vector-like leptons. Considering the pair-production $e^+e^- \rightarrow \tau_4^+\tau_4^-$, the ILC with $\sqrt{s} = 1$ TeV will cover the whole parameter region of the QUE models, while the QDEE model, which is viable for $m_{\tau_{4,5}} \lesssim 700$ GeV, will be fully covered by $\sqrt{s} \gtrsim 1.4$ TeV. Models with relatively large mixing parameters, roughly $\epsilon \gtrsim 0.01$, may also be searched for through the single production process $e^+e^- \rightarrow \tau_4^\pm\tau^\mp$ at smaller collision energies [168, 169].

The discovery prospects for e - and μ -mixed vector-like leptons are considerably brighter than for the τ -mixed case. We have performed Monte Carlo simulations to determine the future prospects of searches at LHC Run 2 with $\sqrt{s} = 14$ TeV. A thorough description of the analysis is given in Appendix C, and the results are summarized in Table 4.2.

4.7.3 Extra Slepton Searches

We now consider searches for the 4th- and 5th-generation sleptons. As stated above, in a small portion of the QDEE parameter region with $200 \text{ GeV} < m_{\ell_4} < 230 \text{ GeV}$ and $420 \text{ GeV} < m_{\tilde{\ell}_4} < 510 \text{ GeV}$, the decay $\tilde{\tau}_{aM} \rightarrow \tau_a + \tilde{B}$ is allowed. As the 4th- and 5th-generation leptons are much lighter than their superpartners in this region, vector-like lepton searches are expected to be more sensitive than extra slepton searches. We therefore concentrate on other parameter regions in which the signature is

$$pp \rightarrow \tilde{\tau}_{aM}^+ \tilde{\tau}_{aM}^- \rightarrow (l^+ \tilde{B})(l^- \tilde{B}) , \quad (4.47)$$

with l being the charged lepton that mixes with τ_a . This signature is equivalent to pair-production of right-handed slepton pairs $\tilde{l}_R^+ \tilde{l}_R^-$ in the MSSM, but with a production cross section that is twice (four times) as large in the QUE (QDEE) models.

Table 4.2: Future prospects for searches for vector-like leptons at the 14 TeV LHC for three values of integrated luminosity. The first table is for the QUE models, and the second for the QDEE models. We consider vector-like leptons with a mass $m_{\ell_4} \geq 200$ GeV; the expressions 0^{+250} GeV etc. show that the central value of exclusion or discovery limit is below our model points and we may achieve the limit of 250 GeV with 1σ statistical fluctuation. In the dashed entries the upper limit is less than 200 GeV even with 1σ statistical fluctuation. The CL_s method is used for statistical treatment, where the statistical uncertainty and a 20% systematic uncertainty for the background contribution are taken into account, while the theoretical uncertainty on the signal cross section as well as the NLO correction are not considered. See Appendix C for further details.

QUE model		300 fb ⁻¹	1000 fb ⁻¹	3000 fb ⁻¹
95% CL exclusion	<i>e</i> -mixed	240 ⁺⁶⁰ GeV	310 ⁺⁵⁰ ₋₆₀ GeV	350 ⁺⁴⁰ ₋₄₀ GeV
	μ -mixed	270 ⁺⁵⁰ GeV	330 ⁺⁴⁰ ₋₆₀ GeV	370 ⁺⁴⁰ ₋₄₀ GeV
3σ discovery	<i>e</i> -mixed	0 ⁺²⁵⁰ GeV	250 ⁺⁶⁰ ₋₄₀ GeV	300 ⁺⁵⁰ ₋₅₀ GeV
	μ -mixed	0 ⁺²⁸⁰ GeV	260 ⁺⁷⁰ ₋₆₀ GeV	320 ⁺⁵⁰ ₋₄₀ GeV
5σ discovery	<i>e</i> -mixed	—	0 ⁺²¹⁰ GeV	220 ⁺²⁰ ₋₂₀ GeV
	μ -mixed	—	0 ⁺²¹⁰ GeV	240 ⁺²⁰ ₋₂₀ GeV

QDEE model		300 fb ⁻¹	1000 fb ⁻¹	3000 fb ⁻¹
95% CL exclusion	<i>e</i> -mixed	350 ⁺⁴⁰ ₋₅₀ GeV	390 ⁺⁴⁰ ₋₄₀ GeV	430 ⁺⁴⁰ ₋₄₀ GeV
	μ -mixed	360 ⁺⁴⁰ ₋₄₀ GeV	400 ⁺⁴⁰ ₋₄₀ GeV	440 ⁺⁴⁰ ₋₄₀ GeV
3σ discovery	<i>e</i> -mixed	290 ⁺⁶⁰ ₋₇₀ GeV	340 ⁺⁶⁰ ₋₄₀ GeV	380 ⁺⁵⁰ ₋₄₀ GeV
	μ -mixed	310 ⁺⁶⁰ ₋₅₀ GeV	360 ⁺⁴⁰ ₋₃₀ GeV	400 ⁺⁴⁰ ₋₃₀ GeV
5σ discovery	<i>e</i> -mixed	0 ⁺²⁰⁰ GeV	260 ⁺⁴⁰ ₋₅₀ GeV	310 ⁺²⁰ ₋₃₀ GeV
	μ -mixed	0 ⁺²⁶⁰ GeV	280 ⁺³⁰ ₋₃₀ GeV	320 ⁺⁴⁰ ₋₂₀ GeV

For the *e*-mixed and μ -mixed cases, we derive the current bound and future sensitivity from studies of slepton ($\tilde{e}_R, \tilde{\mu}_R$) searches, since electrons and muons have a similar acceptance and efficiency at the LHC. Current bounds have been obtained by the ATLAS and CMS Collaborations at the 8 TeV LHC [33, 170], and prospects for LHC Run 2 have been discussed in Ref. [171]. We re-interpret the ATLAS result at the 8 TeV LHC [33] and the results in Ref. [171] in the context of our MSSM4G models.

The results are summarized in Fig. 4.8. For the QUE (QDEE) model, the solid (dashed) lines display the exclusion region; the dark-gray (light-gray) region is excluded by the current 8 TeV bounds, and the other three lines corresponds to the expected sensitivity at 14 TeV LHC with integrated luminosities of 300, 1000, and 3000 fb⁻¹ from left to right. Small dots show

the model point we used in the simulation to determine Run 2 prospects, which is performed with exactly the same method as in Ref. [171], utilizing MADGRAPH5_AMC@NLO [85], PYTHIA 6 [172] with PYTHIA-PGS, and DELPHES 3.2.0 [173] with FASTJET [174,175]. A systematic uncertainty of 5% as well as statistical uncertainty is taken into account.

For the τ -mixed case, the current bounds on $\tilde{\tau}_{4,5}$ are no more than $m_{\tilde{\tau}_4} < 120$ (180) GeV [176,177] in the QUE (QDEE) models, even for $m_{\tilde{B}} = 0$ GeV, which is far below the cosmologically-favored MSSM4G parameter regions. We have estimated the prospects for searches at LHC Run 2 with two methods. One method is Monte Carlo simulation. It is done in a similar way to our analysis of vector-like lepton searches. As another method, we have rescaled the Run 2 prospects for e - and μ -mixed models by the results of the ATLAS Run 1 searches [33,176]. Both analyses give the result that the 14 TeV LHC is sensitive only below $m_{\tilde{B}} < 210$ (140) GeV in the QUE (QDEE) models even with an integrated luminosity of $\int \mathcal{L} = 3000 \text{ fb}^{-1}$. This region is far below the parameter space motivated by the MSSM4G scenario. The extra slepton searches are not sensitive to the MSSM4G scenario with mixings with taus, as long as the only available production process is Drell-Yan pair-production $pp \rightarrow \tilde{\tau}_{aM}^+ \tilde{\tau}_{aM}^-$.

4.7.4 Collider Summary and Discussion

In this section we have discussed the current constraints and future prospects of collider experiments in the MSSM4G models. Let us interpret the results focusing on the cosmologically-motivated parameter space of the MSSM4G scenario (Fig. 1 of Ref. [88]).

First, we found that MSSM4G models with $\epsilon \lesssim 10^{-8}$ are mostly excluded by LLCP searches, regardless of the mixing pattern. A small parameter region of QDEE models with $m_{\ell_4} > 650$ GeV is still valid, and it will be covered in the early stage of the Run 2 LHC. We also briefly discussed the prospects for models with a slightly larger mixing, $10^{-8} \lesssim \epsilon \lesssim 10^{-6}$.

Such models will be investigated by searches for leptons decaying inside the detector as well as long-lived sleptons.

With $\epsilon \gtrsim 10^{-6}$, the extra particles decay promptly at the LHC, and signatures depend on the pattern of their mixing with SM leptons. We discussed this case with two assumptions: the mixings are purely with one of the SM three generations, and only the Drell–Yan production of extra particles ($pp \rightarrow (Z, \gamma) \rightarrow \tau_a^+ \tau_a^-$ and $pp \rightarrow (Z, \gamma) \rightarrow \tilde{\tau}_{aM}^+ \tilde{\tau}_{aM}^-$) are available at the LHC.

For the τ -mixing scenario, i.e., models in which the extra particles mix only with 3rd-generation MSSM leptons and sleptons (τ and $\tilde{\tau}$), we found that the LHC sensitivity is very limited even with 3000 fb^{-1} data. The cosmologically favored MSSM4G parameter region requires $m_{\tilde{\ell}_4} > 220 \text{ GeV}$, but searches for extra sleptons are expected to be insensitive to this region. Only a limited region with $m_{\ell_4} < 234$ (264) GeV of the QUE (QDEE) models is expected to be covered by extra lepton searches [143]. Improvements in tau-tagging techniques may give better, but still limited, sensitivity. Discovery of the extra leptons as well as exclusion of further region requires e^+e^- colliders, or proton–proton colliders with higher energy.

For models with e - or μ -mixing, we found that searches for extra leptons and extra sleptons are both sensitive. The results of our analyses are summarized in Fig. 4.9, restricting to $m_{\ell_4} > 200 \text{ GeV}$ for simplicity. The left (right) figure is for e -mixing QUE (QDEE) models, and similar results are obtained for μ -mixed models. In the color-filled regions, one can tune the lepton mass m_{ℓ_4} so that the models have a DM relic density $\Omega_{\text{DM}} h^2 = 0.12$. The red line in the right figure illustrates $m_{\ell_4} + m_{\tilde{B}} = m_{\tilde{\ell}_4}$. Below this line the extra sleptons decay as $\tilde{\tau}_{aM} \rightarrow \tau_a + \tilde{B}$. Our discussion of extra slepton searches is not applicable to this region. They are valid only above this line, and in all of the (color-filled) region of QUE models, where the extra sleptons decay into e (or μ) and a Bino.

The black lines are the expected exclusion limit at 14 TeV LHC. Those parallel to the m_{ℓ_4} -contours are from the extra lepton searches, and the others are from the extra slepton searches. Dotted, dashed, and solid lines are for integrated luminosities of $\int \mathcal{L} = 300, 1000,$ and 3000 fb^{-1} , respectively. We found that, in most cases, the extra lepton searches are more sensitive than the extra slepton searches. This is because the MSSM4G scenario prefers model points at which the extra sleptons and the Bino are rather close in mass. The degeneracy results in a smaller missing energy from slepton pair-production, and limits the sensitivity of slepton searches. Even so, it is very interesting that a considerably large portion of the parameter space is expected to be investigated by both of the searches; simultaneous appearance of excesses in both searches will be a very strong evidence of the MSSM4G model.

To summarize, the exclusion limit for models with e - or μ -mixing are expected to be $m_{\ell_4} < 350$ (430) GeV for QUE (QDEE) models at the 14 TeV LHC with 3000 fb^{-1} data. Further exploration at collider experiments requires more luminosity, more beam energy, or lepton colliders. For discovery, the extra lepton searches are promising, and their sensitivity is summarized in Table 4.2.

Let us remark again that this discussion for $\epsilon \gtrsim 10^{-6}$ is based on the assumptions that the vector-like lepton(s) has a single dominant mixing and that the other extra particles are not produced. If other MSSM superparticles are within the reach of the LHC, they will also give some event excess in SUSY searches. More interestingly, the other vector-like particles are naturally expected to be within the LHC reach. Extra vector-like quarks are searched for by their characteristic signatures [121, 178, 179], and their superpartners may be found in squark searches. For models in which the extra vector-like leptons (sleptons) are mixed with more than one generation of SM leptons (MSSM sleptons), searches for extra leptons are still promising, while those for the extra sleptons suffer from their multiple decay channels. In general, future prospects for such models are determined by the e - or μ -mixed extra lepton

searches with the signal yield properly reduced.

4.8 Conclusions

In this chapter, we have considered the cosmology of MSSM4G models, in which the MSSM is extended by adding vector-like 4th (and 5th) generation particles. Remarkably, requiring perturbative gauge coupling unification and that the extra particles raise the Higgs boson mass significantly reduces the number of MSSM4G models to two: the QUE and QDEE models.

Here we have shown that these models accommodate an excellent dark matter candidate, the Bino. In the MSSM, Bino dark matter must be lighter than 300 GeV to avoid overclosing the Universe. Such light BinOs are in tension with constraints from the LHC in many scenarios. In contrast, in the MSSM4G models, BinOs may annihilate to extra leptons through $\tilde{B}\tilde{B} \rightarrow \ell_i^+\ell_i^-$, where $i = 4$ in the QUE model, and $i = 4, 5$ in the QDEE model. These annihilation channels are enhanced by the large hypercharges of lepton isosinglets, are not chirality-suppressed, and completely dominate over all of the MSSM annihilation channels combined. We have shown that these extra channels enhance the annihilation cross section to allow Bino masses as large as 470 GeV and 670 GeV in the QUE and QDEE models, respectively, without requiring co-annihilations or resonances. MSSM4G models are therefore motivated by dark matter also, as they accommodate Bino dark matter with the correct relic density in completely generic regions of parameter space.

An interesting question is how to discover supersymmetry if these MSSM4G models are realized in nature. As we have discussed, these models satisfy precision constraints from Higgs boson properties, electroweak physics, and low-energy observables; future improvements in these areas could see hints of anomalies from 4th generation particles, but this is not generic.

These models also have improved naturalness relative to the MSSM, in the sense that the top squarks and 4th generation quarks and squarks, even without left-right mixing, may be lighter than 2 to 3 TeV and still give the correct Higgs boson mass. These are within reach of future runs of the LHC. As noted in Sec. 4.4, however, it is also possible for the stop and 4th generation quarks and squarks to all be beyond the reach of the LHC.

However, the relic density does imply upper bounds on the masses of the 4th generation leptons and sleptons. Given this, it is very interesting to see how one could best search for these at both hadron and lepton colliders. Of course, Bino dark matter can also be searched for through direct and indirect dark matter searches.

Next we investigated the current and future prospects of direct, indirect and collider searches for MSSM4G models, where the MSSM is supplemented with vector-like 4th- (and 5th-) generation particles.

For direct detection, we found that for neutralino–nucleon scattering, the light Higgs boson-mediated processes dominate over the squark-mediated processes for most of the parameter space, despite the fact that the Higgs-mediated diagram is suppressed by Yukawa couplings and the smallness of the dark matter’s Higgsino component. We determined the SI and SD scattering cross sections for various points in MSSM4G parameter space using MICROMEGAS, and for the SI cross section, we derived an accurate analytical expression for the scattering cross section to validate and better understand the results.

SI searches were found to be much more promising than SD searches. Current limits from the LUX experiment already exclude all models with $|\mu| < 500$ GeV, while models up to $|\mu| < 6$ TeV will be probed by future planned experiments. Parameter points with larger $|\mu|$ were found to lie below the neutrino floor and would require other approaches, such as directional dark matter detection [180]. We note, however, that large values of $|\mu|$ are typically considered unnatural and less motivated. MSSM4G dark matter is therefore an

ideal target for current and future direct detection searches.

To discuss indirect detection and collider searches, we needed to be more concrete about the decay channels of the 4th- (and 5th-) generation leptons. We picked three benchmark models in which the 4th- (and 5th-) generation leptons have Yukawa mixings with only one of either electrons, muons, or taus, which leads to decays to $W\nu_l$, Zl , or hl where $l = e, \mu$, or τ .

For indirect detection, Bino annihilation to $\tau_{4(5)}$ followed by decays to SM particles gives a robust gamma-ray signal. Current bounds from the Fermi-MAGIC combined analysis of dwarf spheroidal Milky Way satellites do not yield significant constraints on the MSSM4G parameter space. However, assuming an Einasto (or, in other words, cuspy) dark matter halo profile for the galactic center and 500 hours of observing time, CTA is projected to see a dark matter signal if $m_{\tilde{B}} \gtrsim 340$ GeV in the e - or μ -mixing scenarios, or for the entire range of cosmologically-preferred $m_{\tilde{B}}$ in the τ -mixing scenario. Prospects for indirect detection through neutrinos at IceCube and through positrons at AMS were found to be significantly less promising.

Finally, we examined the sensitivities of collider searches. In the case of Yukawa mixings of $\epsilon \lesssim 10^{-8}$, the 4th- (and 5th-) generation leptons produced at the LHC are long lived and are either excluded or will be covered by Run 2. The case of $10^{-8} \gtrsim \epsilon \gtrsim 10^{-6}$ will also be explored through, for example, displaced vertices.

For larger mixings, both current and projected bounds depend heavily on the decay products of the new leptons/sleptons. Assuming 3000 fb⁻¹ of data at the 14 TeV LHC, the τ -mixing scenario will only be probed up lepton masses of $m_{\ell_4} < 230$ (250) GeV in the QUE (QDEE) model. For the e - and μ -mixing scenarios the sensitivity reach is up to $m_{\ell_4} < 350$ (430) GeV for the QUE (QDEE) model. Interestingly, indirect searches will be sensitive right at the mass threshold where the LHC ceases to be effective, and so the two approaches are highly

complementary.

We also analyzed the special regions in parameter space where the decay $\tilde{\tau}_{4,5} \rightarrow \tau_{4,5} + \tilde{B}$ is allowed. We found that the 14 TeV LHC with 3000 fb^{-1} of data will have poor sensitivity for the τ -mixing case but will fully probe such points for the e - and μ -mixing cases.

We have shown that MSSM4G models are perfectly viable on the one hand and predict diverse and promising experimental signals on the other. Although direct detection experiments have strong sensitivities regardless of the details of the extra generation fields, the indirect detection and collider searches are highly dependent on such details and complement each other. Needless to say, all of those projections come with their own caveats. For instance, the direct detection rates are subject to the small uncertainty in the local dark matter density, indirect detection rates are subject to assumptions about halo profiles and our understanding of astrophysical backgrounds, and collider sensitivities depend on the quality of background estimation at higher energies as well as improvements in particle identification techniques.

We note that there are many variations one could consider. We have assumed many mass unifications to simplify the presentation of our results; these could be relaxed. One could also contemplate left-right mixings for the squarks and their impact on the Higgs boson mass, or allow the lightest neutralino to include Higgsino or Wino components. We believe that the essential point is clear, though: the combination of supersymmetry and vector-like fourth generation particles accommodates an excellent Bino dark matter candidate even in its simplest realizations, and the QUE and QDEE models are among the more motivated and viable supersymmetric extensions of the standard model.

In summary, MSSM4G QUE and QDEE models are among the motivators of both current and proposed experiments from either the pure (or almost pure) Bino dark matter or the extra generation perspective. It is interesting to continue the search for Bino dark matter with

mass $\sim 300\text{--}700$ GeV. At the same time, we demonstrated both the power and limitations of the upgraded LHC, both important points to take into consideration in discussing proposals for future lepton and hadron colliders.

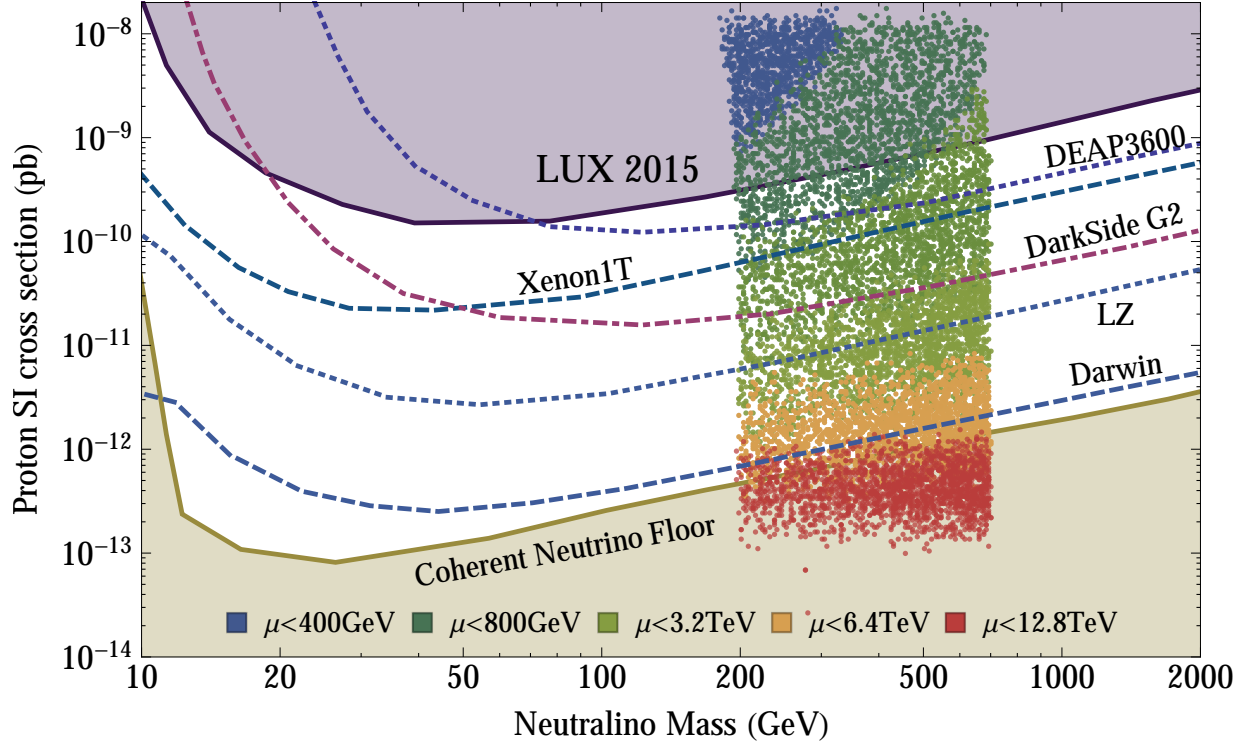


Figure 4.5: Scatter plot of theoretical predictions for MSSM4G models in the $(m_\chi, \sigma_{\text{SI}}^{(p)})$ plane. The points represent QUE and QDEE MSSM4G models that have 125 GeV Higgs bosons, are consistent with all collider bounds, and have the correct thermal relic density. QUE models populate the mass range $200 \text{ GeV} \lesssim m_\chi \lesssim 540 \text{ GeV}$, and QDEE models populate the full range $200 \text{ GeV} \lesssim m_\chi \lesssim 700 \text{ GeV}$. The points are color-coded by the value of $|\mu|$ in each model point. The upper shaded region is excluded by the current bound from LUX [22], and the dashed contours indicate the projected future sensitivities for DEAP3600 [23], Xenon 1T [24], DarkSide G2 [25], LZ [26], and Darwin [27]. In the lower shaded region, coherent neutrino scattering is a background.

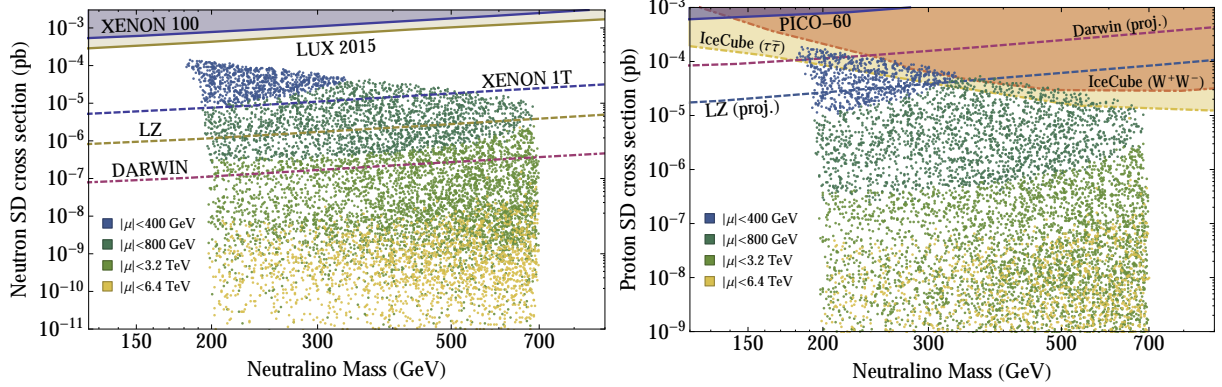


Figure 4.6: Left: Predictions for the neutron SD cross section in MSSM4G models, along with experimental bounds. The shaded regions show the excluded parameter space from Xenon 100 [28] and LUX [29], and the projected sensitivities of LZ [29], Xenon1T and DARWIN [30] are given by dashed lines. Right: Predictions of the proton SD cross section in MSSM4G models, along with existing bounds from PICO-60 [31] and IceCube [32] and the projected sensitivities of LZ and DARWIN. The IceCube bounds assume dark matter pair annihilates to W^+W^- or $\tau^+\tau^-$, as indicated.

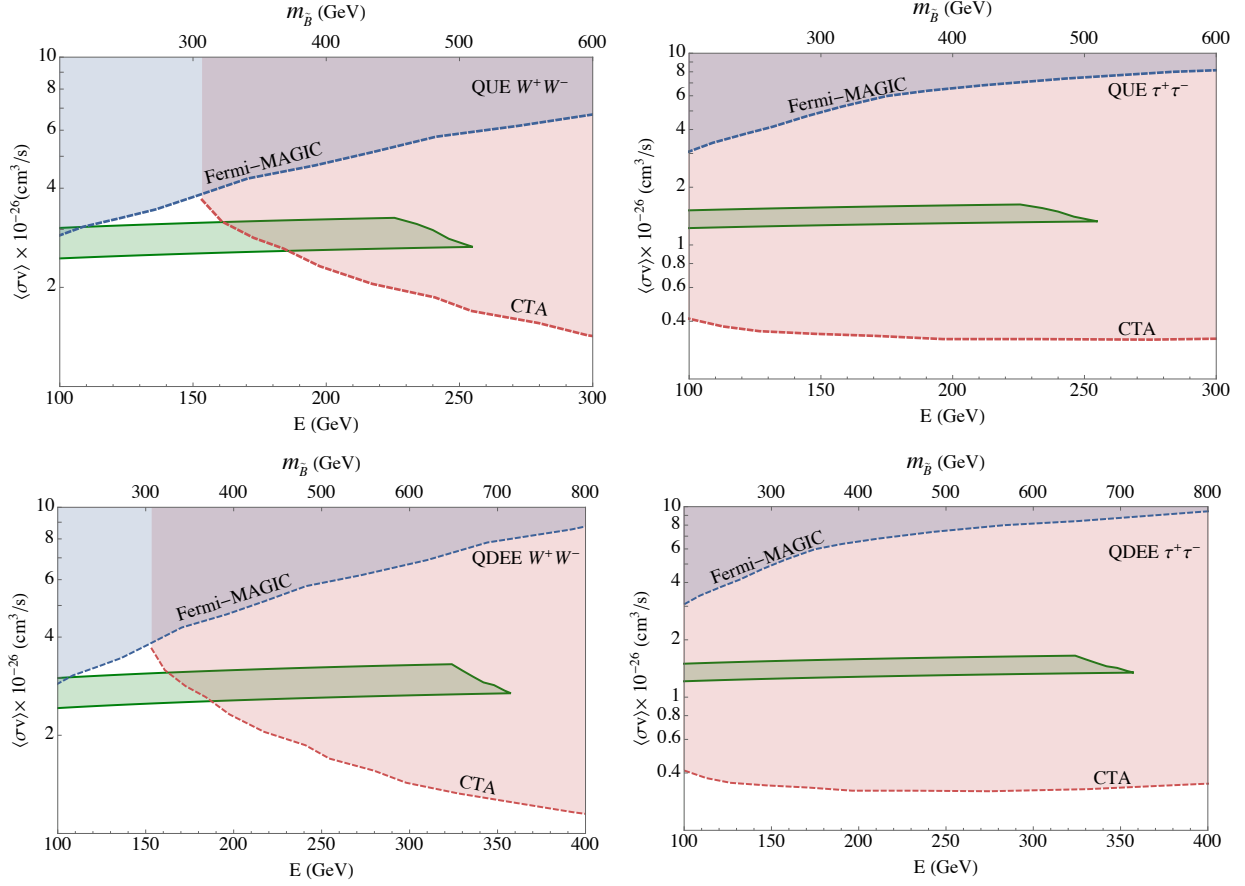


Figure 4.7: Theoretical predictions for, and current and future experimental sensitivities to, the annihilation cross sections to W^+W^- (left) and $\tau^+\tau^-$ (right) final states in the QUE (top) and QDEE (bottom) MSSM4G models as functions of the dark matter mass (top axis) and average energy $\bar{E} = m_{\bar{B}}/2$ of the annihilation products (bottom axis). The green-shaded regions are the theoretical predictions for models with thermal relic density in the range $\Omega_{\text{DM}}h^2 = 0.12 \pm 0.012$; decays to 3rd-generation leptons are assumed for the $\tau^+\tau^-$ panels. The dashed blue lines are the existing dwarf bounds from the combined MAGIC and Fermi-LAT data, and the dashed red lines are the CTA projections for Galactic Center sensitivities assuming 500 hours of observation time and an Einasto dark matter profile.

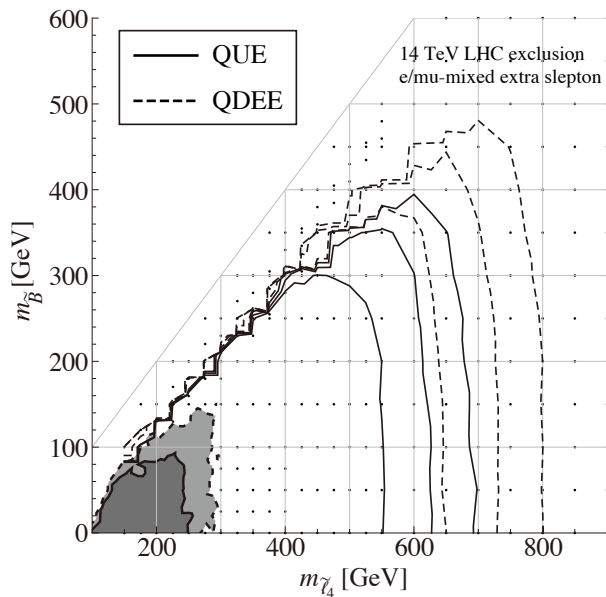


Figure 4.8: Current bounds and LHC Run 2 discovery prospects for searches for extra sleptons $\tilde{\tau}_{4(5)}$ in MSSM4G models with e -mixed or μ -mixed extra lepton generations. For the QUE (QDEE) model, the dark-gray (light-gray) region is excluded by 8 TeV searches [33], and the solid (dashed) contours outline the expected exclusion sensitivities of the 14 TeV LHC with integrated luminosities of 300, 1000, and 3000 fb^{-1} , from left to right. The small dots show the parameter points we simulated to determine the Run 2 prospects.

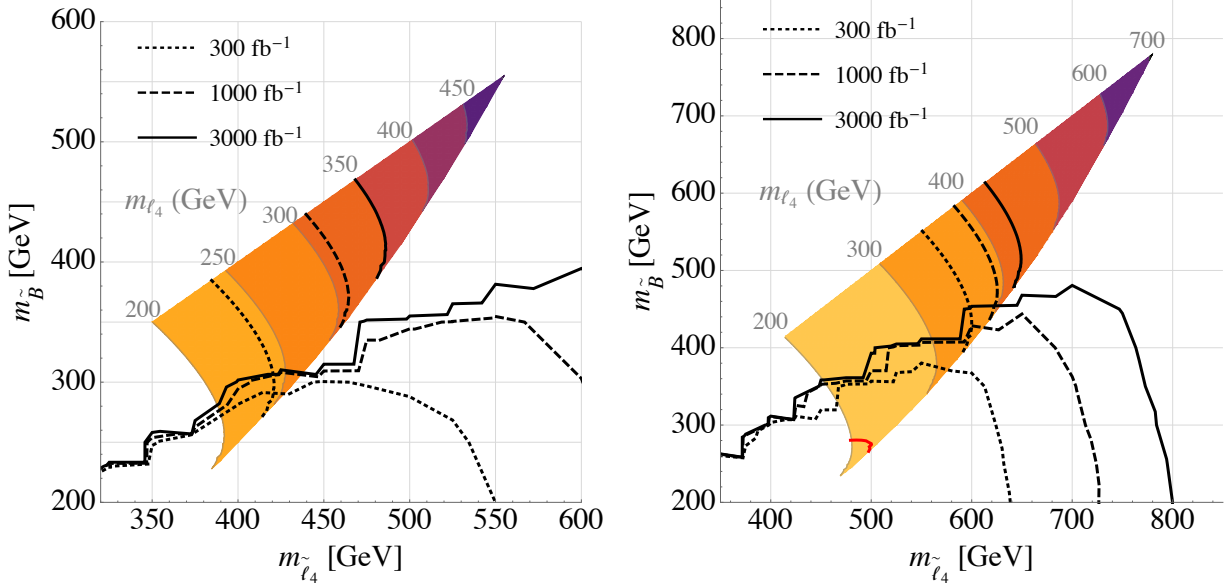


Figure 4.9: The cosmologically preferred parameter space of QUE (left) and QDEE (right) MSSM4G models, and the exclusion sensitivity of LHC searches in the e -mixing case. The μ -mixing case results in almost identical sensitivity, while the LHC is expected to be insensitive to the τ -mixing case. In both panels, the unified mass relations are assumed and we consider $m_{\ell_4} > 200$ GeV. In the shaded regions, m_{ℓ_4} is can be tuned so that the model has $\Omega_{\text{DM}} h^2 = 0.12$; contours of constant m_{ℓ_4} are shown in gray. Outside the shaded regions, the model cannot satisfy $\Omega_{\text{DM}} h^2 = 0.12$ with $m_{\ell_4} > 200$ GeV. The black lines are the expected exclusion limits at the 14 TeV LHC. Those parallel to the m_{ℓ_4} -contours are from extra lepton searches. The other lines are from extra slepton searches; they are not limited to the color-filled region because they are independent of m_{ℓ_4} . For both searches, dotted, dashed, and solid lines are for an integrated luminosities of $\int \mathcal{L} = 300, 1000, \text{ and } 3000 \text{ fb}^{-1}$, respectively. On the red contour in the right plot, the masses satisfy the relation $m_{\ell_4} + m_{\tilde{B}} = m_{\tilde{\ell}_4}$.

Chapter 5

Flavored Gauge Mediation, A Heavy Higgs, and Supersymmetric Alignment

Based on arXiv:1209.4904 [181]

5.1 Introduction

The null results of direct searches for supersymmetry suggest that it does not manifest itself in the form of light, flavor-blind superpartners. Furthermore, if the recently discovered scalar at 126 GeV [2,3] is indeed the Higgs boson, its relatively large mass requires either a large stop mixing or very heavy stops, at least in the context of the Minimal Supersymmetric Standard Model (MSSM) [182]. These results are especially problematic for Gauge-Mediated Supersymmetry Breaking (GMSB) models [183,184], which predict zero A -terms and flavor-blind spectra at the messenger scale. Low scale gauge mediation is therefore strongly disfavored by the Higgs mass, and even high-scale models, with A -terms generated by the running below the messenger scale, require stop masses of around 8–10 TeV [185,186] in the context of minimal gauge mediation [184]. Given the tight relations between squark and gluino masses

in minimal GMSB (mGMSB), this implies that all superpartners are very heavy in these models, and beyond the reach of any foreseeable experiment.

From a purely theoretical point of view, however, GMSB models are very attractive, since both the breaking of supersymmetry and its mediation are described by well understood quantum field theories, as opposed to unknown Planck-scale physics. Indeed, flavor-blind extensions of gauge mediation have been extensively discussed in recent years [187]. These extensions too are only consistent with a 126 GeV Higgs for high messenger scales, unless the stops or the gluino are very heavy [188]. Here we will study instead a flavor-dependent extension of gauge mediation, specifically, the Flavored Gauge Mediation (FGM) models of [189]. In these models, the flavor structure of GMSB is in principle modified, due to superpotential couplings of the messengers to SM fields [190]. We will show that these messenger-matter couplings can yield significant stop A -terms¹, as well as new contributions to the stop soft masses, resulting in a heavy Higgs and fairly light superpartners for a wide range of messenger scales.

The superpartner masses in FGM models are generated by both the SM gauge interactions, and by Yukawa-type superpotential couplings of the messengers to the SM matter fields. Thus, while the interactions mediating the breaking are not purely gauge interactions, they are still completely “visible”—occurring within simple field theoretic extensions of the MSSM, and potentially at low scales. Since the matter-messenger couplings are in principle flavor dependent, they are strongly constrained by the non-observation of flavor changing neutral currents. As stressed in [189], however, there are good reasons to consider these couplings. At the very least, given our ignorance about the origin of the SM Yukawas structure, it is conceivable that the messenger-matter couplings have some special structure, which results in an acceptable pattern of soft terms. Indeed, the structure of the SM fermion masses hints at some theory of flavor, and any such theory will necessarily also control the

¹Scenarios where non-trivial flavor structure leads to maximal flavor mixing have also been considered in the context of horizontal symmetries and MSSM, see for example [191]

sizes of matter-messenger couplings. Furthermore, as superpartner masses are pushed to higher values by direct searches (as well as by the large Higgs mass), there is more room for non-degenerate spectra. From the point of view of LHC searches for supersymmetry, the assumption of Minimal Flavor Violation (MFV), which underlies many analyses, can result in reduced sensitivity to non-MFV spectra [192–194]. So when searching for gauge-mediated supersymmetry, it is important to keep the possibility of flavor-dependent spectra in mind, and FGM models provide useful examples of such spectra.

The main new ingredient in our models will be superpotential messenger-matter interactions, with the up-type Higgs (or also the down-type Higgs) replaced by a messenger field of the same gauge charges. Since we would like to generate a large top A -term, the messengers need only couple to the top. As a concrete realization of this scenario, we invoke a flavor symmetry under which the Higgs and messenger field have identical charges. Flavor constraints in our models are thus satisfied by a combination of degeneracy — coming from the pure gauge contributions, and alignment [189]. Unlike in the original alignment models of [195], in which the flavor symmetry controls the soft terms directly, here it controls the *supersymmetric* messenger-matter couplings so that they are aligned with the SM Yukawas. The soft terms therefore inherit this structure, even though they are generated at the messenger scale, which is typically much lower than the flavor-symmetry breaking scale.

We note that three other works appeared recently [196–198] which rely on messenger-SM couplings to raise the Higgs mass. The differences between our models and the models of [196–198] arise due to the different choices of symmetries and, as a result, the allowed messenger-SM couplings. In [196], the messengers are chosen to have the same R-parity as the SM matter fields, so the relevant coupling is the analog of the Yukawa coupling with one SM matter field replaced by a messenger. Messengers in $5+\bar{5}$ representations of $SU(5)$ in these models do not affect the u^c mass, and as a result can raise the Higgs mass only to around 118 GeV for stops below 1.5 TeV. Therefore [196] uses messengers in $10+\bar{10}$.

In [197, 198], a coupling of the type Higgs-messenger-messenger is used, with one messenger being a SM gauge singlet. Since none of the fields involved is colored, the effect of this coupling is moderate, so that the Higgs mass is viable only at low messenger scales, where the negative one-loop contributions to the Higgs soft masses-squared are important [198]. It is interesting that, although the new messenger couplings in our models do not involve the Higgs at all, they have a significant effect on the Higgs mass. The reason is that the key feature needed for getting a large Higgs mass is a modified stop spectrum, which only requires that the messengers couple to the top.

To calculate the 2-loop contributions to the soft terms we use analytic continuation [199]. The messenger-Higgs mixing present in the models has led to some erroneous results in the literature (including in an earlier version of this article²). We clarify this issue and discuss the calculation in detail in the Appendix. The key point is the correct identification of the relevant couplings and wave function renormalizations, for which one must match the high-energy and low-energy theories correctly. We give a simple and intuitive prescription for the calculation by identifying the physical messenger field, given by the heavy combination, and the physical Higgs field, given by the light combination, and their respective running couplings.

The resulting spectra are rich and quite unusual. There are essentially two different regions of the parameter space which lead to an enhanced Higgs mass. In the first region, the stop A -terms are substantial, while the LL and RR stop masses are largely unmodified, because they receive both positive and negative contributions from the new couplings. Since these negative contributions are dominated by 1-loop effects which are higher order in the supersymmetry breaking, this region occurs for relatively low messenger scales. The resulting spectra can be very light, with colored superpartners even well below 2 TeV. In the second region, the LL and RR stop masses are enhanced as well, so that the large Higgs mass is driven not by the

²Specifically, our results for the Higgs masses were correct, but our results for the remaining scalars were wrong. We thank M. Ibe for pointing this out to us.

large mixing but rather by large stop masses. Thus a 125 GeV Higgs requires heavy stops. While only the stop masses are modified at the messenger scale, the running to the weak scale can affect the remaining masses dramatically, since the stop masses are large. While most colored superpartners are above 2 TeV in this case, the weak gauginos and sleptons can be light. Furthermore, the new contributions to the soft masses can reverse the effect of the stops on the remaining sfermions through the RGEs, leading to novel spectra with the NLSP being either the neutralino, or a L-handed slepton.

The organization of this chapter is as follows. In Section 5.2.1 we briefly review FGM and introduce the symmetries and the superpotential of our models. In Section 5.2.2 we give expressions for the soft terms in the limit of third-generation dominance. In Section 5.3 we present the Higgs mass and superpartner spectra for different choices of parameters. Our conclusions and discussion of the results are presented in Section 5.4. We present the calculation of the soft masses in the Appendix. In A.1, we derive the soft terms in a simple toy model with Higgs-messenger mixing. We generalize this to the models of interest in A.4. Full expressions for the soft terms for general 3×3 coupling matrices in generation space are presented in A.5. As a cross-check, we also calculated the relevant terms explicitly. We describe this calculation in A.6.

5.2 Models

5.2.1 The models and supersymmetric alignment.

We begin by briefly reviewing FGM models [189]. The starting point in these models is mGMSB [184]. Specifically, we will take N sets of messengers transforming as $5 + \bar{5}$ of $SU(5)$, coupled to a supersymmetry-breaking singlet $\langle X \rangle = M + F\theta^2$. We use capital letters to denote the messenger fields, with $5 = T + D$ and $\bar{5} = \bar{T} + \bar{D}$, where T (\bar{T}) and D (\bar{D}) are

fundamentals (anti-fundamentals) of $SU(3)$ and $SU(2)$ respectively. The SM gauge symmetry permits different couplings of the messengers to SM fields, and these would generically give rise to flavor-dependent soft-terms [190, 199–203]³.

As in [189], we will assume that the SM fermion masses are explained by a flavor symmetry. This symmetry then also controls the messenger-matter couplings⁴. In the models we will consider, these coupling matrices will be aligned with the SM Yukawa matrices, so that flavor constraints are satisfied. Naively, one would think that alignment can only be relevant for high-scale supersymmetry breaking. This is indeed the case in the original alignment models of [195]. In these models, a Froggatt-Nielsen flavor symmetry [19] dictates the structure of the soft-term matrices at the supersymmetry-breaking scale. As explained above however, the non-universal parts of the soft terms in FGM models are generated by superpotential matter-messenger couplings. These *supersymmetric* coupling matrices are the ones controlled by the flavor symmetry at high scales, and their near-diagonal structure is inherited by the soft terms, which are generated at much lower scales. We therefore refer to this type of alignment as “supersymmetric alignment”.

In addition to the flavor symmetry and R-parity, we impose a Z_3 symmetry with charges given in Table 5.1. The following superpotential is then allowed by the symmetries,

$$\begin{aligned}
 W = X (X^2 + T_I \bar{T}_I + D_I \bar{D}_I) &+ H_U q Y_U u^c + H_D q Y_D d^c + H_L l Y_L e^c \\
 &+ \bar{D}_1 q y_U u^c + D_2 q y_D d^c + D_2 l y_L e^c , \quad (5.1)
 \end{aligned}$$

where $I = 1, \dots, N$ runs over messenger pairs, y_U, y_D, y_L are messenger-matter Yukawa matrices, Y_U, Y_D, Y_L are the SM Yukawa matrices, and q, u^c, d^c, l, e^c are the MSSM chiral multiplets. We assume that the μ -term(s) are forbidden by some U(1) symmetry. Note that to have messenger couplings to both up quarks and down quarks we need at least two sets

³The model of [201] relies on an extra dimension in order to obtain MFV couplings.

⁴In general, some messenger fields may be charged under the flavor symmetry.

Superfield	R -parity	Z_3
X	even	1
D_1	even	-1
\bar{D}_1	even	0
D_2	even	0
\bar{D}_2	even	-1
$T_I, \bar{T}_I, D_{I>2}, \bar{D}_{I>2}$	even	1
q, u^c, d^c, l, e^c	odd	0
H_U, H_D	even	0

Table 5.1: R-parity and Z_3 charges.

of messengers [189, 201]. We also display here the term X^3 , required in mGMSB in order to generate the X VEVs, and motivating our choice of a Z_3 symmetry. In the following, however, we will limit ourselves to treating X as a supersymmetry breaking spurion.

At this point, D_2 and H_D , as well as \bar{D}_1 and H_U , have identical charges under all the symmetries, and therefore the following terms are allowed as well,

$$XD_1H_U + XH_D\bar{D}_2 . \quad (5.2)$$

However, we can set these couplings to zero without loss of generality. Consider for concreteness the H_U and \bar{D}_1 couplings

$$y_{Uij}\bar{D}_1q_iu_j^c + Y_{Uij}H_Uq_iu_j^c , \quad (5.3)$$

where i, j are generation indices. Taking H_U and \bar{D}_1 to have the same charges under the flavor symmetry, we can define the combination of \bar{D}_1 and H_U that couples to X to be the messenger (indeed, this is the massive eigenstate), and the orthogonal combination to be the Higgs. A similar redefinition can be done for D_2 and H_d . Thus (5.1) is the most general superpotential and the entries y_{Uij} and Y_{Uij} are the same up to order-one coefficients⁵.

⁵The running between the UV scale and the messenger scale will introduce, of course, some mixing

Since the only order-one entry of Y_U is Y_{U33} , the two matrices Y_U and y_U are approximately diagonal, and the soft terms inherit this structure. Inter-generational mixings are thus suppressed by supersymmetric alignment⁶.

5.2.2 A -terms and scalar masses

At leading order in F/M^2 , the messenger-matter couplings of Eq. (5.1) generate one-loop contributions to the A -terms, and two-loop contributions to the sfermion masses-squared. We present full expressions for the soft terms in Appendix A. In the case of interest, only the 3-3 entries of the coupling matrices are important and the soft terms (at the messenger scale) simplify to,

$$\begin{aligned}
 A_{33}^U &= -\frac{1}{16\pi^2} [3y_t^2 + y_b^2] \frac{F}{M} \\
 A_{33}^D &= -\frac{1}{16\pi^2} [3y_b^2 + y_t^2] \frac{F}{M} \\
 A_{33}^L &= -\frac{3y_\tau^2}{16\pi^2} \frac{F}{M} \ ,
 \end{aligned}
 \tag{5.4}$$

where $Y_t \equiv Y_{U33}$ and similarly for the remaining couplings, and,

between H_U and \bar{D}_1 , but the only effect of this running is to modify the order-one coefficients of y_U and Y_U .

⁶ It is also possible to choose different charges for H_U and \bar{D}_1 , (and similarly for H_D and D_2) such that the terms (5.2) are either forbidden or very suppressed. In this case, y_U and Y_U will have different textures, and these can be chosen to be compatible with flavor constraints [189].

$$\begin{aligned}
\tilde{m}_{H_U}^2 &= \frac{1}{128\pi^4} \left\{ -\frac{3}{2}Y_t^2(3y_t^2 + y_b^2) + N \left(\frac{3}{4}g_2^4 + \frac{3}{20}g_1^4 \right) \right\} \left| \frac{F}{M} \right|^2 \\
\tilde{m}_{H_D}^2 &= \frac{1}{128\pi^4} \left\{ -\frac{3}{2}Y_b^2(3y_b^2 + y_t^2) - \frac{3}{2}Y_\tau^2 y_\tau^2 + N \left(\frac{3}{4}g_2^4 + \frac{3}{20}g_1^4 \right) \right\} \left| \frac{F}{M} \right|^2 \\
(\tilde{m}_q^2)_{33} &= \frac{1}{128\pi^4} \left\{ \left(y_t^2 + 3y_b^2 + 3Y_b^2 + \frac{1}{2}y_\tau^2 - \frac{8}{3}g_3^2 - \frac{3}{2}g_2^2 - \frac{7}{30}g_1^2 \right) y_b^2 \right. \\
&\quad + \left(3y_t^2 + 3Y_t^2 - \frac{8}{3}g_3^2 - \frac{3}{2}g_2^2 - \frac{13}{30}g_1^2 \right) y_t^2 + Y_b y_b Y_\tau y_\tau \\
&\quad \left. + N \left(\frac{4}{3}g_3^4 + \frac{3}{4}g_2^4 + \frac{1}{60}g_1^4 \right) \right\} \left| \frac{F}{M} \right|^2 \\
(\tilde{m}_{u^c}^2)_{33} &= \frac{1}{128\pi^4} \left\{ \left(6y_t^2 + y_b^2 + Y_b^2 + 6Y_t^2 - \frac{16}{3}g_3^2 - 3g_2^2 - \frac{13}{15}g_1^2 \right) y_t^2 - Y_t^2 y_b^2 \right. \\
&\quad \left. + N \left(\frac{4}{3}g_3^4 + \frac{4}{15}g_1^4 \right) \right\} \left| \frac{F}{M} \right|^2 \\
(\tilde{m}_{d^c}^2)_{33} &= \frac{1}{128\pi^4} \left\{ \left(6y_b^2 + y_\tau^2 + y_t^2 + Y_t^2 + 6Y_b^2 - \frac{16}{3}g_3^2 - 3g_2^2 - \frac{7}{15}g_1^2 \right) y_b^2 - y_t^2 Y_b^2 \right. \\
&\quad \left. + 2Y_b y_b Y_\tau y_\tau + N \left(\frac{4}{3}g_3^4 + \frac{1}{15}g_1^4 \right) \right\} \left| \frac{F}{M} \right|^2, \\
(\tilde{m}_l^2)_{33} &= \frac{1}{128\pi^4} \left\{ \left(\frac{3}{2}y_b^2 + 2y_\tau^2 - \frac{3}{2}g_2^2 - \frac{9}{10}g_1^2 \right) y_\tau^2 + (Y_\tau^2 y_\tau^2 + 3Y_b y_b Y_\tau y_\tau) \right. \\
&\quad \left. + N \left(\frac{3}{4}g_2^4 + \frac{3}{20}g_1^4 \right) \right\} \left| \frac{F}{M} \right|^2 \\
(\tilde{m}_{e^c}^2)_{33} &= \frac{1}{128\pi^4} \left\{ \left(3y_b^2 + 4y_\tau^2 - 3g_2^2 - \frac{9}{5}g_1^2 \right) y_\tau^2 + (2Y_\tau^2 y_\tau^2 + 6Y_b y_b Y_\tau y_\tau) + \frac{3}{5}N g_1^4 \right\} \left| \frac{F}{M} \right|^2.
\end{aligned} \tag{5.5}$$

If the messenger scale M is below roughly 10^7 GeV, the one-loop $\mathcal{O}(F^4/M^6)$ contributions [190] to the soft masses may be important. In the limit of third-generation dominance,

these contributions are given by,

$$\begin{aligned}
(\delta\tilde{m}_q^2)_{33} &= -\frac{1}{6} \frac{1}{16\pi^2} (y_t^2 + y_b^2) \frac{F^4}{M^6} \\
(\delta\tilde{m}_{u^c}^2)_{33} &= -\frac{1}{3} \frac{1}{16\pi^2} y_t^2 \frac{F^4}{M^6} \\
(\delta\tilde{m}_{d^c}^2)_{33} &= -\frac{1}{3} \frac{1}{16\pi^2} y_b^2 \frac{F^4}{M^6} \\
(\delta\tilde{m}_l^2)_{33} &= -\frac{1}{6} \frac{1}{16\pi^2} y_\tau^2 \frac{F^4}{M^6} \\
(\delta\tilde{m}_{e^c}^2)_{33} &= -\frac{1}{3} \frac{1}{16\pi^2} y_\tau^2 \frac{F^4}{M^6} .
\end{aligned} \tag{5.6}$$

For completeness we also show the next-to-leading contribution in F/M^2 to the top A -term,

$$\delta A_{33}^U = -\frac{1}{16\pi^2} y_t^2 \frac{F^3}{M^5} . \tag{5.7}$$

Comparing the new contributions to the mGMSB expressions, we see that the importance of the new contributions relative to the mGMSB expressions is maximal for the smallest possible number of messengers. Thus we will take $N = 1$ when the only new Yukawa coupling is y_t , and $N = 2$ if y_b and/or y_τ are present as well.

As is well known [182], at one-loop, the Higgs mass is approximately given by,

$$m_h^2 = m_Z^2 \cos^2 2\beta + \frac{3m_t^4}{4\pi^2 v^2} \left[\log \frac{M_S^2}{m_t^2} + \frac{X_t^2}{M_S^2} \left[1 - \frac{X_t^2}{12M_S^2} \right] \right] , \tag{5.8}$$

where $X_t = A_t - \mu \cot \beta$ is the LR stop mixing and $M_S \equiv (m_{\tilde{t}_1} m_{\tilde{t}_2})^{1/2}$ is the average stop mass. Clearly, the Higgs mass can be increased either by increasing the average stop mass, so that the log term is large, or by increasing the stop mixing, so that X_t/M_S is large, with the maximal m_h^2 obtained for X_t/M_S of around 2.4 [204].

Since our main objective is to obtain the correct Higgs mass with superpartners within LHC reach, we need a large X_t/M_S , and therefore a large A_t . As can be seen from equations (5.5), a

non-zero y_t , which generates A_t , also gives new contributions to the stop masses, proportional to y_t^4 . These contributions are positive, so that M_S is increased as well. Note that the new coupling also gives rise to negative contributions to the stop masses, proportional to $y_t^2 g^2$, but there is an accidental cancellation between these and the positive $y_t^2 Y_t^2$ contribution. At low messenger scales however, the one-loop contributions are important, and since these are negative, one can obtain large X_t/M_S with low M_S .

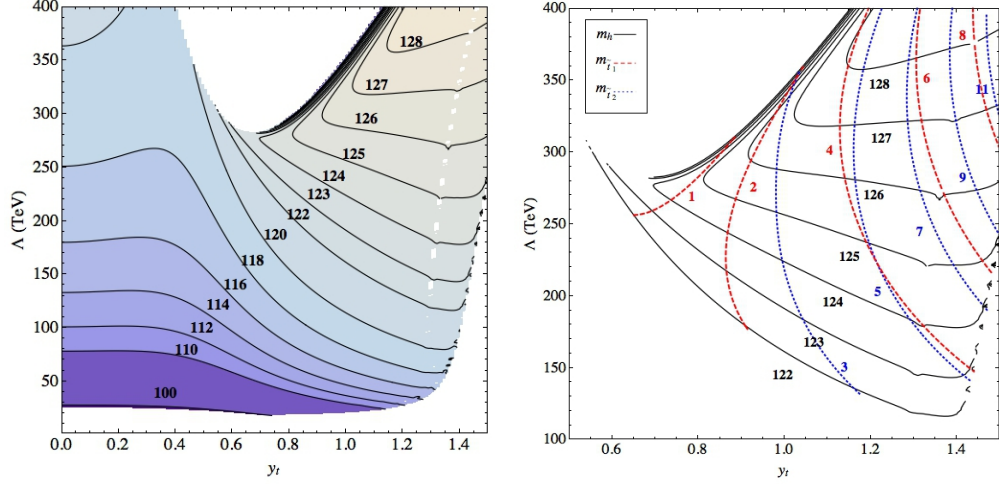
Thus, at low messenger scales, our models can give a heavy Higgs together with light stops, while at high scales, a heavy Higgs necessitates heavy stops. The messenger-scale masses of the remaining superpartner remain unchanged, and will only be modified by the running.

5.3 Higgs mass and superpartner masses

5.3.1 The Higgs and stop masses

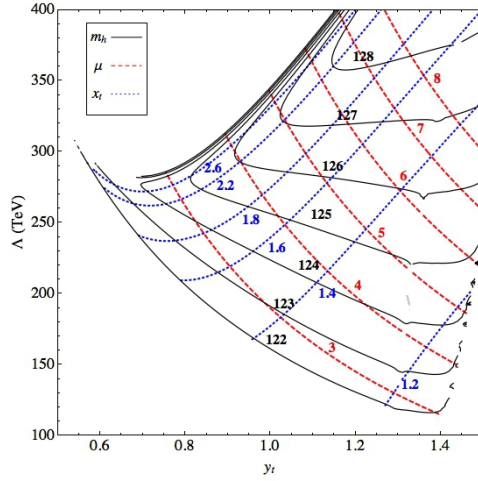
We first consider models with one set of messengers. With the Z_3 charges of Table 5.1, only the \bar{D}_1 messenger couplings to matter are allowed. Moreover, since we assume that \bar{D}_1 and H_U have the same charge under the flavor symmetry of the model, the only significant messenger coupling is $y_t \equiv (y_U)_{33}$. We use SOFTSUSY [205] to calculate the Higgs mass for different choices of the GMSB parameters and y_t . Given the theoretical uncertainty in the calculation of the Higgs mass, it is interesting to study Higgs masses in the 124–128 GeV window.

In Fig. 5.1 we show contours of the Higgs and stop masses as a function of $\Lambda \equiv F/M$ and y_t , for a low messenger scale of $M = 900$ TeV, with $\tan \beta = 10$. For such a low messenger scale, the one-loop $\mathcal{O}(F^4/M^6)$ corrections are not necessarily negligible and have been taken into account. Fig. 5.1a shows the Higgs mass contours for a wide range of y_t . The white region



(a)

(b)



(c)

Figure 5.1: The Higgs and stop masses for $N = 1$, $M = 900 \text{ TeV}$, $\tan \beta = 10$. Fig. 5.1a shows the Higgs mass for a wide range of y_t . The predictions of minimal gauge mediation can be read off from the line $y_t = 0$. The white region is excluded because it leads to tachyonic stops (see text). In Fig. 5.1b, we show Higgs mass (solid), heavy stop mass (dotted) and light stop mass (dashed) contour lines in a smaller region of y_t . In Fig. 5.1c we show Higgs (solid), μ (dashed) and $x_t = |X_t/M_S|$ (dotted) contour lines in the same region.

for intermediate values of y_t is excluded. In this region, the stops are either tachyonic or too light for successful electroweak symmetry breaking. As explained above, for these values of y_t , the negative one-loop contribution to the stop mass-squared is comparable to the positive contributions from pure GMSB. As y_t is increased, the y_t^4 contribution to the stop masses guarantees that the stops are non-tachyonic, but because of the partial cancellation between the 1-loop and 2-loop contributions, the A -term becomes appreciable compared to the stop masses and the resulting large mixing allows for a heavy Higgs. As y_t is increased further, the stops become heavy relative to the other superpartners. In this regime, the heavy stops and large A -terms both play a crucial role in making the Higgs heavy.

In Fig. 5.1b, we zoom in on the interesting range $y_t \sim 1$, and show contours of the Higgs mass together with the two stop masses, with the remaining parameters being the same as in Fig. 5.1a. In Fig. 5.1c, we also show contours of μ and the mixing parameter $x_t = |X_t/M_S|$. As expected, the largest values of x_t are obtained close to the excluded regions where one of the stops is relatively light. Thus, appreciable A -terms can be obtained without a large increase in the stop squared masses. Indeed, as can be seen in Fig. 5.1b, for these large values of x_t , the Higgs mass can be large even for low Λ 's, such that the stops are light. For $y_t \sim 1$ we can therefore find at least one stop below 2 TeV.

We can get even lighter stops by lowering the messenger scale, which allows for a lower Λ . In Fig. 5.2 we show the behavior of the models for $M = 400$ TeV. Note that since we only know the leading F/M^2 behavior of the new contributions to the soft masses, we keep $F/M^2 < 0.5$ (the pure GMSB higher-order corrections are known to be small [206]). Indeed, a Higgs mass of 125 GeV is obtained with both stops between 1.5 and 2 TeV, and stops below 1.5 TeV allow for Higgs masses above 124 GeV (as mentioned above, one should bear in mind the uncertainty in our Higgs mass calculation). The remaining squarks will be quite light too in this region, and we will give a few example spectra to illustrate this in the next Section.

For higher messengers scales, the behavior of the models is qualitatively different. To demon-

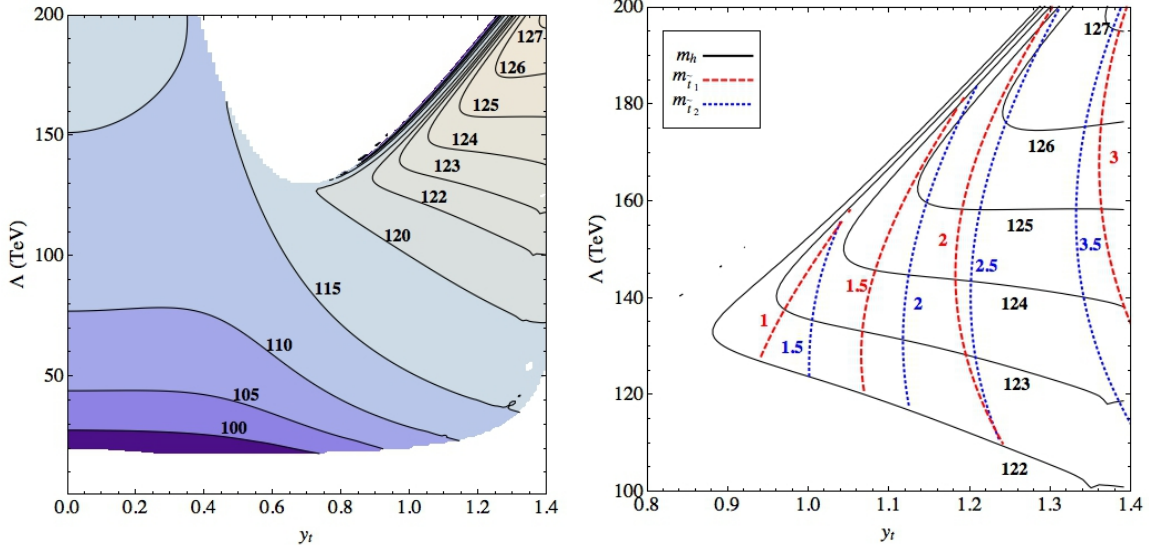


Figure 5.2: Same plots as in Fig 5.1a and 5.1b with $M = 400 \text{ TeV}$ and $\tan \beta = 10$

strate this, we present similar plots for two other messenger scales, $M = 10^{12} \text{ GeV}$ in Fig 5.3 and $M = 10^8 \text{ GeV}$ in Fig 5.4. Clearly, the tachyonic stop region for moderate y_t is absent for these high scales, since the negative one-loop contribution is negligible. Thus a 125 GeV Higgs requires heavy stops, above 4 TeV. It is interesting to compare our results for high messenger scales with models of minimal gauge mediation. As is well known, with a lot of running, appreciable A -terms can be generated in pure GMSB models. This is, however, not sufficient—as was shown in Ref. [186], even with a high messenger scale a heavy Higgs requires very heavy stops near 8-10 TeV. For example, with $M = 7.9 \cdot 10^{12} \text{ GeV}$ and $\tan \beta = 10$, a Higgs mass of 125 GeV can be achieved if $\Lambda = 1.3 \cdot 10^6 \text{ GeV}$ [186]. With such a high value of Λ , one of the stops is the lightest squark and has a mass of 7.9 TeV. In contrast, if we choose the same messenger scale in the FGM model with $y_t = 1.1$, a Higgs mass of 124.2 GeV can be achieved with $\Lambda = 3.35 \cdot 10^5 \text{ GeV}$. While the stops are still very heavy (around 5 TeV) due to the messenger Yukawa contributions, the remaining superpartners are significantly lighter, with the gluino and right handed up and charm squarks around 2.3–2.4 TeV, and a 461 GeV bino NLSP.

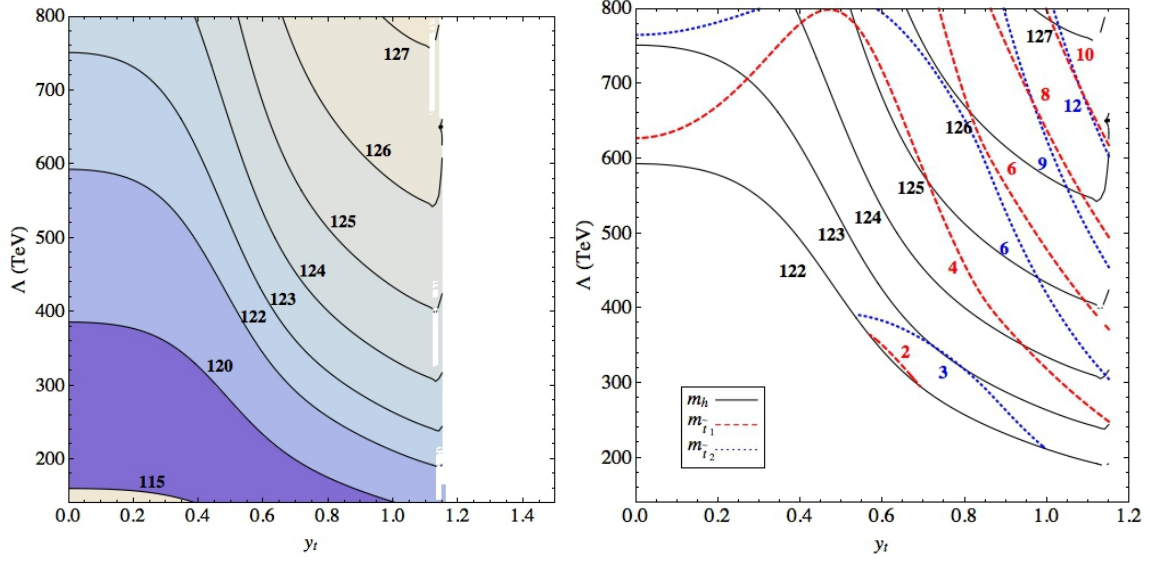


Figure 5.3: Same plots as in Fig 5.1a and 5.1b with $M = 10^{12}$ GeV and $\tan \beta = 10$

While the models with only messenger-top Yukawas are the most economical ones, viable models with additional messenger-bottom and messenger-tau couplings may also be viable. As an example, in Fig. 5.5 we present Higgs mass contours in the $y_t - y_b$ plane for $N = 2$, with $M = 10^8$ GeV, $\Lambda = 230$ TeV, and $\tan \beta = 10$. For large values of y_b , the sleptons become tachyonic, leading to the white excluded region on the right.

Since we are turning on order-one superpotential couplings, it is interesting to ask at what scales these become non-perturbative. For example, if $N = 1$ the high scale models with $M = 10^{12}$ GeV remain perturbative even above the GUT scale. For $M = 10^8$ GeV, one loses perturbativity at around $10^{12} - 10^{13}$ GeV for $y_t \sim 1$. Finally, with $M = 900$ TeV, the models stay perturbative up to $10^9 - 10^{10}$ GeV for y_t above 1, and for a smaller $y_t \sim 0.9$ (as is the case with one of the lighter spectra we show below. See Table 5.2) up to scales of around 10^{13} GeV. In the case of $N = 2$ the couplings remain perturbative for a few order of magnitude above the messenger scale.

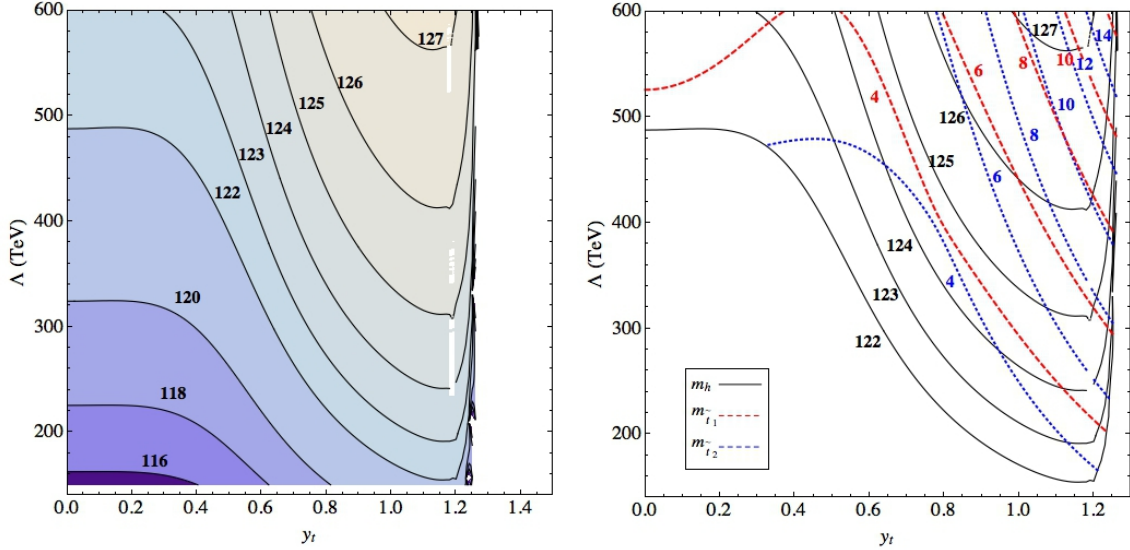


Figure 5.4: Same plots as in Fig 5.1a and and 5.1b with $M = 10^8$ GeV, $\tan \beta = 20$.

5.3.2 Superpartner spectra and LHC signatures

To understand the phenomenology of our FGM models, we present in Table 5.2

complete superpartner spectra for several choices of the parameters at low, intermediate and high messenger scales. A detailed analysis of the experimental signatures is beyond the scope of this chapter, and these spectra are only meant to illustrate the general features of the models. Thus for example, spectrum 1, which has a light gluino and first generation squarks, is ruled out by jets-plus-missing-energy searches like [207,208] and possibly by specific GMSB searches [209,210]. It is nonetheless useful to point out a few key features.

First, large regions of the parameter space yield gluino and squark masses that will hopefully be accessible in the 14 TeV LHC. Indeed, in many of the examples shown in Table 5.2, the gluino and some first generation squarks are below 2.5 TeV, and sometimes considerably lighter.

Second, even with a single messenger pair, for which mGMSB models usually predict a

Parameter	Spect. 1	Spect. 2	Spect. 3	Spect. 4	Spect. 5	Spect. 6	Spect. 7	Spect. 8
M_{mess}	$2 \cdot 10^5$	$4 \cdot 10^5$	$9 \cdot 10^5$	$1 \cdot 10^8$	$1 \cdot 10^8$	$1 \cdot 10^{12}$	$1 \cdot 10^{12}$	$7.9 \cdot 10^{12}$
Λ	$1.05 \cdot 10^5$	$1.65 \cdot 10^5$	$3.03 \cdot 10^5$	$3.08 \cdot 10^5$	$2.74 \cdot 10^5$	$4.00 \cdot 10^5$	$3.55 \cdot 10^5$	$3.35 \cdot 10^5$
$\tan \beta$	10	10	10	20	20	10	10	10
y_t	1.45	1.20	0.92	1.19	1.18	1.13	1.14	1.10
μ	2606	3165	4053	6405	5648	7844	7091	6278
h_0	124.9	125.4	126.0	125.0	124.5	125.0	124.5	124.2
A	2686	3281	4248	6570	5792	8107	7319	6493
H_0	2686	3281	4250	6567	5791	8105	7319	6493
H_{\pm}	2687	3283	4249	6571	5792	8107	7320	6494
t_1	1620	1997	1795	5698	4986	6243	5634	4899
t_2	2050	2315	2623	7232	6305	7576	6855	5826
b_L	1680	2069	2615	5654	4948	6195	5591	4864
b_R	1119	1683	2918	2721	2439	3359	3007	2803
u_L, c_L	1179	1780	3116	2987	2672	3616	3229	3029
u_R, c_R	1096	1668	2950	2508	2257	2704	2401	2281
d_L, s_L	1182	1781	3117	2987	2673	3617	3230	3030
d_R, s_R	1133	1698	2950	2844	2546	3403	3048	2839
e_L, μ_L	305	525	1039	569	523	578	417	620
e_R, μ_R	356	458	618	1514	1333	2378	2149	1991
τ_L	244	550	1038	505	462	555	390	603
τ_R	392	418	604	1476	1303	2363	2135	1979
ν_e	295	519	1035	555	509	562	397	606
ν_{μ}, ν_{τ}	295	519	1036	563	516	571	408	614
χ_1	151	233	425	426	378	552	488	461
χ_2	299	457	822	826	732	1056	935	880
χ_3	2642	3208	4107	6573	5793	8010	7239	6403
χ_4	2643	3209	4108	6573	5793	8010	7240	6404
χ_1^{\pm}	299	458	823	826	733	1056	935	880
χ_2^{\pm}	2643	3210	4109	6573	5794	8011	7240	6404
g	894	1315	2240	2251	2024	2832	2540	2404

Table 5.2: Model parameters, and resulting Higgs parameters and spectra for eight sample models. All mass parameters are given in GeV.

neutralino NLSP, the NLSP in our models can be either a bino, a left-handed charged slepton, or a sneutrino, depending on the choice of parameters. This is due to the fact that the $U(1)_Y$ contributions to the RG evolution of sfermion masses contain a term proportional to $S \equiv \text{Tr}[Y_j m_{\phi_j}^2]$, where the trace is taken over all the SM sfermions. Normally this contribution suppresses the right-handed sfermions masses, but in flavored GMSB the sign of S changes for sufficiently large y_t . Furthermore, since for large y_t the stop masses are much larger than the remaining soft-terms, the effect of S through the running is dramatic. As a result, in some regions of the parameter space, the right-handed sleptons become heavy while the left-handed ones are relatively light.

While squarks are generically heavy in this class of models, the sleptons, charginos and neutralinos can be quite light, and may therefore be discovered even if produced directly. This depends of course on the details of the spectrum, and in particular on the identity and lifetime of the NLSP. Whether or not the NLSP decays inside the detector depends on the gravitino mass, which involves a lot of uncertainty⁷. In any case, the fact that the gravitino is the LSP in these models can provide additional handles for their discovery, using either prompt NLSP decays to the gravitino as in [209, 210], or the long lifetime of a charged NLSP. Thus for example, the current bound on a long-lived charged slepton NLSP in mGMSB is 300 GeV [212] and the model-independent bound on Drell-Yan produced right-handed sleptons just somewhat below that. These bounds are likely to improve considerably for long-lived charged left-handed sleptons at the 14 TeV LHC.

It would also be interesting to study models with more messenger pairs. Since the pure gauge contribution to the scalar squared masses is proportional to N , we expect that for such models the cancellation between the negative new contributions and pure gauge contributions will

⁷ If F_X is the dominant F -term, the gravitino mass in our models varies between about 100 eV for $M = 900$ TeV to a GeV for the high-scale models. It is quite plausible however that there are much higher F terms in the supersymmetry-breaking sector, as is often the case in calculable models, in which case F_X is generated through several small couplings from a higher F -term. For large values of the gravitino mass, the NLSP would decay outside the detector. Heavy gravitinos from late NLSP decay could also supply warm dark matter [186, 211].

be less dramatic than for the $N = 1$ models, so that very light spectra would not occur. Such models would typically give rise to gluino masses above squark masses, and to slepton or sneutrino NLSPs.

5.4 Conclusions

We have shown that gauge-mediated models with messenger-matter couplings can give rise to an acceptable Higgs mass, with colored superpartners within LHC reach. The important new ingredient in these models is the messenger-scale top A -term, which gives rise to significant stop mixing, and therefore enhances the Higgs mass. While a heavy Higgs can be obtained for a wide range of messenger scales, the details of the superpartner spectra may vary significantly. For low messenger scales, the one-loop $\mathcal{O}(F^4)$ negative contributions to the stop masses are important, so that the stops are relatively light while the Higgs mass is raised largely due to the A -terms. For large messenger scales, the stops become heavy due to large positive contributions proportional to the messenger Yukawas. As a result, the Higgs mass is raised both due to the A -terms and to the large stop masses.

The messenger Yukawas often lead to another novel effect – the $U(1)_Y$ contribution to sfermion RGE's may change sign so that left-handed sleptons become light. We see that the resulting spectra can be quite diverse with either a neutralino or slepton NLSP. We leave a detailed study of the phenomenology of these models for future work. It would also be interesting to examine models with down-type messenger couplings, which may lead to rather different phenomenology. We further note that while we have concentrated on models with only a single pair of messengers and a messenger-top coupling, the results can be easily generalized to models with several messenger pairs, with or without messenger down-type couplings.

The structure of the matter-messenger couplings can naturally be the same as the structure of the usual Yukawas, since the new couplings are obtained by replacing H_U and/or H_D by the messenger of the same gauge charge. The models are therefore protected against flavor-violation by *supersymmetric alignment*. This can be simply realized in the context of flavor symmetries if the Higgs and corresponding messenger have the same charges under the flavor symmetry.

The amount of tuning in our models is related to the tuning of the new messenger-matter coupling y_t . As can be seen in Table 5.2, for spectrum 1, which relies on a finely-dialed y_t to obtain a light spectrum, the μ -term is 2.6 TeV, while less tuned choices of y_t require larger μ -terms, around 6 or 8 TeV. Generating an acceptable μ -term in our models is an important direction to pursue. If there is a successful mechanism for generating the μ -term, the tuning question would translate into the question of how finely one needs to tune the coupling y_t . It is probably far from trivial to find a successful mechanism for generating the μ -term, and even if it is found, the required tuning of y_t is likely to be significant. Still, since y_t is a superpotential coupling, the tuning involved is qualitatively different from the tuning of the Higgs mass in the standard model.

Note added

After posting the original version of this article on the archive, M. Ibe drew our attention to [213, 214], which use the same messenger-top coupling in order to raise the Higgs mass. There is thus some overlap between our work and [213, 214] as concerns the implications of a heavy Higgs. The origin of the messenger-matter coupling is different however in [213, 214], with the result that these models are MFV. Also, while we calculate the new contributions of the full 3-generation coupling matrices, [213, 214] only consider third generation couplings. While completing this revised version, Ref. [215] appeared, which surveys different messenger-

matter couplings. Our results for the soft masses now agree with [213–215], but our approach to the calculation differs from theirs.

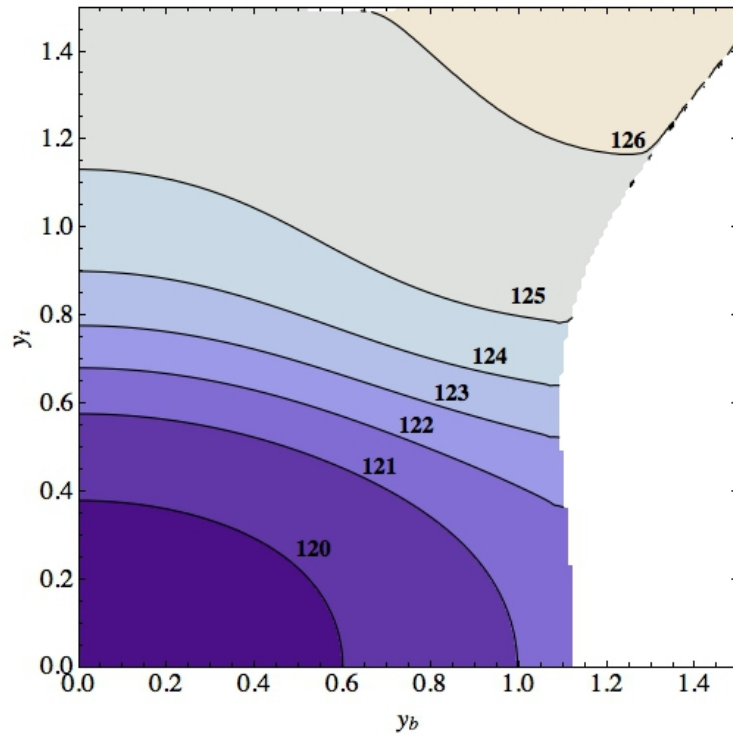


Figure 5.5: Higgs mass contours in the $y_t - y_b$ plane with $M = 10^8 \text{ GeV}$, $\Lambda = 230 \text{ TeV}$, and $\tan \beta = 10$.

Chapter 6

Conclusion

The hierarchy problem, in association with other standing puzzles such as dark matter, baryogenesis, neutrino masses, flavor hierarchy, and gauge coupling unification, gives us great hope that some new physics exists at the TeV scale. In this work, we have presented various approaches of searching for such new phenomena utilizing a variety of experimental techniques.

In Ch. 2 we presented a systematic way of looking for new resonances at the LHC based on classifying the final state topology. We analyzed the future prospects for a concrete example, namely a 2-lepton and 2-jets topology which has not been well studied. In constructing a simple toy model to perform the analysis we were forced to consider existing limits on the model using alternative channels that are well explored in the literature, and it is not clear whether our chosen topology would continue to provide complementary results at future LHC runs. Although, the simplicity of the approach and the flexibility of the result presentation remain attractive features nonetheless. This idea has been pursued further by Ref. [225].

In Ch. 3, we investigated a model of spin-3/2 leptons using LHC data supplemented with effective operators inspired by fermion compositeness. Such model, while possible within

some theoretical framework, has not been well explored due to the lack of such fields in popular new physics models. Limits based on current LHC data were presented.

An extension of the MSSM has been studied in Ch. 4, where it was supplemented by extra vector-like matter. We showed that, in addition to the well known motivations of solving the hierarchy problem and preserving perturbative gauge coupling unification, this model can significantly expand on the parameter space of viable bino dark matter.

Additionally, the current and future sensitivities of colliders, direct detection, and indirect detection experiments has been presented. We found that the parameter space will be comprehensively covered by a combination of those experiments.

Finally, we delved deeper into the structure of the MSSM in Ch. 5 to better understand the extent to which fine-tuning can be reduced if gauge mediation is relied upon as the primary mechanism of transmitting supersymmetry breaking to the observable sector. We concluded that additional flavor interactions can induce desirable corrections to the Higgs mass while maintaining an experimentally accessible spectrum of superpartners. However, the additional structure suffers from its own sources if fine-tuning as well as a loss of perturbativity at high energy. The model still serves as useful proof of principle for constructing models of supersymmetry breaking.

We have a great amount of experimental and observational resources at our disposal, and with the infinite possibilities of new discoveries to be made, a balance needs to be made in deciding on search strategies. In exploring a variety of different approaches, we hope that, in addition to the results specific to each model, their advantages and disadvantages has been highlighted and will serve to help guide the searches of new physics in the exciting years to come.

Bibliography

- [1] C. Patrignani *et al.* [Particle Data Group], *Chin. Phys. C* **40**, no. 10, 100001 (2016). doi:10.1088/1674-1137/40/10/100001
- [2] G. Aad *et al.* [ATLAS Collaboration], *Phys. Lett. B* **716**, 1 (2012) doi:10.1016/j.physletb.2012.08.020 [arXiv:1207.7214 [hep-ex]].
- [3] S. Chatrchyan *et al.* [CMS Collaboration], *Phys. Lett. B* **716**, 30 (2012) doi:10.1016/j.physletb.2012.08.021 [arXiv:1207.7235 [hep-ex]].
- [4] F. Englert and R. Brout, *Phys. Rev. Lett.* **13**, 321 (1964). doi:10.1103/PhysRevLett.13.321
- [5] P. W. Higgs, *Phys. Lett.* **12**, 132 (1964). doi:10.1016/0031-9163(64)91136-9
- [6] P. W. Higgs, *Phys. Rev. Lett.* **13**, 508 (1964). doi:10.1103/PhysRevLett.13.508
- [7] G. S. Guralnik, C. R. Hagen and T. W. B. Kibble, *Phys. Rev. Lett.* **13**, 585 (1964). doi:10.1103/PhysRevLett.13.585
- [8] P. W. Higgs, *Phys. Rev.* **145**, 1156 (1966). doi:10.1103/PhysRev.145.1156
- [9] T. W. B. Kibble, *Phys. Rev.* **155**, 1554 (1967). doi:10.1103/PhysRev.155.1554
- [10] E. Gildener and S. Weinberg, *Phys. Rev. D* **13**, 3333 (1976). doi:10.1103/PhysRevD.13.3333
- [11] E. Gildener, *Phys. Rev. D* **14**, 1667 (1976). doi:10.1103/PhysRevD.14.1667
- [12] A. de Gouvea, D. Hernandez and T. M. P. Tait, *Phys. Rev. D* **89**, no. 11, 115005 (2014) doi:10.1103/PhysRevD.89.115005 [arXiv:1402.2658 [hep-ph]].
- [13] **Planck** Collaboration, P. A. R. Ade *et al.*, “Planck 2015 results. XIII. Cosmological parameters,” arXiv:1502.01589 [astro-ph.CO].
- [14] G. Bertone and D. Hooper, [arXiv:1605.04909 [astro-ph.CO]].
- [15] A. D. Sakharov, *Pisma Zh. Eksp. Teor. Fiz.* **5**, 32 (1967) [*JETP Lett.* **5**, 24 (1967)] [*Sov. Phys. Usp.* **34**, 392 (1991)] [*Usp. Fiz. Nauk* **161**, 61 (1991)]. doi:10.1070/PU1991v034n05ABEH002497

- [16] M. Fairbairn and P. Grothaus, “Baryogenesis and Dark Matter with Vector-like Fermions,” *JHEP* **10** (2013) 176, [arXiv:1307.8011 \[hep-ph\]](#).
- [17] P. Minkowski, *Phys. Lett.* **67B**, 421 (1977). doi:10.1016/0370-2693(77)90435-X
- [18] M. Fukugita and T. Yanagida, *Phys. Lett. B* **174**, 45 (1986). doi:10.1016/0370-2693(86)91126-3
- [19] C. D. Froggatt and H. B. Nielsen, “Hierarchy of Quark Masses, Cabibbo Angles and CP Violation,” *Nucl. Phys.* **B147** (1979) 277–298.
- [20] H. Fritzsch and P. Minkowski, *Annals Phys.* **93**, 193 (1975). doi:10.1016/0003-4916(75)90211-0
- [21] **ATLAS** Collaboration, G. Aad *et al.*, “Search for new phenomena in events with three or more charged leptons in pp collisions at $\sqrt{s} = 8$ TeV with the ATLAS detector,” *JHEP* **08** (2015) 138, [arXiv:1411.2921 \[hep-ex\]](#).
- [22] **LUX** Collaboration, D. S. Akerib *et al.*, “Improved Limits on Scattering of Weakly Interacting Massive Particles from Reanalysis of 2013 LUX Data,” *Phys. Rev. Lett.* **116** (2016) 161301, [arXiv:1512.03506 \[astro-ph.CO\]](#).
- [23] **DEAP** Collaboration, P. A. Amaudruz *et al.*, “DEAP-3600 Dark Matter Search,” in *Proceedings, 37th International Conference on High Energy Physics (ICHEP 2014)*, vol. 273-275, pp. 340–346. 2016. [arXiv:1410.7673 \[physics.ins-det\]](#).
- [24] **XENON** Collaboration, E. Aprile *et al.*, “Physics reach of the XENON1T dark matter experiment,” *JCAP* **1604** (2016) 027, [arXiv:1512.07501 \[physics.ins-det\]](#).
- [25] C. E. Aalseth *et al.*, “The DarkSide Multiton Detector for the Direct Dark Matter Search,” *Adv. High Energy Phys.* **2015** (2015) 541362.
- [26] **LZ** Collaboration, D. S. Akerib *et al.*, “LUX-ZEPLIN (LZ) Conceptual Design Report,” [arXiv:1509.02910 \[physics.ins-det\]](#).
- [27] **DARWIN** Collaboration, J. Aalbers *et al.*, “DARWIN: towards the ultimate dark matter detector,” [arXiv:1606.07001 \[astro-ph.IM\]](#).
- [28] **XENON100 Collaboration** Collaboration, E. Aprile *et al.*, “Limits on Spin-Dependent Wimp-Nucleon Cross Sections from 225 Live Days of Xenon100 Data,” *Phys.Rev.Lett.* **111** (2013) no. 2, 021301, [arXiv:1301.6620 \[astro-ph.CO\]](#).
- [29] **LUX** Collaboration, D. S. Akerib *et al.*, “Results on the Spin-Dependent Scattering of Weakly Interacting Massive Particles on Nucleons from the Run 3 Data of the LUX Experiment,” *Phys. Rev. Lett.* **116** (2016) no. 16, 161302, [arXiv:1602.03489 \[hep-ex\]](#).

- [30] M. Schumann, L. Baudis, L. BÄijtikofer, A. Kish, and M. Selvi, “Dark matter sensitivity of multi-ton liquid xenon detectors,” *JCAP* **1510** (2015) 016, arXiv:1506.08309 [physics.ins-det].
- [31] **PICO** Collaboration, C. Amole *et al.*, “Dark matter search results from the PICO-60 CF₃I bubble chamber,” *Phys. Rev.* **D93** (2016) no. 5, 052014, arXiv:1510.07754 [hep-ex].
- [32] **IceCube** Collaboration, M. G. Aartsen *et al.*, “Improved limits on dark matter annihilation in the Sun with the 79-string IceCube detector and implications for supersymmetry,” *JCAP* **1604** (2016) no. 04, 022, arXiv:1601.00653 [hep-ph].
- [33] **ATLAS** Collaboration, G. Aad *et al.*, “Search for direct production of charginos, neutralinos and sleptons in final states with two leptons and missing transverse momentum in pp collisions at $\sqrt{s} = 8$ TeV with the ATLAS detector,” *JHEP* **05** (2014) 071, arXiv:1403.5294 [hep-ex].
- [34] **LHC New Physics Working Group** Collaboration, D. Alves *et al.*, “Simplified Models for LHC New Physics Searches,” *J.Phys.* **G39** (2012) 105005, arXiv:1105.2838 [hep-ph].
- [35] N. D. Christensen and C. Duhr, “FeynRules - Feynman rules made easy,” *Comput. Phys. Commun.* **180** (2009) 1614–1641, arXiv:0806.4194 [hep-ph].
- [36] B. A. Dobrescu and F. Yu, “Coupling-Mass Mapping of Dijet Peak Searches,” *Phys.Rev.* **D88** (2013) no. 3, 035021, arXiv:1306.2629 [hep-ph].
- [37] M. Abdullah *et al.*, *Phys. Rev. D* **89**, no. 9, 095002 (2014) doi:10.1103/PhysRevD.89.095002 [arXiv:1401.1462 [hep-ph]].
- [38] P. Papacz [CMS Collaboration], arXiv:1201.5577 [hep-ex].
- [39] T. Aaltonen *et al.* [CDF Collaboration], *Phys. Rev. D* **78**, 012002 (2008) [arXiv:0712.1311 [hep-ex]].
- [40] F. D. Aaron *et al.* [H1 Collaboration], *Phys. Lett. B* **674**, 257 (2009) [arXiv:0901.0507 [hep-ex]].
- [41] W. Buchmuller and D. Wyler, *Phys. Lett. B* **177**, 377 (1986).
- [42] N. D. Christensen and C. Duhr, *Comput. Phys. Commun.* **180**, 1614 (2009) [arXiv:0806.4194 [hep-ph]].
- [43] J. Alwall, M. Herquet, F. Maltoni, O. Mattelaer and T. Stelzer, *JHEP* **1106**, 128 (2011) [arXiv:1106.0522 [hep-ph]].
- [44] P. J. Fox, J. Liu, D. Tucker-Smith and N. Weiner, *Phys. Rev. D* **84**, 115006 (2011) [arXiv:1104.4127 [hep-ph]].

- [45] P. Batra, B. A. Dobrescu and D. Spivak, *J. Math. Phys.* **47**, 082301 (2006) [hep-ph/0510181].
- [46] K. Cranmer and I. Yavin, *JHEP* **1104**, 038 (2011) [arXiv:1010.2506 [hep-ex]].
- [47] T. Sjostrand, S. Mrenna and P. Z. Skands, *JHEP* **0605**, 026 (2006) [hep-ph/0603175].
- [48] S. Ovin, X. Rouby and V. Lemaitre, arXiv:0903.2225 [hep-ph].
- [49] J. M. Campbell, R. K. Ellis and C. Williams, *JHEP* **1107**, 018 (2011)
- [50] J. R. Andersen *et al.* [SM and NLO Multileg Working Group Collaboration], arXiv:1003.1241 [hep-ph].
- [51] M. Aliev, H. Lacker, U. Langenfeld, S. Moch, P. Uwer and M. Wiedermann, *Comput. Phys. Commun.* **182**, 1034 (2011)
- [52] L. Moneta *et al.* [arXiv:1009.1003]
- [53] G. Cowan, K. Cranmer, E. Gross and O. Vitells, *Eur. Phys. J. C* **71**, 1554 (2011) [arXiv:1007.1727 [physics.data-an]].
- [54] A. Rajaraman and F. Yu, *Phys. Lett. B* **700**, 126 (2011) [arXiv:1009.2751 [hep-ph]].
- [55] CMS PAS SUS-13-002
- [56] ATLAS-CONF-2013-036
- [57] G. Aad *et al.* [ATLAS Collaboration], *Eur. Phys. J. C* **73**, 2263 (2013)
- [58] S. Chatrchyan *et al.* [CMS Collaboration], *Phys. Rev. Lett.* **110**, 141802 (2013)
- [59] T. Aaltonen *et al.* [CDF Collaboration], *Phys. Rev. Lett.* (2013) [arXiv:1303.2699 [hep-ex]].
- [60] ATLAS-CONF-2013-017
- [61] F. Abe *et al.* [CDF Collaboration], *Phys. Rev. D* **55**, 5263 (1997)
- [62] T. Aaltonen *et al.* [CDF Collaboration], *Phys. Rev. D* **79**, 112002 (2009)
- [63] S. Chatrchyan *et al.* [CMS Collaboration], *Phys. Lett. B* **704**, 123 (2011)
- [64] G. Aad *et al.* [ATLAS Collaboration], *Phys. Lett. B* **712**, 22 (2012)
- [65] CMS Collaboration [CMS Collaboration], CMS-PAS-SUS-13-002.
- [66] S. Bhattacharya, E. Ma and D. Wegman, arXiv:1308.4177 [hep-ph].
- [67] M. Abdullah, K. Bauer, L. Gutierrez, J. Sandy and D. Whiteson, *Phys. Rev. D* **95**, no. 3, 035008 (2017) doi:10.1103/PhysRevD.95.035008 [arXiv:1609.05251 [hep-ph]].

- [68] E. Eichten, K. D. Lane, and M. E. Peskin, “New Tests for Quark and Lepton Substructure,” *Phys. Rev. Lett.* **50** (1983) 811–814. [,369(1983)].
- [69] R. Contino, T. Kramer, M. Son, and R. Sundrum, “Warped/composite phenomenology simplified,” *JHEP* **05** (2007) 074, arXiv:hep-ph/0612180 [hep-ph].
- [70] B. Lillie, J. Shu, and T. M. P. Tait, “Top Compositeness at the Tevatron and LHC,” *JHEP* **04** (2008) 087, arXiv:0712.3057 [hep-ph].
- [71] R. S. Chivukula and H. Georgi, “Composite Technicolor Standard Model,” *Phys.Lett.* **B188** (1987) 99.
- [72] M. A. Shupe, “A Composite Model of Leptons and Quarks,” *Phys. Lett.* **B86** (1979) 87–92.
- [73] D. A. Dicus, D. Karabacak, S. Nandi, and S. K. Rai, “Search for spin-3/2 quarks at the Large Hadron Collider,” *Phys. Rev.* **D87** (2013) no. 1, 015023, arXiv:1208.5811 [hep-ph].
- [74] A. Lenz, “Constraints on a fourth generation of fermions from Higgs Boson searches,” *Adv. High Energy Phys.* **2013** (2013) 910275.
- [75] H. Krebs, E. Epelbaum, and U. G. Meissner, “Redundancy of the off-shell parameters in chiral effective field theory with explicit spin-3/2 degrees of freedom,” *Phys. Lett.* **B683** (2010) 222–228, arXiv:0905.2744 [hep-th].
- [76] **SLD Electroweak Group, DELPHI, ALEPH, SLD, SLD Heavy Flavour Group, OPAL, LEP Electroweak Working Group, L3 Collaboration, S. Schael et al.**, “Precision electroweak measurements on the Z resonance,” *Phys. Rept.* **427** (2006) 257–454, arXiv:hep-ex/0509008 [hep-ex].
- [77] M. E. Peskin and T. Takeuchi, “A New constraint on a strongly interacting Higgs sector,” *Phys. Rev. Lett.* **65** (1990) 964–967.
- [78] **CMS Collaboration, S. Chatrchyan et al.**, “Searches for long-lived charged particles in pp collisions at $\sqrt{s}=7$ and 8 TeV,” *JHEP* **07** (2013) 122, arXiv:1305.0491 [hep-ex].
- [79] **ATLAS Collaboration, G. Aad et al.**, “Searches for heavy long-lived charged particles with the ATLAS detector in proton-proton collisions at $\sqrt{s} = 8$ TeV,” *JHEP* **01** (2015) 068, arXiv:1411.6795 [hep-ex].
- [80] **ATLAS Collaboration, G. Aad et al.**, “Search for metastable heavy charged particles with large ionisation energy loss in pp collisions at $\sqrt{s} = 8$ TeV using the ATLAS experiment,” *Eur. Phys. J.* **C75** (2015) 407, arXiv:1506.05332 [hep-ex].
- [81] **ATLAS Collaboration, G. Aad et al.**, “Search for excited leptons in proton-proton collisions at $\sqrt{s} = 7$ TeV with the ATLAS detector,” *Phys. Rev.* **D85** (2012) 072003, arXiv:1201.3293 [hep-ex].

- [82] **ATLAS** Collaboration, G. Aad *et al.*, “Search for heavy lepton resonances decaying to a Z boson and a lepton in pp collisions at $\sqrt{s} = 8$ TeV with the ATLAS detector,” *JHEP* **09** (2015) 108, [arXiv:1506.01291 \[hep-ex\]](#).
- [83] **ATLAS** Collaboration, G. Aad *et al.*, “Search for type-III Seesaw heavy leptons in pp collisions at $\sqrt{s} = 8$ TeV with the ATLAS Detector,” *Phys. Rev.* **D92** (2015) no. 3, 032001, [arXiv:1506.01839 \[hep-ex\]](#).
- [84] **ATLAS** Collaboration, G. Aad *et al.*, “Search for anomalous production of prompt same-sign lepton pairs and pair-produced doubly charged Higgs bosons with $\sqrt{s} = 8$ TeV pp collisions using the ATLAS detector,” *JHEP* **03** (2015) 041, [arXiv:1412.0237 \[hep-ex\]](#).
- [85] J. Alwall, R. Frederix, S. Frixione, V. Hirschi, F. Maltoni, O. Mattelaer, H. S. Shao, T. Stelzer, P. Torrielli, and M. Zaro, “The automated computation of tree-level and next-to-leading order differential cross sections, and their matching to parton shower simulations,” *JHEP* **07** (2014) 079, [arXiv:1405.0301 \[hep-ph\]](#).
- [86] N. D. Christensen, P. de Aquino, N. Deutschmann, C. Duhr, B. Fuks, C. Garcia-Cely, O. Mattelaer, K. Mawatari, B. Oexl, and Y. Takaesu, “Simulating spin- $\frac{3}{2}$ particles at colliders,” *Eur. Phys. J.* **C73** (2013) no. 10, 2580, [arXiv:1308.1668 \[hep-ph\]](#).
- [87] T. Sjostrand, S. Mrenna, and P. Z. Skands, “PYTHIA 6.4 Physics and Manual,” *JHEP* **05** (2006) 026, [arXiv:hep-ph/0603175 \[hep-ph\]](#).
- [88] M. Abdullah and J. L. Feng, “Reviving bino dark matter with vectorlike fourth generation particles,” *Phys. Rev.* **D93** (2016) 015006, [arXiv:1510.06089 \[hep-ph\]](#).
- [89] M. Abdullah, J. L. Feng, S. Iwamoto and B. Lillard, *Phys. Rev. D* **94**, no. 9, 095018 (2016) [doi:10.1103/PhysRevD.94.095018 \[arXiv:1608.00283 \[hep-ph\]\]](#).
- [90] L. Maiani, “Proceedings: Summer school on particle physics,” Paris, France, 1979.
- [91] M. J. G. Veltman, “The Infrared - Ultraviolet Connection,” *Acta Phys. Polon.* **B12** (1981) 437.
- [92] E. Witten, “Dynamical Breaking of Supersymmetry,” *Nucl. Phys.* **B188** (1981) 513.
- [93] R. K. Kaul, “Gauge Hierarchy in a Supersymmetric Model,” *Phys. Lett.* **B109** (1982) 19.
- [94] S. Dimopoulos, S. Raby, and F. Wilczek, “Supersymmetry and the Scale of Unification,” *Phys. Rev.* **D24** (1981) 1681–1683.
- [95] N. Sakai, “Naturalness in Supersymmetric Guts,” *Z. Phys.* **C11** (1981) 153.
- [96] L. E. Ibanez and G. G. Ross, “Low-Energy Predictions in Supersymmetric Grand Unified Theories,” *Phys. Lett.* **B105** (1981) 439.

- [97] M. B. Einhorn and D. R. T. Jones, “The Weak Mixing Angle and Unification Mass in Supersymmetric SU(5),” *Nucl. Phys.* **B196** (1982) 475.
- [98] H. Goldberg, “Constraint on the Photino Mass from Cosmology,” *Phys. Rev. Lett.* **50** (1983) 1419. [Erratum: *Phys. Rev. Lett.* 103, 099905 (2009)].
- [99] J. R. Ellis, J. S. Hagelin, D. V. Nanopoulos, K. A. Olive, and M. Srednicki, “Supersymmetric Relics from the Big Bang,” *Nucl. Phys.* **B238** (1984) 453–476.
- [100] J. L. Feng, “Naturalness and the Status of Supersymmetry,” *Ann. Rev. Nucl. Part. Sci.* **63** (2013) 351–382, [arXiv:1302.6587 \[hep-ph\]](#).
- [101] N. Craig, “The State of Supersymmetry after Run I of the LHC,” in *Beyond the Standard Model after the first run of the LHC Arcetri, Florence, Italy, May 20-July 12, 2013*. 2013. [arXiv:1309.0528 \[hep-ph\]](#).
- [102] M. E. Peskin and T. Takeuchi, “Estimation of oblique electroweak corrections,” *Phys. Rev.* **D46** (1992) 381–409.
- [103] **Particle Data Group** Collaboration, K. A. Olive *et al.*, “Review of Particle Physics,” *Chin. Phys.* **C38** (2014) 090001.
- [104] G. D. Kribs, T. Plehn, M. Spannowsky, and T. M. P. Tait, “Four generations and Higgs physics,” *Phys. Rev.* **D76** (2007) 075016, [arXiv:0706.3718 \[hep-ph\]](#).
- [105] S. Bar-Shalom, M. Geller, S. Nandi, and A. Soni, “Two Higgs doublets, a 4th generation and a 125 GeV Higgs: A review.,” *Adv. High Energy Phys.* **2013** (2013) 672972, [arXiv:1208.3195 \[hep-ph\]](#).
- [106] S. A. R. Ellis, R. M. Godbole, S. Gopalakrishna, and J. D. Wells, “Survey of vector-like fermion extensions of the Standard Model and their phenomenological implications,” *JHEP* **09** (2014) 130, [arXiv:1404.4398 \[hep-ph\]](#).
- [107] **ATLAS, CMS** Collaboration, G. Aad *et al.*, “Combined Measurement of the Higgs Boson Mass in pp Collisions at $\sqrt{s} = 7$ and 8 TeV with the ATLAS and CMS Experiments,” *Phys. Rev. Lett.* **114** (2015) 191803, [arXiv:1503.07589 \[hep-ex\]](#).
- [108] H. E. Haber and R. Hempfling, “Can the mass of the lightest Higgs boson of the minimal supersymmetric model be larger than $m(Z)$?,” *Phys. Rev. Lett.* **66** (1991) 1815–1818.
- [109] Y. Okada, M. Yamaguchi, and T. Yanagida, “Upper bound of the lightest Higgs boson mass in the minimal supersymmetric standard model,” *Prog. Theor. Phys.* **85** (1991) 1–6.
- [110] J. R. Ellis, G. Ridolfi, and F. Zwirner, “Radiative corrections to the masses of supersymmetric Higgs bosons,” *Phys. Lett.* **B257** (1991) 83–91.

- [111] T. Moroi and Y. Okada, “Radiative corrections to Higgs masses in the supersymmetric model with an extra family and antifamily,” *Mod. Phys. Lett.* **A7** (1992) 187–200.
- [112] T. Moroi and Y. Okada, “Upper bound of the lightest neutral Higgs mass in extended supersymmetric Standard Models,” *Phys. Lett.* **B295** (1992) 73–78.
- [113] K. S. Babu, I. Gogoladze, and C. Kolda, “Perturbative unification and Higgs boson mass bounds,” [arXiv:hep-ph/0410085](#) [[hep-ph](#)].
- [114] K. S. Babu, I. Gogoladze, M. U. Rehman, and Q. Shafi, “Higgs Boson Mass, Sparticle Spectrum and Little Hierarchy Problem in Extended MSSM,” *Phys. Rev.* **D78** (2008) 055017, [arXiv:0807.3055](#) [[hep-ph](#)].
- [115] S. P. Martin, “Extra vector-like matter and the lightest Higgs scalar boson mass in low-energy supersymmetry,” *Phys. Rev.* **D81** (2010) 035004, [arXiv:0910.2732](#) [[hep-ph](#)].
- [116] P. W. Graham, A. Ismail, S. Rajendran, and P. Saraswat, “A Little Solution to the Little Hierarchy Problem: A Vector-like Generation,” *Phys. Rev.* **D81** (2010) 055016, [arXiv:0910.3020](#) [[hep-ph](#)].
- [117] S. W. Ham, S.-A. Shim, C. M. Kim, and S. K. Oh, “Higgs boson masses in an extension of the MSSM with vector-like quarks,” [arXiv:1004.1974](#) [[hep-ph](#)].
- [118] T. Li and D. V. Nanopoulos, “General Gauge and Anomaly Mediated Supersymmetry Breaking in Grand Unified Theories with Vector-Like Particles,” *JHEP* **10** (2011) 090, [arXiv:1005.3798](#) [[hep-ph](#)].
- [119] M. Endo, K. Hamaguchi, S. Iwamoto, and N. Yokozaki, “Higgs Mass and Muon Anomalous Magnetic Moment in Supersymmetric Models with Vector-Like Matters,” *Phys. Rev.* **D84** (2011) 075017, [arXiv:1108.3071](#) [[hep-ph](#)].
- [120] T. Moroi, R. Sato, and T. T. Yanagida, “Extra Matters Decree the Relatively Heavy Higgs of Mass about 125 GeV in the Supersymmetric Model,” *Phys. Lett.* **B709** (2012) 218–221, [arXiv:1112.3142](#) [[hep-ph](#)].
- [121] M. Endo, K. Hamaguchi, S. Iwamoto, and N. Yokozaki, “Higgs mass, muon $g-2$, and LHC prospects in gauge mediation models with vector-like matters,” *Phys. Rev.* **D85** (2012) 095012, [arXiv:1112.5653](#) [[hep-ph](#)].
- [122] S. P. Martin and J. D. Wells, “Implications of gauge-mediated supersymmetry breaking with vector-like quarks and a 125 GeV Higgs boson,” *Phys. Rev.* **D86** (2012) 035017, [arXiv:1206.2956](#) [[hep-ph](#)].
- [123] M. Endo, K. Hamaguchi, K. Ishikawa, S. Iwamoto, and N. Yokozaki, “Gauge Mediation Models with Vectorlike Matters at the LHC,” *JHEP* **01** (2013) 181, [arXiv:1212.3935](#) [[hep-ph](#)].

- [124] W.-Z. Feng and P. Nath, “Higgs diphoton rate and mass enhancement with vectorlike leptons and the scale of supersymmetry,” *Phys. Rev.* **D87** (2013) 075018, arXiv:1303.0289 [hep-ph].
- [125] A. Joglekar, P. Schwaller, and C. E. M. Wagner, “A Supersymmetric Theory of Vector-like Leptons,” *JHEP* **07** (2013) 046, arXiv:1303.2969 [hep-ph].
- [126] R. Dermisek and A. Raval, “Explanation of the Muon $g-2$ Anomaly with Vectorlike Leptons and its Implications for Higgs Decays,” *Phys. Rev.* **D88** (2013) 013017, arXiv:1305.3522 [hep-ph].
- [127] W. Fischler and W. Tangarife, “Vector-like Fields, Messenger Mixing and the Higgs mass in Gauge Mediation,” *JHEP* **05** (2014) 151, arXiv:1310.6369 [hep-ph].
- [128] X. Chang and R. Huo, “Electroweak baryogenesis in the MSSM with vectorlike superfields,” *Phys. Rev.* **D89** (2014) no. 3, 036005, arXiv:1402.4204 [hep-ph].
- [129] C. Faroughy and K. Grizzard, “Raising the Higgs mass in supersymmetry with $t-t'$ mixing,” *Phys. Rev.* **D90** (2014) 035024, arXiv:1405.4116 [hep-ph].
- [130] Y.-L. Tang, “Unification of gauge couplings and the Higgs mass in vectorlike particle theories extended into NMSSM,” *Phys. Rev.* **D90** (2014) 075020, arXiv:1409.5858 [hep-ph].
- [131] Z. Lalak, M. Lewicki, and J. D. Wells, “Higgs boson mass and high-luminosity LHC probes of supersymmetry with vectorlike top quark,” *Phys. Rev.* **D91** (2015) 095022, arXiv:1502.05702 [hep-ph].
- [132] K. Nickel and F. Staub, “Precise determination of the Higgs mass in supersymmetric models with vectorlike tops and the impact on naturalness in minimal GMSB,” *JHEP* **07** (2015) 139, arXiv:1505.06077 [hep-ph].
- [133] K. A. Olive and M. Srednicki, “New Limits on Parameters of the Supersymmetric Standard Model from Cosmology,” *Phys. Lett.* **B230** (1989) 78.
- [134] K. Griest, M. Kamionkowski, and M. S. Turner, “Supersymmetric Dark Matter Above the W Mass,” *Phys. Rev.* **D41** (1990) 3565–3582.
- [135] **ATLAS** Collaboration, G. Aad *et al.*, “Search for squarks and gluinos with the ATLAS detector in final states with jets and missing transverse momentum using $\sqrt{s} = 8$ TeV proton–proton collision data,” *JHEP* **09** (2014) 176, arXiv:1405.7875 [hep-ex].
- [136] **CMS** Collaboration, V. Khachatryan *et al.*, “Searches for Supersymmetry using the M_{T2} Variable in Hadronic Events Produced in pp Collisions at 8 TeV,” *JHEP* **05** (2015) 078, arXiv:1502.04358 [hep-ex].
- [137] K. Griest and D. Seckel, “Three exceptions in the calculation of relic abundances,” *Phys.Rev.* **D43** (1991) 3191–3203.

- [138] R. H. Cyburt, J. Ellis, B. D. Fields, F. Luo, K. A. Olive, and V. C. Spanos, “Nucleosynthesis Constraints on a Massive Gravitino in Neutralino Dark Matter Scenarios,” *JCAP* **0910** (2009) 021, [arXiv:0907.5003 \[astro-ph.CO\]](#).
- [139] Y. Konishi, S. Ohta, J. Sato, T. Shimomura, K. Sugai, and M. Yamanaka, “First evidence of the constrained minimal supersymmetric standard model is appearing soon,” *Phys. Rev.* **D89** (2014) 075006, [arXiv:1309.2067 \[hep-ph\]](#).
- [140] N. Desai, J. Ellis, F. Luo, and J. Marrouche, “Closing in on the Tip of the CMSSM Stau Coannihilation Strip,” *Phys. Rev.* **D90** (2014) 055031, [arXiv:1404.5061 \[hep-ph\]](#).
- [141] J. L. Feng, S. Iwamoto, Y. Shadmi, and S. Tarem, “Long-Lived Sleptons at the LHC and a 100 TeV Proton Collider,” [arXiv:1505.02996 \[hep-ph\]](#).
- [142] A. Joglekar, P. Schwaller, and C. E. M. Wagner, “Dark Matter and Enhanced Higgs to Di-photon Rate from Vector-like Leptons,” *JHEP* **12** (2012) 064, [arXiv:1207.4235 \[hep-ph\]](#).
- [143] N. Kumar and S. P. Martin, “Vectorlike leptons at the Large Hadron Collider,” *Phys. Rev.* **D92** (2015) 115018, [arXiv:1510.03456 \[hep-ph\]](#).
- [144] E. W. Kolb and M. S. Turner, *The Early Universe*. Addison-Wesley, Redwood City, CA, 1990.
- [145] M. Carena, J. R. Espinosa, M. Quiros, and C. E. M. Wagner, “Analytical expressions for radiatively corrected Higgs masses and couplings in the MSSM,” *Phys. Lett.* **B355** (1995) 209–221, [arXiv:hep-ph/9504316 \[hep-ph\]](#).
- [146] M. Drees and M. Nojiri, “Neutralino - nucleon scattering revisited,” *Phys. Rev.* **D48** (1993) 3483–3501, [arXiv:hep-ph/9307208 \[hep-ph\]](#).
- [147] G. B aflanger, F. Boudjema, A. Pukhov, and A. Semenov, “micrOMEGAs4.1: two dark matter candidates,” *Comput. Phys. Commun.* **192** (2015) 322–329, [arXiv:1407.6129 \[hep-ph\]](#).
- [148] P. Junnarkar and A. Walker-Loud, “Scalar strange content of the nucleon from lattice QCD,” *Phys. Rev.* **D87** (2013) 114510, [arXiv:1301.1114 \[hep-lat\]](#).
- [149] J. M. Alarcon, L. S. Geng, J. Martin Camalich, and J. A. Oller, “The strangeness content of the nucleon from effective field theory and phenomenology,” *Phys. Lett.* **B730** (2014) 342–346, [arXiv:1209.2870 \[hep-ph\]](#).
- [150] J. M. Alarcon, J. Martin Camalich, and J. A. Oller, “The chiral representation of the πN scattering amplitude and the pion-nucleon sigma term,” *Phys. Rev.* **D85** (2012) 051503, [arXiv:1110.3797 \[hep-ph\]](#).
- [151] M. Hoferichter, J. Ruiz de Elvira, B. Kubis, and U.-G. Meißner, “High-Precision Determination of the Pion-Nucleon σ Term from Roy-Steiner Equations,” *Phys. Rev. Lett.* **115** (2015) 092301, [arXiv:1506.04142 \[hep-ph\]](#).

- [152] G. Belanger, F. Boudjema, A. Pukhov, and A. Semenov, “micrOMEGAs: Version 1.3,” *Comput. Phys. Commun.* **174** (2006) 577–604, [arXiv:hep-ph/0405253](#) [hep-ph].
- [153] J. L. Feng *et al.*, “Planning the Future of U.S. Particle Physics (Snowmass 2013): Chapter 4: Cosmic Frontier,” in *Community Summer Study 2013: Snowmass on the Mississippi (CSS2013) Minneapolis, MN, USA, July 29-August 6, 2013*. 2014. [arXiv:1401.6085](#) [hep-ex].
- [154] **PICO** Collaboration, C. Amole *et al.*, “Dark Matter Search Results from the PICO-2L C₃F₈ Bubble Chamber,” *Phys. Rev. Lett.* **114** (2015) no. 23, 231302, [arXiv:1503.00008](#) [astro-ph.CO].
- [155] **Fermi-LAT**, **MAGIC** Collaboration, M. L. Ahnen *et al.*, “Limits to dark matter annihilation cross-section from a combined analysis of MAGIC and Fermi-LAT observations of dwarf satellite galaxies,” *JCAP* **1602** (2016) 039, [arXiv:1601.06590](#) [astro-ph.HE].
- [156] **CTA Consortium** Collaboration, J. Carr *et al.*, “Prospects for Indirect Dark Matter Searches with the Cherenkov Telescope Array (CTA),” in *Proceedings, 34th International Cosmic Ray Conference (ICRC 2015)*. 2015. [arXiv:1508.06128](#) [astro-ph.HE].
- [157] K. N. Abazajian and R. E. Keeley, “Bright gamma-ray Galactic Center excess and dark dwarfs: Strong tension for dark matter annihilation despite Milky Way halo profile and diffuse emission uncertainties,” *Phys. Rev.* **D93** (2016) no. 8, 083514, [arXiv:1510.06424](#) [hep-ph].
- [158] **Fermi-LAT** Collaboration, M. Ackermann *et al.*, “Searching for Dark Matter Annihilation from Milky Way Dwarf Spheroidal Galaxies with Six Years of Fermi Large Area Telescope Data,” *Phys. Rev. Lett.* **115** (2015) no. 23, 231301, [arXiv:1503.02641](#) [astro-ph.HE].
- [159] V. Bonnivard *et al.*, “Dark matter annihilation and decay in dwarf spheroidal galaxies: The classical and ultrafaint dSphs,” *Mon. Not. Roy. Astron. Soc.* **453** (2015) no. 1, 849–867, [arXiv:1504.02048](#) [astro-ph.HE].
- [160] **IceCube** Collaboration, M. G. Aartsen *et al.*, “Search for Dark Matter Annihilation in the Galactic Center with IceCube-79,” *Eur. Phys. J.* **C75** (2015) 492, [arXiv:1505.07259](#) [astro-ph.HE].
- [161] M. Di Mauro, F. Donato, N. Fornengo, and A. Vittino, “Dark matter vs. astrophysics in the interpretation of AMS-02 electron and positron data,” *JCAP* **1605** (2016) 031, [arXiv:1507.07001](#) [astro-ph.HE].
- [162] Y. D. A. Coutinho, J. A. Martins Simoes, C. M. Porto, and P. P. Queiroz Filho, “Single heavy lepton production in hadron hadron collisions,” *Phys. Rev.* **D57** (1998) 6975–6980.

- [163] CMS Collaboration, “Searches for Long-lived Charged Particles in Proton-Proton Collisions at $\sqrt{s} = 13$ TeV,”. CMS-PAS-EXO-15-010.
- [164] A. Falkowski, D. M. Straub, and A. Vicente, “Vector-like leptons: Higgs decays and collider phenomenology,” *JHEP* **05** (2014) 092, arXiv:1312.5329 [hep-ph].
- [165] CMS Collaboration, S. Chatrchyan *et al.*, “Search for anomalous production of events with three or more leptons in pp collisions at $\sqrt{s} = 8$ TeV,” *Phys. Rev.* **D90** (2014) 032006, arXiv:1404.5801 [hep-ex].
- [166] R. Dermisek, J. P. Hall, E. Lunghi, and S. Shin, “Limits on Vectorlike Leptons from Searches for Anomalous Production of Multi-Lepton Events,” *JHEP* **12** (2014) 013, arXiv:1408.3123 [hep-ph].
- [167] L3 Collaboration, P. Achard *et al.*, “Search for heavy neutral and charged leptons in e^+e^- annihilation at LEP,” *Phys. Lett.* **B517** (2001) 75–85, arXiv:hep-ex/0107015 [hep-ex].
- [168] E. De Pree, M. Sher, and I. Turan, “Production of single heavy charged leptons at a linear collider,” *Phys. Rev.* **D77** (2008) 093001, arXiv:0803.0996 [hep-ph].
- [169] A. Djouadi, J. Ellis, R. Godbole, and J. Quevillon, “Future Collider Signatures of the Possible 750 GeV State,” *JHEP* **03** (2016) 205, arXiv:1601.03696 [hep-ph].
- [170] CMS Collaboration, V. Khachatryan *et al.*, “Searches for electroweak production of charginos, neutralinos, and sleptons decaying to leptons and W, Z, and Higgs bosons in pp collisions at 8 TeV,” *Eur. Phys. J.* **C74** (2014) 3036, arXiv:1405.7570 [hep-ex].
- [171] J. Eckel, M. J. Ramsey-Musolf, W. Shepherd, and S. Su, “Impact of LSP Character on Slepton Reach at the LHC,” *JHEP* **11** (2014) 117, arXiv:1408.2841 [hep-ph].
- [172] T. Sjostrand, S. Mrenna, and P. Z. Skands, “PYTHIA 6.4 Physics and Manual,” *JHEP* **05** (2006) 026, arXiv:hep-ph/0603175.
- [173] DELPHES 3 Collaboration, J. de Favereau, C. Delaere, P. Demin, A. Giammanco, V. Lemaître, A. Mertens, and M. Selvaggi, “DELPHES 3, A modular framework for fast simulation of a generic collider experiment,” *JHEP* **02** (2014) 057, arXiv:1307.6346 [hep-ex].
- [174] M. Cacciari and G. P. Salam, “Dispelling the N^3 myth for the k_t jet-finder,” *Phys. Lett.* **B641** (2006) 57–61, arXiv:hep-ph/0512210 [hep-ph].
- [175] M. Cacciari, G. P. Salam, and G. Soyez, “FastJet User Manual,” *Eur. Phys. J.* **C72** (2012) 1896, arXiv:1111.6097 [hep-ph].
- [176] ATLAS Collaboration, G. Aad *et al.*, “Search for the direct production of charginos, neutralinos and staus in final states with at least two hadronically decaying taus and missing transverse momentum in pp collisions at $\sqrt{s} = 8$ TeV with the ATLAS detector,” *JHEP* **10** (2014) 096, arXiv:1407.0350 [hep-ex].

- [177] CMS Collaboration, “Search for electroweak production of charginos in final states with two tau leptons in pp collisions at $\sqrt{s} = 8$ TeV,”. CMS-PAS-SUS-14-022.
- [178] K. Harigaya, S. Matsumoto, M. M. Nojiri, and K. Tobioka, “Search for the Top Partner at the Lhc Using Multi-B-Jet Channels,” *Phys.Rev.* **D86** (2012) 015005, arXiv:1204.2317 [hep-ph].
- [179] M. Endo, K. Hamaguchi, K. Ishikawa, and M. Stoll, “Reconstruction of Vector-like Top Partner from Fully Hadronic Final States,” *Phys. Rev.* **D90** (2014) no. 5, 055027, arXiv:1405.2677 [hep-ph].
- [180] F. Mayet *et al.*, “A review of the discovery reach of directional Dark Matter detection,” *Phys. Rept.* **627** (2016) 1–49, arXiv:1602.03781 [astro-ph.CO].
- [181] M. Abdullah, I. Galon, Y. Shadmi, and Y. Shirman, “Flavored Gauge Mediation, A Heavy Higgs, and Supersymmetric Alignment,” *JHEP* **06** (2013) 057, arXiv:1209.4904 [hep-ph].
- [182] M. Carena and H. E. Haber, “Higgs boson theory and phenomenology,” *Prog. Part. Nucl. Phys.* **50** (2003) 63–152, arXiv:hep-ph/0208209 [hep-ph].
- [183] M. Dine, W. Fischler and M. Srednicki, *Nucl. Phys. B* **189**, 575 (1981); S. Dimopoulos and S. Raby, *Nucl. Phys. B* **192**, 353 (1981); M. Dine and W. Fischler, *Phys. Lett. B* **110**, 227 (1982); M. Dine and M. Srednicki, *Nucl. Phys. B* **202**, 238 (1982); L. Alvarez-Gaume, M. Claudson and M. B. Wise, *Nucl. Phys. B* **207**, 96 (1982); C. R. Nappi and B. A. Ovrut, *Phys. Lett. B* **113**, 175 (1982).
- [184] M. Dine, A. E. Nelson and Y. Shirman, *Phys. Rev. D* **51**, 1362 (1995) [hep-ph/9408384]; M. Dine, A. E. Nelson, Y. Nir and Y. Shirman, *Phys. Rev. D* **53**, 2658 (1996) [hep-ph/9507378].
- [185] M. A. Ajaib, I. Gogoladze, F. Nasir, and Q. Shafi, “Revisiting mGMSB in Light of a 125 GeV Higgs,” *Phys. Lett.* **B713** (2012) 462–468, arXiv:1204.2856 [hep-ph].
- [186] J. L. Feng, Z. Surujon, and H.-B. Yu, “Confluence of Constraints in Gauge Mediation: The 125 GeV Higgs Boson and Goldilocks Cosmology,” *Phys. Rev.* **D86** (2012) 035003, arXiv:1205.6480 [hep-ph].
- [187] P. Meade, N. Seiberg, and D. Shih, “General Gauge Mediation,” *Prog. Theor. Phys. Suppl.* **177** (2009) 143–158, arXiv:0801.3278 [hep-ph].
- [188] P. Draper, P. Meade, M. Reece, and D. Shih, “Implications of a 125 GeV Higgs for the MSSM and Low-Scale SUSY Breaking,” *Phys. Rev.* **D85** (2012) 095007, arXiv:1112.3068 [hep-ph].
- [189] Y. Shadmi and P. Z. Szabo, “Flavored Gauge-Mediation,” *JHEP* **06** (2012) 124, arXiv:1103.0292 [hep-ph].

- [190] M. Dine, Y. Nir, and Y. Shirman, “Variations on minimal gauge mediated supersymmetry breaking,” *Phys. Rev.* **D55** (1997) 1501–1508, arXiv:hep-ph/9607397 [hep-ph].
- [191] M. Badziak, E. Dudas, M. Olechowski, and S. Pokorski, “Inverted Sfermion Mass Hierarchy and the Higgs Boson Mass in the MSSM,” *JHEP* **07** (2012) 155, arXiv:1205.1675 [hep-ph].
- [192] J. L. Feng, C. G. Lester, Y. Nir, and Y. Shadmi, “The Standard Model and Supersymmetric Flavor Puzzles at the Large Hadron Collider,” *Phys. Rev.* **D77** (2008) 076002, arXiv:0712.0674 [hep-ph].
- [193] I. Galon and Y. Shadmi, “Kinematic Edges with Flavor Splitting and Mixing,” *Phys. Rev.* **D85** (2012) 015010, arXiv:1108.2220 [hep-ph].
- [194] Y. Shadmi, “Flavor and LHC Searches for New Physics,” *Eur. Phys. J.* **C72** (2012) 2104, arXiv:1201.5275 [hep-ph].
- [195] Y. Nir and N. Seiberg, “Should squarks be degenerate?,” *Phys. Lett.* **B309** (1993) 337–343, arXiv:hep-ph/9304307 [hep-ph].
- [196] A. Albaid and K. S. Babu, “Higgs boson of mass 125 GeV in GMSB models with messenger-matter mixing,” *Phys. Rev.* **D88** (2013) 055007, arXiv:1207.1014 [hep-ph].
- [197] Z. Kang, T. Li, T. Liu, C. Tong, and J. M. Yang, “A Heavy SM-like Higgs and a Light Stop from Yukawa-Deflected Gauge Mediation,” *Phys. Rev.* **D86** (2012) 095020, arXiv:1203.2336 [hep-ph].
- [198] N. Craig, S. Knapen, D. Shih, and Y. Zhao, “A Complete Model of Low-Scale Gauge Mediation,” *JHEP* **03** (2013) 154, arXiv:1206.4086 [hep-ph].
- [199] G. F. Giudice and R. Rattazzi, “Extracting supersymmetry breaking effects from wave function renormalization,” *Nucl. Phys.* **B511** (1998) 25–44, arXiv:hep-ph/9706540 [hep-ph].
- [200] T. Han and R.-J. Zhang, “Direct messenger - matter interactions in gauge - mediated supersymmetry breaking models,” *Phys. Lett.* **B428** (1998) 120–128, arXiv:hep-ph/9802422 [hep-ph].
- [201] Z. Chacko and E. Ponton, “Yukawa deflected gauge mediation,” *Phys. Rev.* **D66** (2002) 095004, arXiv:hep-ph/0112190 [hep-ph].
- [202] F. R. Joaquim and A. Rossi, “Gauge and Yukawa mediated supersymmetry breaking in the triplet seesaw scenario,” *Phys. Rev. Lett.* **97** (2006) 181801, arXiv:hep-ph/0604083 [hep-ph].
- [203] F. R. Joaquim and A. Rossi, “Phenomenology of the triplet seesaw mechanism with Gauge and Yukawa mediation of SUSY breaking,” *Nucl. Phys.* **B765** (2007) 71–117, arXiv:hep-ph/0607298 [hep-ph].

- [204] H. E. Haber, R. Hempfling, and A. H. Hoang, “Approximating the radiatively corrected Higgs mass in the minimal supersymmetric model,” *Z. Phys.* **C75** (1997) 539–554, arXiv:hep-ph/9609331 [hep-ph].
- [205] B. C. Allanach, “SOFTSUSY: a program for calculating supersymmetric spectra,” *Comput. Phys. Commun.* **143** (2002) 305–331, arXiv:hep-ph/0104145 [hep-ph].
- [206] S. P. Martin, *Phys. Rev. D* **55**, 3177 (1997) [hep-ph/9608224]; S. Dimopoulos, G. F. Giudice and A. Pomarol, *Phys. Lett. B* **389**, 37 (1996) [hep-ph/9607225].
- [207] **ATLAS** Collaboration, “Search for squarks and gluinos with the ATLAS detector using final states with jets and missing transverse momentum and 5.8 fb^{-1} of $\sqrt{s}=8$ TeV proton-proton collision data,”.
- [208] S. Chatrchyan *et al.* [CMS Collaboration], arXiv:1303.2985 [hep-ex].
- [209] **ATLAS** Collaboration, G. Aad *et al.*, “Search for diphoton events with large missing transverse momentum in 7 TeV proton-proton collision data with the ATLAS detector,” *Phys. Lett.* **B718** (2012) 411–430, arXiv:1209.0753 [hep-ex].
- [210] J. Barnard, B. Farmer, T. Gherghetta, and M. White, “Natural gauge mediation with a bino NLSP at the LHC,” *Phys. Rev. Lett.* **109** (2012) 241801, arXiv:1208.6062 [hep-ph].
- [211] J. L. Feng, B. T. Smith, and F. Takayama, “Goldilocks Supersymmetry: Simultaneous Solution to Dark Matter and Flavor Problems of Supersymmetry,” *Phys. Rev. Lett.* **100** (2008) 021302, arXiv:0709.0297 [hep-ph].
- [212] **ATLAS** Collaboration, G. Aad *et al.*, “Searches for heavy long-lived sleptons and R-Hadrons with the ATLAS detector in pp collisions at $\sqrt{s} = 7$ TeV,” *Phys. Lett.* **B720** (2013) 277–308, arXiv:1211.1597 [hep-ex].
- [213] J. L. Evans, M. Ibe, and T. T. Yanagida, “Relatively Heavy Higgs Boson in More Generic Gauge Mediation,” *Phys. Lett.* **B705** (2011) 342–348, arXiv:1107.3006 [hep-ph].
- [214] J. L. Evans, M. Ibe, S. Shirai, and T. T. Yanagida, “A 125GeV Higgs Boson and Muon $g-2$ in More Generic Gauge Mediation,” *Phys. Rev.* **D85** (2012) 095004, arXiv:1201.2611 [hep-ph].
- [215] J. A. Evans and D. Shih, “Surveying Extended GMSB Models with $m_h=125$ GeV,” *JHEP* **08** (2013) 093, arXiv:1303.0228 [hep-ph].
- [216] N. Arkani-Hamed, G. F. Giudice, M. A. Luty, and R. Rattazzi, “Supersymmetry breaking loops from analytic continuation into superspace,” *Phys. Rev.* **D58** (1998) 115005, arXiv:hep-ph/9803290 [hep-ph].
- [217] S. P. Ahlen, F. T. Avignone, R. L. Brodzinski, A. K. Drukier, G. Gelmini, and D. N. Spergel, “Limits on Cold Dark Matter Candidates from an Ultralow Background Germanium Spectrometer,” *Phys. Lett.* **B195** (1987) 603–608.

- [218] G. Jungman, M. Kamionkowski, and K. Griest, “Supersymmetric dark matter,” *Phys. Rept.* **267** (1996) 195–373, arXiv:hep-ph/9506380 [hep-ph].
- [219] J. Anderson *et al.*, “Snowmass Energy Frontier Simulations,” in *Community Summer Study 2013: Snowmass on the Mississippi (CSS2013) Minneapolis, MN, USA, July 29-August 6, 2013*. 2013. arXiv:1309.1057 [hep-ex].
- [220] A. Avetisyan *et al.*, “Methods and Results for Standard Model Event Generation at $\sqrt{s} = 14$ TeV, 33 TeV and 100 TeV Proton Colliders (A Snowmass Whitepaper),” in *Community Summer Study 2013: Snowmass on the Mississippi (CSS2013) Minneapolis, MN, USA, July 29-August 6, 2013*. 2013. arXiv:1308.1636 [hep-ex].
- [221] A. Avetisyan *et al.*, “Snowmass Energy Frontier Simulations using the Open Science Grid (A Snowmass 2013 whitepaper),” in *Community Summer Study 2013: Snowmass on the Mississippi (CSS2013) Minneapolis, MN, USA, July 29-August 6, 2013*. 2013. arXiv:1308.0843 [hep-ex].
- [222] M. Cacciari, G. P. Salam, and G. Soyez, “The Anti-k(t) jet clustering algorithm,” *JHEP* **04** (2008) 063, arXiv:0802.1189 [hep-ph].
- [223] **ATLAS** Collaboration, G. Aad *et al.*, “Search for direct production of charginos and neutralinos in events with three leptons and missing transverse momentum in $\sqrt{s} = 8$ TeV *pp* collisions with the ATLAS detector,” *JHEP* **04** (2014) 169, arXiv:1402.7029 [hep-ex].
- [224] A. L. Read, “Presentation of search results: The CL(s) technique,” *J. Phys.* **G28** (2002) 2693–2704.
- [225] N. Craig, P. Draper, K. Kong, Y. Ng and D. Whiteson, arXiv:1610.09392 [hep-ph].

Appendix A

Derivation of the soft terms

In this Appendix, we describe the calculation of the soft terms. As pointed out in [199], these can be extracted from the wave function renormalizations of the light fields, treating the heavy threshold as a spurion. The main advantage of this method is that the running of the wave function renormalizations, as well as of the various couplings, is only needed at one-loop. The method of [199] was used in [201] to obtain the soft terms in models with messenger-matter couplings. However, the analysis of [201], as well as the analysis in an earlier version of this article, did not treat the matter-messenger mixing correctly. In A.1 we clarify this issue by discussing a simple toy model. In A.4, we generalize the results to models with multiple fields and couplings. Our final results are given in A.5. As a double check of our derivation, we explicitly calculate the relevant contributions, namely the mixed $y^2 Y^2$ terms, in A.6.

A.1 Analytic continuation in the presence of mixing

To discuss the calculation of the soft terms in the presence of messenger-SM mixings, we first consider a simple toy model, with the superpotential

$$W = X\bar{D}D + (y^0 D + Y^0 H)le. \quad (\text{A.1})$$

Here $X = M + F\theta^2$ is the SUSY breaking spurion, \bar{D} , D , H , l and e are singlet fields, and we use the superscript ⁰ to denote the superpotential couplings y^0 and Y^0 in order to distinguish them from the running couplings.

Our analysis closely follows [201], which applied the method of [199] to models with multiple couplings, in which one cannot integrate the one-loop RGEs to obtain closed-form expressions for the wave function renormalizations and couplings. The necessary ingredients in the calculation are the RGE's for the various couplings, and the boundary conditions for these couplings. In the absence of mixing between the messengers and SM fields, there is a clear distinction between the messengers and light fields. In our toy model however, H and D mix, and as a result, there is some ambiguity in the identification of the messenger and Higgs couplings. The key in the calculation is therefore the correct matching of the high-energy and low-energy theories, which we will perform by identifying the *physical* heavy and light combinations of messenger and Higgs fields, and by demanding that the physical coupling of the light combination is continuous across the threshold.

Let us first recall the main results of [199]. At leading order in F/M^2 , the soft mass of the light field f can be extracted from its wave function renormalization Z_f ,

$$m_f^2(\mu) = -\frac{1}{4} \frac{\partial^2 \ln Z_f(\mu)}{\partial \ln M^2} \frac{F^2}{M^2}, \quad (\text{A.2})$$

at $\mu \leq M$. This relies on the fact that, at this order, the only threshold dependence

enters through the one-loop running of Z_f , and therefore one can obtain the soft masses by promoting M to a superfield. Specifically, as argued in [199] based on symmetries and holomorphy, $Z_f(M) \rightarrow Z_f(\sqrt{X^\dagger X})$. Note that, since the theory is defined at a scale Λ above M , the derivatives with respect to M are taken while holding the physical couplings at Λ fixed. It is therefore natural to choose a canonical Kähler potential at Λ , and to hold the superpotential couplings fixed while taking derivatives with respect to M .

It will be convenient to rewrite our model by defining, $\phi_1 \equiv D$, $\phi_2 \equiv H$, $y_1^0 \equiv y^0$ and $y_2^0 \equiv Y^0$. The high energy theory is then defined at the cutoff Λ , by the superpotential

$$W = X \bar{D} \phi_1 + y_i^0 \phi_i l e \quad (\text{A.3})$$

where $i = 1, 2$. As noted above, we take the Kähler potential to be canonical at Λ .

At any scale μ below Λ and above the messenger scale, the renormalized fields are

$$\phi_r(\mu)_i \equiv Z^{1/2}(\mu)_{ij} \phi_j \quad l_r(\mu) \equiv Z_l^{1/2}(\mu) l, \quad e_r(\mu) \equiv Z_e^{1/2}(\mu) e, \quad (\text{A.4})$$

Here $Z^{1/2}$ is the square-root of the two-by-two wave-function renormalization matrix Z . The running couplings are given by

$$y_i(\mu) = Z_l^{-1/2}(\mu) Z_e^{-1/2}(\mu) Z^{-1/2}(\mu)_{ji} y_j^0. \quad (\text{A.5})$$

Note that Z is a real superfield. At one loop, Z runs according to

$$\frac{dZ}{dt} = Z^{1/2} \gamma Z^{1/2}, \quad (\text{A.6})$$

where γ is the two-by-two matrix of anomalous dimensions.

At the messenger scale μ_X , we have a heavy combination $\tilde{\phi}_{r1}$ and (the orthogonal) light

combination $\tilde{\phi}_{r2}$,

$$\tilde{\phi}_{r1} = [Z^{-1/2}(\mu_X)_{11}\phi_{r1} + Z^{-1/2}(\mu_X)_{12}\phi_{r2}] / C(\mu_X) \quad (\text{A.7})$$

$$\tilde{\phi}_{r2} = [Z^{-1/2}(\mu_X)_{11}\phi_{r2} - Z^{-1/2}(\mu_X)_{21}\phi_{r1}] / C(\mu_X) \quad (\text{A.8})$$

where

$$C(\mu_X) = \sqrt{(Z^{-1/2}(\mu_X)_{11})^2 + |Z^{-1/2}(\mu_X)_{12}|^2} \quad (\text{A.9})$$

and where we used

$$(Z^{-1/2*})_{ij} = (Z^{-1/2})_{ji} \quad (\text{A.10})$$

We can now find the physical couplings at the threshold. The physical coupling of the heavy combination $\tilde{\phi}_{r1}$ to l and e is,

$$\tilde{y}_1(\mu_X) = Z_l^{-1/2}(\mu_X) Z_e^{-1/2}(\mu_X) C(\mu_X) \left[y_1^0 + \frac{y_2^0 Z_{21}^{-1/2}(\mu_X) (Z_{11}^{-1/2}(\mu_X) + Z_{22}^{-1/2}(\mu_X))}{C(\mu_X)^2} \right], \quad (\text{A.11})$$

and the physical coupling of the light combination $\tilde{\phi}_{r2}$ to l and e is,

$$\tilde{y}_2(\mu_X) = Z_l^{-1/2}(\mu_X) Z_e^{-1/2}(\mu_X) \frac{Z^{-1/2}(\mu_X)_{11}Z^{-1/2}(\mu_X)_{22} - |Z^{-1/2}(\mu_X)_{12}|^2}{\sqrt{|Z^{-1/2}(\mu_X)_{11}|^2 + |Z^{-1/2}(\mu_X)_{12}|^2}} y_2^0. \quad (\text{A.12})$$

The physical messenger scale is

$$\mu_X^2 = (|Z^{-1/2}(\mu_X)_{11}|^2 + |Z^{-1/2}(\mu_X)_{12}|^2) X^\dagger X. \quad (\text{A.13})$$

To leading order, we can replace μ_X^2 by $X^\dagger X$, since the difference between the two gives a 3-loop correction to the soft masses (see also [216]). In the following we will therefore set $\mu_X = M$. Furthermore, the expression for the soft masses (A.2) involves the running of Z and the couplings at one-loop only. Thus we only need to match the couplings at the

threshold at one-loop, and at this order the coupling of the heavy combination is

$$\tilde{y}_1(M) = Z_l^{-1/2}(M) Z_e^{-1/2}(M) Z^{-1/2}(M)_{11} (y_1^0 + 2Z^{-1/2}(M)_{21} y_2^0) , \quad (\text{A.14})$$

while the coupling of the light combination is,

$$\tilde{y}_2(M) = Z_l^{-1/2}(M) Z_e^{-1/2}(M) Z^{-1/2}(M)_{22} y_2^0 . \quad (\text{A.15})$$

Equations (A.14) and (A.15) are the key results of the preceding analysis, and lead to the main difference between our results and the results of [201]. The point is that these couplings do not coincide with the running couplings $y_i(M)$ of eqn. (A.5). In particular, the coupling of the light combination at the threshold, $\tilde{y}_2(M)$, does not involve either y_1^0 or the mixed anomalous dimension γ_{12} since at one loop $(Z^{-1/2})_{22}$ only depends on γ_{22} . Consequently, as we will see below, the soft mass of the light combination H does not depend on the mixed anomalous dimension γ_{12} . This is precisely what one would expect intuitively¹. On the other hand, the coupling of the heavy combination (A.14) involves both y_1^0 and y_2^0 , with the latter multiplied by the mixed anomalous dimension γ_{12} . However, this contribution appears with a factor of 2 compared to the analogous term in the running coupling $y_1(M)$.

The two conclusions of the above discussion, namely, the absence of γ_{12} in the coupling of the light combination, and the factor of 2 multiplying γ_{12} in the coupling of the heavy combination, only involve the fields H and D , and are not affected by the structure of the couplings to the remaining fields l and e . These conclusions therefore carry over trivially to the full 3-generation model. In other words, we only need to integrate out the heavy field once, and at one-loop, this procedure only involves the wave-function renormalizations of H and D .

¹In fact, in the earlier version of this article, this intuition motivated us to ignore the contributions of γ_{12} in the soft masses. This is indeed correct for H , but not for the other SM fields.

We can now turn to the low energy theory. Clearly, this theory can be written in terms of the fields l , e , and H . Its coupling is defined by matching to the high scale theory at the threshold. That is, we require that the running coupling in the low-energy theory, $Y(\mu)$ match the physical coupling of the light combination at the threshold M at one-loop,

$$Y(M) = \tilde{y}_2(M) \tag{A.16}$$

with $\tilde{y}_2(M)$ given by eqn. (A.15). The low-energy theory is therefore defined by

$$W = Y^0 H l e \tag{A.17}$$

with $Z_l(M)$, $Z_e(M)$ and $Z_H(M)$ continuous across the threshold. More precisely, for the latter²,

$$Z_H(M) = Z_{22}(M). \tag{A.18}$$

Thus, both the wave-function renormalization and the physical coupling of the light combination are continuous across the threshold as one would expect, but, as noted above, the coupling of this combination is different from the running coupling $y_2(M)$.

Note that, since we only have a single combination of ϕ_1 and ϕ_2 in the low-energy theory, we have reverted to the original notation and replaced y_2^0 by Y^0 . The running coupling below M is therefore

$$Y(t) = \frac{Z_l^{-1/2}(t)}{Z_l^{-1/2}(M)} \frac{Z_e^{-1/2}(t)}{Z_e^{-1/2}(M)} \frac{Z_H^{-1/2}(t)}{Z_H^{-1/2}(M)} \tilde{y}_2(M). \tag{A.19}$$

²Note that at one loop, $(Z_{22}^{-1/2})^2 = Z_{22}^{-1}$.

A.2 slepton mass

Let us use this to calculate the l mass following [201]. For $\mu < M$,

$$\ln Z_l(\mu) = - \int_{\ln M}^{\ln \Lambda} \gamma_l^>(t') dt' - \int_t^{\ln M} \gamma_l^<(t') dt', \quad (\text{A.20})$$

with $t = \ln \mu$. We use the superscript $>$ ($<$) to denote the theory above (below) M .

We have

$$\frac{\partial}{\partial \ln M} \ln Z_l(\mu) = \gamma_l^>(M) - \gamma_l^<(M) - \int_t^{\ln M} \frac{\partial}{\partial \ln M} \gamma_l^<(t') dt', \quad (\text{A.21})$$

and

$$\frac{\partial^2}{\partial \ln M^2} \ln Z_l(M) = \frac{\partial}{\partial \ln M} (\gamma_l^>(M) - \gamma_l^<(M)) - \frac{\partial}{\partial \ln M} \gamma_l^<(t)|_{t=\ln M}. \quad (\text{A.22})$$

The jump in the l anomalous dimension is given by the contribution of the heavy field to γ_l .

Therefore,

$$\gamma_l^>(M) - \gamma_l^<(M) = -\frac{2}{16\pi^2} |\tilde{y}_1(M)|^2. \quad (\text{A.23})$$

The l anomalous dimension at scales below M is given by

$$\gamma_l^<(t) = -\frac{2}{16\pi^2} |Y(t)|^2, \quad (\text{A.24})$$

with

$$|Y(t)|^2 = \frac{Z_l(M)}{Z_l(\mu)} \frac{Z_e(M)}{Z_e(\mu)} \frac{Z_h(M)}{Z_h(\mu)} Y(M) = Z_l^{-1}(\mu) Z_e^{-1}(\mu) Z_H^{-1}(\mu) |y_2^0|^2. \quad (\text{A.25})$$

Thus,

$$m_i^2(M) = -\frac{1}{4} \left| \frac{F}{M} \right|^2 \frac{\partial^2}{\partial \ln M^2} \ln Z_l(M) \quad (\text{A.26})$$

$$= \frac{1}{4} \left| \frac{F}{M} \right|^2 \frac{2}{16\pi^2} \left[\frac{\partial}{\partial \ln M} |\tilde{y}_1(M)|^2 + \frac{\partial}{\partial \ln M} |Y(t)|^2|_{t=\ln M} \right]. \quad (\text{A.27})$$

The derivatives in the expression above involve of course the beta functions of the two couplings, which in turn are combinations of the various anomalous dimensions. The derivative of the first term can be obtained from eqn. (A.14), and, as explained above, involves *double* the usual contribution of γ_{12} .

In contrast, the derivative of the second term does not contain γ_{12} at all, since γ_{12} cannot appear in the theory below M , and does not appear in $Y(M)$ as we saw above. To obtain the second term of eqn. (A.26), we can use first eqn. (A.20) which gives at one loop,

$$\frac{\partial}{\partial \ln M} \ln Z_l(\mu) = \Delta\gamma_l(M) = \gamma_l^>(M) - \gamma_l^<(M) \quad (\text{A.28})$$

so that

$$\frac{\partial}{\partial \ln M} Z_l^{-1}(\mu) = -\Delta\gamma_l(M). \quad (\text{A.29})$$

We also need the analogous expression for Z_H ,

$$\ln Z_H(\mu) = \ln Z_{22}(M) - \int_t^{\ln M} \gamma_H dt' \quad (\text{A.30})$$

so at one-loop

$$\frac{\partial}{\partial \ln M} Z_H(\mu) = \gamma_{22}(M) - \gamma_H(M) = 0. \quad (\text{A.31})$$

Plugging these in eqn. (A.26), we have,

$$m_l^2(M) = \frac{1}{4} \frac{2}{16\pi^2} [(\gamma_l^> + \gamma_e^> + \gamma_{11}^>)y^2 + 2\gamma_{12}yY - [\Delta\gamma_l + \Delta\gamma_e]Y^2] \left| \frac{F}{M} \right|^2 \quad (\text{A.32})$$

with everything evaluated at the scale M . Substituting in the values of the anomalous dimensions one gets

$$m_l^2 = \frac{1}{(4\pi)^4} (4y^4 + 2y^2Y^2) \left| \frac{F}{M} \right|^2, \quad (\text{A.33})$$

or for a simplified model where all fields are singlets

$$m_l^2 \Big|_{\text{simplified}} = \frac{1}{(4\pi)^4} (3y^4 + 2y^2 Y^2) \left| \frac{F}{M} \right|^2, \quad (\text{A.34})$$

Alternatively, we can rewrite eqn. (A.32) in a way that is more similar to the expression of [201],

$$\tilde{m}^2(M) = -\frac{1}{4} \left(\frac{d\Delta\gamma}{dy} [\beta_y^<]_{\gamma_{12}=0} - \gamma_{12} \frac{d\Delta\gamma}{dy} Y - \frac{d\gamma^<}{dY} [\Delta\beta_Y]_{\gamma_{12}=0} \right) \left| \frac{F}{M} \right|^2. \quad (\text{A.35})$$

Here the various β 's and anomalous dimensions are the standard ones, and $\square_{\gamma_{12}=0}$ indicates that γ_{12} should be set to zero in the expression for the relevant β . One could in principle denote the couplings collectively by λ , as in [201], but $\Delta\gamma$ only depends on the messenger couplings y , whereas $\gamma^<$ only depends on the Higgs couplings Y .

A.3 Higgs mass

To calculate the Higgs mass we again need to take two derivatives of

$$\ln Z_H(\mu) = \ln Z_{22}(M) - \int_t^{\ln M} \gamma_H^<(t') dt'. \quad (\text{A.36})$$

Since there is no jump in the anomalous dimension of H , one could immediately start with the analog of eqn. (A.22) and set $\Delta\gamma_H = 0$. We can also derive this result more carefully.

Writing

$$Z_{22}(M) = 1 - \int_{\ln M}^{\ln \Lambda} (Z^{1/2} \gamma Z^{1/2})_{22} dt \quad (\text{A.37})$$

we find (dropping 3-loop terms)

$$\frac{\partial^2}{\partial \ln M^2} \ln Z_H(M) = \frac{\partial}{\partial \ln M} \gamma_{22}(M) + |\gamma_{12}|^2(M). \quad (\text{A.38})$$

Then

$$\frac{\partial^2}{\partial \ln M^2} \ln Z_H(M) \Big|_{\mu=M} = \frac{\partial}{\partial \ln M} (\gamma_{22}(M) - \gamma_H(M)) + |\gamma_{12}|^2 - \frac{\partial}{\partial \ln M} \gamma_H^{\leq}(t) \Big|_{t=\ln M}. \quad (\text{A.39})$$

Note that $\gamma_{22}(M)$ and $\gamma_H(M)$ differ at one-loop:

$$\gamma_{22}(M) = \frac{-2}{16\pi^2} |y_2(M)|^2 = \frac{-2}{16\pi^2} \left[|y_2^0|^2 Z_{22}^{-1}(M) Z_l^{-1}(M) Z_e^{-1}(M) + \left(y_1^0 y_2^{0*} Z_{12}^{-1/2}(M) + cc \right) \right], \quad (\text{A.40})$$

whereas

$$\gamma_H(M) = \frac{-2}{16\pi^2} |\tilde{y}_2(M)|^2 = \frac{-2}{16\pi^2} |y_2^0|^2 Z_{22}^{-1}(M) Z_l^{-1}(M) Z_e^{-1}(M). \quad (\text{A.41})$$

Therefore

$$\frac{\partial}{\partial \ln M} (\gamma_{22}(M) - \gamma_H(M)) = \frac{-2}{16\pi^2} \frac{\partial}{\partial \ln M} \left(y_1^0 y_2^{0*} Z_{12}^{-1/2}(M) + cc \right) = -|\gamma_{12}(M)|^2, \quad (\text{A.42})$$

which precisely cancels the third term in (A.39). We are then left with

$$\frac{\partial^2}{\partial \ln M^2} \ln Z_H(M) \Big|_{\mu=M} = -\frac{\partial}{\partial \ln M} \gamma_H(t) \Big|_{t=\ln M}. \quad (\text{A.43})$$

In this case, the soft mass only depends on the anomalous dimension in the low-energy theory, and therefore does not involve the mixed anomalous dimension γ_{12} as explained in the previous section.

Using the results of the last section we find,

$$m_H^2 = \frac{1}{4} \frac{2}{16\pi^2} [\Delta\gamma_l + \Delta\gamma_e] |Y|^2 \left| \frac{F}{M} \right|^2 = -\frac{1}{(4\pi)^4} (3|y|^2 |Y|^2) \left| \frac{F}{M} \right|^2, \quad (\text{A.44})$$

or for a simplified model where all fields are singlets

$$m_H^2 = -\frac{1}{(4\pi)^4} (2|y|^2 |Y|^2) \left| \frac{F}{M} \right|^2. \quad (\text{A.45})$$

Again, we can rewrite this in analogy with eq.(A.35),

$$\tilde{m}_H^2(M) = \frac{1}{4} \frac{d\gamma_H^<}{dY} [\Delta\beta_Y]_{\gamma_{12}=0} \left| \frac{F}{M} \right|^2, \quad (\text{A.46})$$

where we used $\Delta\gamma_H = 0$.

A.4 Multiple couplings

We can now generalize these results to models with multiple fields and couplings. Specifically, we will take the superpotential to be

$$W = X\bar{D}D + (y_{a\alpha}^0 D + Y_{a\alpha}^0 H)l_a e_\alpha, \quad (\text{A.47})$$

where the different fields can have different multiplicities³. As before we define $\phi_1 \equiv D$, $\phi_2 \equiv H$, $y_{1a\alpha}^0 \equiv y_{a\alpha}^0$ and $y_{2a\alpha}^0 \equiv Y_{a\alpha}^0$. The various wave-function renormalizations are now all matrices, and the expressions for the soft masses at 2-loops generalize to

$$m_l^2(\mu) = -\frac{1}{4} \left[\frac{\partial^2 Z(\mu)}{\partial \ln M^2} - \left(\frac{\partial Z(\mu)}{\partial \ln M} \right)^2 \right] \left| \frac{F}{M} \right|^2, \quad (\text{A.48})$$

and similarly for e . Using the RGE for the matrix Z_l (in analogy with eqn. (A.6)) this can be written as (at $\mu = M$),

$$m_l^2(M) = -\frac{1}{4} \left[\frac{\partial}{\partial \ln M} \Delta\gamma_l(M) - \frac{\partial}{\partial \ln M} \gamma_l^<(\mu) \Big|_{\mu=M} \right] \left| \frac{F}{M} \right|^2, \quad (\text{A.49})$$

³This covers also the models with both down-quark and lepton couplings, with $a = 1 \dots 3$ running over quarks and $a = 4 \dots 6$ over leptons etc.

and similarly for e . For completeness we display again the expression for the Higgs mass,

$$m_H^2(M) = \frac{1}{4} \frac{\partial}{\partial \ln M} \gamma_H^<(\mu) \Big|_{\mu=M} \left| \frac{F}{M} \right|^2. \quad (\text{A.50})$$

Note that the second term of (A.49) is common to all the SM fields including H and $\gamma^<$ is given by the square of the low-energy coupling Y . On the other hand the first term of (A.49) does not appear in the H mass (since its anomalous dimension is continuous across the threshold), and $\Delta\gamma(M)$ is given by the square of $\tilde{y}(M)$.

It is now easy to evaluate these expressions. Let us do this explicitly for the l mass. The first term of (A.49) is then

$$\begin{aligned} \frac{\partial}{\partial \ln M} \Delta\gamma_l(M)_{ba} &= \left(-\frac{2}{16\pi^2} \right) \left[\tilde{y}_{b\alpha}^* \frac{\partial}{\partial \ln M} \tilde{y}_{a\alpha} + \text{cc} \right] \\ &= -\frac{1}{2} \left(-\frac{2}{16\pi^2} \right) [y_{b\alpha}^* (\gamma_{11}^> y_{a\alpha} + \gamma_{ba}^> y_{b\alpha} + \gamma_{\beta\alpha}^> y_{a\beta} + 2\gamma_{12}^> Y_{a\alpha}) + \text{cc}] \end{aligned} \quad (\text{A.51})$$

where in the second line we omitted the tildes because the expression is already of two-loop order. The second term of (A.49) is,

$$\begin{aligned} \frac{\partial}{\partial \ln M} \gamma_l^<(\mu) \Big|_{\mu=M} &= \left(-\frac{2}{16\pi^2} \right) \left[\tilde{Y}_{b\alpha}^* \frac{\partial}{\partial \ln M} \tilde{Y}_{a\alpha} + \text{cc} \right] \\ &= -\frac{1}{2} \left(-\frac{2}{16\pi^2} \right) [y_{b\alpha}^* (\Delta\gamma_{ba} y_{b\alpha} + \Delta\gamma_{\beta\alpha} y_{a\beta}) + \text{cc}]. \end{aligned} \quad (\text{A.52})$$

Finally we need to substitute,

$$\Delta\gamma_{ba} = \left(-\frac{2}{16\pi^2} \right) (yy^\dagger) \quad (\text{A.53})$$

and the analogous expression for e . Here again we used the fact that $\Delta\gamma \sim \tilde{y}(M)^2$, but to leading order $\tilde{y} = y$.

A.5 Soft terms in the three generation model

We are now ready to present the soft terms resulting from general coupling matrices y_U , y_D and y_L .

Note that our couplings Y_U are actually the complex conjugates of the commonly used standard-model Yukawas, which we denote by y_u . To conform with the standard notation we will therefore express the soft terms in terms of Y_u and y_u (and similarly for the down and lepton couplings with

$$\begin{aligned} Y_u &= Y_U^*, & Y_d &= Y_D^*, & Y_l &= Y_L^*, \\ y_u &= y_U^*, & y_d &= y_D^*, & y_l &= y_L^*. \end{aligned} \tag{A.54}$$

The 2-loop soft squared masses at $\mu = M$ are

$$\begin{aligned} \tilde{m}_q^2 &= \frac{1}{(4\pi)^4} \left| \frac{F}{M} \right|^2 \left\{ \begin{aligned} &\left(3Tr(y_u^\dagger y_u) - \frac{16}{3}g_3^2 - 3g_2^2 - \frac{13}{15}g_1^2 \right) y_u y_u^\dagger \\ &+ \left(Tr(3y_d^\dagger y_d + y_l^\dagger y_l) - g_3^2 \frac{16}{3} - 3g_2^2 - \frac{7}{15}g_1^2 \right) y_d y_d^\dagger \\ &+ 3y_u y_u^\dagger y_u y_u^\dagger + 3y_d y_d^\dagger y_d y_d^\dagger + y_u y_u^\dagger y_d y_d^\dagger + y_d y_d^\dagger y_u y_u^\dagger \\ &+ 2y_u Y_u^\dagger Y_u y_u^\dagger + 2y_d Y_d^\dagger Y_d y_d^\dagger - 2Y_u y_u^\dagger y_u Y_u^\dagger - 2Y_d y_d^\dagger y_d Y_d^\dagger \\ &+ y_u Y_u^\dagger Tr(3y_u^\dagger Y_u) + Y_u y_u^\dagger Tr(3Y_u^\dagger y_u) \\ &+ y_d Y_d^\dagger Tr(3y_d^\dagger Y_d + y_l^\dagger Y_l) + Y_d y_d^\dagger Tr(3Y_d^\dagger y_d + Y_l^\dagger y_l) \\ &+ 2N_5 \left(\frac{4}{3}g_3^4 + \frac{3}{4}g_2^4 + \frac{1}{60}g_1^4 \right) 1_{3 \times 3} \end{aligned} \right\} \end{aligned} \tag{A.55}$$

$$\begin{aligned}
\tilde{m}_{uR}^2 &= \frac{1}{(4\pi)^4} \left| \frac{F}{M} \right|^2 \left\{ 2 \left(3\text{Tr} (y_u^\dagger y_u) - \frac{16}{3}g_3^2 - 3g_2^2 - \frac{13}{15}g_1^2 \right) y_u^\dagger y_u \right. \\
&\quad + 6y_u^\dagger y_u y_u^\dagger y_u + 2y_u^\dagger Y_u Y_u^\dagger y_u + 2y_u^\dagger Y_d Y_d^\dagger y_u + 2y_u^\dagger y_d y_d^\dagger y_u \\
&\quad - 2Y_u^\dagger y_u y_u^\dagger Y_u - 2Y_u^\dagger y_d y_d^\dagger Y_u + 2y_u^\dagger Y_u \text{Tr} (3Y_u^\dagger y_u) \\
&\quad \left. + 2Y_u^\dagger y_u \text{Tr} (3y_u^\dagger Y_u) + 2 \left(\frac{4}{3}g_3^4 + \frac{4}{15} \right) N_5 g_1^4 1_{3 \times 3} \right\} \quad (\text{A.56})
\end{aligned}$$

$$\begin{aligned}
\tilde{m}_{dR}^2 &= \frac{1}{(4\pi)^4} \left| \frac{F}{M} \right|^2 \left\{ 2 \left(\text{Tr} (3y_d^\dagger y_d + y_l^\dagger y_l) - \frac{16}{3}g_3^2 - 3g_2^2 - \frac{7}{15}g_1^2 \right) y_d^\dagger y_d \right. \\
&\quad + 6y_d^\dagger y_d y_d^\dagger y_d + 2y_d^\dagger Y_u Y_u^\dagger y_d + 2y_d^\dagger y_u y_u^\dagger y_d + 2y_d^\dagger Y_d Y_d^\dagger y_d \\
&\quad - 2Y_d^\dagger y_u y_u^\dagger Y_d - 2Y_d^\dagger y_d y_d^\dagger Y_d \\
&\quad + 2y_d^\dagger Y_d \text{Tr} (3Y_d^\dagger y_d + Y_l^\dagger y_l) + 2Y_d^\dagger y_d \text{Tr} (3y_d^\dagger Y_d + y_l^\dagger Y_l) \\
&\quad \left. + 2N_5 \left(\frac{4}{3}g_3^4 + \frac{1}{15}g_1^4 \right) 1_{3 \times 3} \right\} \quad (\text{A.57})
\end{aligned}$$

$$\begin{aligned}
\tilde{m}_L^2 &= \frac{1}{(4\pi)^4} \left| \frac{F}{M} \right|^2 \left\{ \left(\text{Tr} (3y_d^\dagger y_d + y_l^\dagger y_l) - 3g_2^2 - \frac{9}{5}g_1^2 \right) y_l y_l^\dagger \right. \\
&\quad + 3y_l y_l^\dagger y_l y_l^\dagger + 2y_l Y_l^\dagger Y_l y_l^\dagger - 2Y_l y_l^\dagger y_l Y_l^\dagger \\
&\quad + y_l Y_l^\dagger \text{Tr} (3y_d^\dagger Y_d + y_l^\dagger Y_l) + Y_l y_l^\dagger \text{Tr} (3Y_d^\dagger y_d + Y_l^\dagger y_l) \\
&\quad \left. + 2N_5 \left(\frac{3}{4}g_2^4 + \frac{3}{20}g_1^4 \right) 1_{3 \times 3} \right\} \quad (\text{A.58})
\end{aligned}$$

$$\begin{aligned}
\tilde{m}_{e_R}^2 &= \frac{1}{(4\pi)^4} \left| \frac{F}{M} \right|^2 \left\{ 2 \left(\text{Tr} \left(3y_d^\dagger y_d + y_l^\dagger y_l \right) - 3g_2^2 - \frac{9}{5}g_1^2 \right) y_l^\dagger y_l \right. \\
&\quad + 6y_l^\dagger y_l y_l^\dagger y_l + 2y_l^\dagger Y_l Y_l^\dagger y_l - 2Y_l^\dagger y_l y_l^\dagger Y_l \\
&\quad + 2y_l^\dagger Y_l \text{Tr} \left(3Y_d^\dagger y_d + Y_l^\dagger y_l \right) + 2Y_l^\dagger y_l \text{Tr} \left(3y_d^\dagger Y_d + y_l^\dagger Y_l \right) \\
&\quad \left. + \frac{6}{5} N_5 g_1^4 1_{3 \times 3} \right\} \tag{A.59}
\end{aligned}$$

$$\begin{aligned}
\tilde{m}_{H^u}^2 &= \frac{1}{(4\pi)^4} \left| \frac{F}{M} \right|^2 \left\{ -3 \text{Tr} \left(Y_u^\dagger y_u y_u^\dagger Y_u + Y_u^\dagger y_d y_d^\dagger Y_u + 2Y_u^\dagger Y_u y_u^\dagger y_u \right) \right. \\
&\quad \left. + 2N_5 \left(\frac{3}{4}g_2^4 + \frac{3}{20}g_1^4 \right) \right\} \tag{A.60}
\end{aligned}$$

$$\begin{aligned}
\tilde{m}_{H^d}^2 &= \frac{1}{(4\pi)^4} \left| \frac{F}{M} \right|^2 \left\{ -3 \text{Tr} \left(Y_d^\dagger y_u y_u^\dagger Y_d + Y_d^\dagger y_d y_d^\dagger Y_d + 2Y_d^\dagger Y_d y_d^\dagger y_d \right) \right. \\
&\quad \left. - \text{Tr} \left(Y_l^\dagger y_l y_l^\dagger Y_l + 2Y_l^\dagger Y_l y_l^\dagger y_l \right) + 2N_5 \left(\frac{3}{4}g_2^4 + \frac{3}{20}g_1^4 \right) \right\} \tag{A.61}
\end{aligned}$$

In addition, we give here the fully-flavored 1-loop contributions to the soft masses,

$$\delta m_{qL}^2 = -\frac{1}{(4\pi)^2} \frac{1}{6} \left(y_u y_u^\dagger + y_d y_d^\dagger \right) \frac{F^4}{M^6} \quad (\text{A.62})$$

$$\delta m_{uR}^2 = -\frac{1}{(4\pi)^2} \frac{1}{3} \left(y_u^\dagger y_u \right) \frac{F^4}{M^6} \quad (\text{A.63})$$

$$\delta m_{dR}^2 = -\frac{1}{(4\pi)^2} \frac{1}{3} \left(y_d^\dagger y_d \right) \frac{F^4}{M^6} \quad (\text{A.64})$$

$$\delta m_l^2 = -\frac{1}{(4\pi)^2} \frac{1}{6} \left(y_l y_l^\dagger \right) \frac{F^4}{M^6} \quad (\text{A.65})$$

$$\delta m_{e^c}^2 = -\frac{1}{(4\pi)^2} \frac{1}{3} \left(y_l^\dagger y_l \right) \frac{F^4}{M^6}. \quad (\text{A.66})$$

The A-terms, i.e the coefficients of the Lagrangian terms $L \supset (A_u)_{i,j} \tilde{q}_{Li} \tilde{u}_{Rj}^* H_U$
 $+ (A_d)_{i,j} \tilde{q}_{Li} \tilde{d}_{Rj}^* H_d + (A_l)_{i,j} \tilde{L}_{Li} \tilde{e}_{Rj}^* H_d$ at the scale M are,

$$A_u^* = -\frac{1}{16\pi^2} \left[\left(y_u y_u^\dagger + y_d y_d^\dagger \right) Y_u + 2Y_u \left(y_u^\dagger y_u \right) \right] \frac{F}{M} \quad (\text{A.67})$$

$$A_d^* = -\frac{1}{16\pi^2} \left[\left(y_u y_u^\dagger + y_d y_d^\dagger \right) Y_d + 2Y_d \left(y_d^\dagger y_d \right) \right] \frac{F}{M} \quad (\text{A.68})$$

$$A_l^* = -\frac{1}{16\pi^2} \left[\left(y_l y_l^\dagger \right) Y_l + 2Y_l \left(y_l^\dagger y_l \right) \right] \frac{F}{M} \quad (\text{A.69})$$

A.6 Explicit 2-loop Calculation

A cross-check of the calculation described above, we have also calculated the mixed $y^2 Y^2$ terms explicitly. Since we are only interested in verifying the two loop contributions, which are only known to leading order in F/M^2 , we work in the limit $F \ll M^2$, treating F as an insertion.

The scalar interaction Lagrangian is

$$\begin{aligned}
L_{scalar} &\supset -F D \bar{D} - F^* D^* \bar{D}^* - |F_D|^2 - |F_{\bar{D}}|^2 - |F_H|^2 - |F_l|^2 - |F_e|^2 \\
&= -F D \bar{D} - F^* D^* \bar{D}^* - |M \bar{D} + y l e|^2 - |M D|^2 - |Y l e|^2 \\
&\quad - |Y H e + y D e|^2 - |Y H l + y D l|^2 \\
&= -F D \bar{D} - F^* D^* \bar{D}^* - |M|^2 D^* D - |M|^2 \bar{D}^* \bar{D} \\
&\quad - M y^* \bar{D} l^* e^* - M^* y \bar{D}^* l e - (|Y|^2 + |y|^2) l^* l e^* e \\
&\quad - (|Y|^2 H^* H + |y|^2 D^* D + Y y^* H D^* + Y^* y H^* D) e^* e \\
&\quad - (|Y|^2 H^* H + |y|^2 D^* D + Y y^* H D^* + Y^* y H^* D) l^* l
\end{aligned} \tag{A.70}$$

and the fermion Lagrangian is

$$-L_{fermion} = M \psi_D \psi_{\bar{D}} + Y (H \psi_l \psi_e + e \psi_l \psi_H + l \psi_H \psi_e) + y (D \psi_l \psi_e + e \psi_l \psi_D + l \psi_D \psi_e) + c.c \tag{A.71}$$

For the sake of brevity we will define

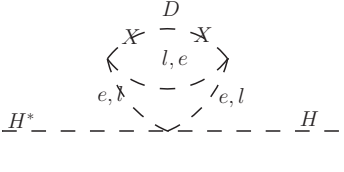
$$\int d\varphi = \int \frac{d^4 p}{(2\pi)^4} \int \frac{d^4 k}{(2\pi)^4} \tag{A.72}$$

While we are working in the $F/M^2 \ll 1$ limit, it is important to remember that the sfermions obtain small soft mass (of order F^4/M^2) already at one loop. Indeed, loops of massless scalars

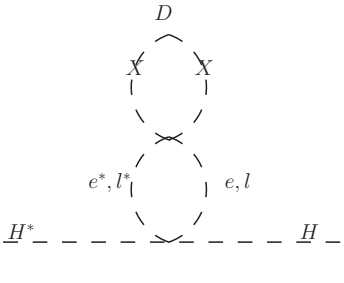
in the calculation presented below lead to spurious IR divergences which manifest themselves in the fact that the results of the calculation appear to depend on the order of integration. The presence of non-vanishing scalar masses cuts off these divergences leading to a finite result independent of the order of integration. For the sake of brevity, below we choose the order of integration which gives the correct result even when light scalars are treated as massless.

A.7 H field soft mass squared

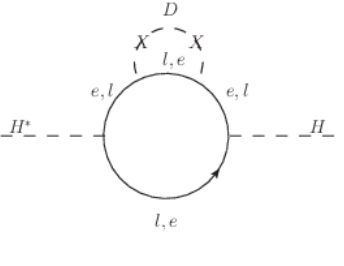
The four 2-loop diagrams with two insertions of the SUSY breaking spurion and their contributions are given by,



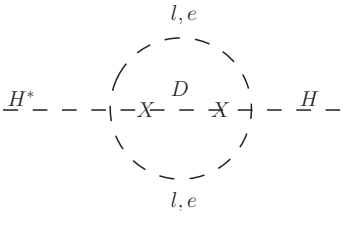
$$= i|F|^2|yY|^2 \int d\varphi \frac{M^2}{p^4(k^2 - M^2)^3(p - k)^2} \quad (\text{A.73})$$



$$= i|F|^2|yY|^2 \int d\varphi \frac{1}{p^4(k^2 - M^2)^3} \quad (\text{A.74})$$



$$= -i|F|^2|yY|^2 \int d\varphi \frac{2p \cdot (p - k)}{p^4(p - k)^2(k^2 - M^2)^3} \quad (\text{A.75})$$



$$= i|F|^2|yY|^2 \int d\varphi \frac{1}{(k^2 - M^2)^3(p - k)^2 p^2} \quad (\text{A.76})$$

The integrals on the right-hand side represent contributions of either l or e propagating in the loop. Multiplying the results by a factor of two to account for the number of fields in

the loop and summing the diagrams we obtain

$$\begin{aligned}
I &= 2i|Yy|^2|F|^2 \int d\varphi \frac{1}{p^2(k^2 - M^2)^3} \left(\frac{M^2}{p^2(p-k)^2} + \frac{1}{p^2} + \frac{1}{(p-k)^2} - \frac{2p \cdot (p-k)}{p^2(p-k)^2} \right) \\
&= 2i|Yy|^2|F|^2 \int d\varphi \frac{k^2 + M^2}{p^4(k^2 - M^2)^3(p-k)^2}
\end{aligned} \tag{A.77}$$

As discussed above, to avoid spurious IR divergences we will choose to perform the k integral, associated with the massive messenger loop momentum, first followed by the p integral.

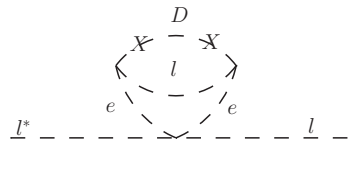
The resulting Higgs mass squared is

$$m_H^2 = -\frac{2|Yy|^2}{(4\pi)^4} \left| \frac{F}{M} \right|^2 \tag{A.78}$$

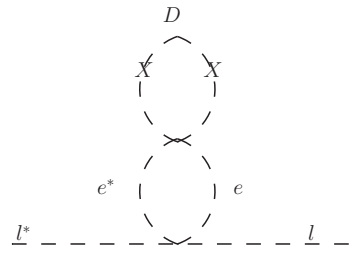
consistent with the results obtained using analytic continuation in Equation (A.45).

A.7.1 l field mass squared

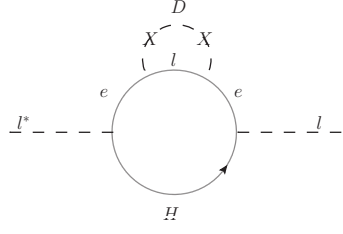
The diagrams contributing to the l -field soft mass squared which contain a $|yY|^2$ term are



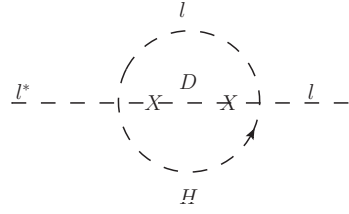
$$= i|F|^2|y|^2(|y|^2 + |Y|^2) \int d\varphi \frac{|M|^2}{(k^2 - M^2)^3(p-k)^2 p^4} \tag{A.79}$$



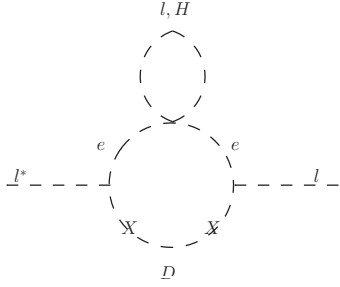
$$= i|F|^2|y|^2(|y|^2 + |Y|^2) \int d\varphi \frac{1}{(k^2 - M^2)^3 p^4} \tag{A.80}$$



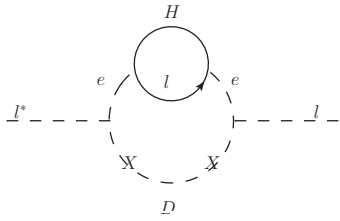
$$= -2i|F|^2|yY|^2 \int d\varphi \frac{p \cdot (p - k)}{(k^2 - M^2)^3(p - k)^2 p^4} \quad (\text{A.81})$$



$$= 2i|F|^2|yY|^2 \int d\varphi \frac{1}{(k^2 - M^2)^3(p - k)^2 p^2} \quad (\text{A.82})$$



$$= i|F|^2|yM|^2(|y|^2 + 2|Y|^2) \int d\varphi \frac{1}{(k^2 - M^2)^3 k^4 p^2} \quad (\text{A.83})$$



$$= -2i|F|^2|M|^2|yY|^2 \int d\varphi \frac{p \cdot (p - k)}{(k^2 - M^2)^3 k^4 (p - k)^2 p^2} \quad (\text{A.84})$$

$$\begin{aligned}
& \text{Diagram 1} + \text{Diagram 2} \\
& = 2i|F|^2|y|^2(|y|^2 + |Y|^2) \int d\varphi \frac{|M|^2}{(k^2 - M^2)^3 k^2 (p-k)^2 p^2}
\end{aligned} \tag{A.85}$$

$$= -4i|F|^2|yY|^2 \int d\varphi \frac{p \cdot (p-k)}{(k^2 - M^2)^3 k^2 (p-k)^2 p^2} \tag{A.86}$$

$$= 4i|F|^2|yY|^2 \int d\varphi \frac{1}{(k^2 - M^2)^3 k^2 p^2} \tag{A.87}$$

We note that contributions of Feynman diagrams A.80-A.82 are identical to the diagrams contributing to the Higgs mass. The last of these diagrams, A.82, has an additional factor of two due to two possible choices of “chirality” for D and H propagators. The $|yY|^2$ contribution to the l soft squared mass in the diagrams of Eqs. A.80-A.87 can be written as a sum of three integrals,

$$\begin{aligned}
\mathcal{I} &= \int d\varphi \frac{k^2 + M^2}{(k^2 - M^2)^3 (p-k)^2 p^4} = \frac{1}{(4\pi)^4 M^2} \\
\mathcal{II} &= 3 \int d\varphi \frac{k^2 + M^2}{k^2 (k^2 - M^2)^3 (p-k)^2 p^2} = -\frac{3}{(4\pi)^4 M^2} \\
\mathcal{III} &= \int d\varphi \frac{(p-k)^2 - p^2}{(k^2 - M^2)^3 (p-k)^2 p^2} \left(\frac{2}{k^2} + \frac{M^2}{k^4} \right) = 0.
\end{aligned} \tag{A.88}$$

Summing all contributions, the $|yY|^2$ part of the l soft squared mass reads

$$m_l^2 \Big|_{|yY|^2} = \frac{2|Yy|^2}{(4\pi)^4} \left| \frac{F}{M} \right|^2 \quad (\text{A.89})$$

consistent with the results obtained in the revised analytic continuation in Equation (A.34).

Appendix B

Spin-Independent Scattering Cross Section of Bino-Like Neutralinos

In this Appendix, we derive a simple expression for the differential cross section for SI neutralino–nucleus scattering in the limit where the neutralino is Bino-like. The resulting expression will require some additional approximations, but will provide an analytic cross-check for the numerical results derived in the body of the paper.

The SI cross section for neutralinos χ scattering off a nucleus N , with nuclear charge Z and mass number A , is [146]

$$\frac{d\sigma}{d|\vec{q}|^2} = \frac{1}{\pi v^2} [Z f_p + (A - Z) f_n]^2 F^2(Q) , \quad (\text{B.1})$$

where \vec{q} is the momentum transferred in the interaction; v is the velocity of the dark matter; f_p and f_n are the effective couplings to protons and neutrons, respectively; and $F(Q)$ is the nuclear form factor, where Q is the energy transfer.

For the form factor, a common parameterization is [217]

$$F^2(Q) = e^{-Q/Q_0} , \quad (\text{B.2})$$

where

$$Q_0 = \frac{1.5}{m_N R_0^2} \quad R_0 = \left[0.3 + 0.91 \left(\frac{m_N}{\text{GeV}} \right)^{1/3} \right] \times 10^{-15} \text{ m} . \quad (\text{B.3})$$

In the non-relativistic limit, the maximum energy transfer from elastic scattering of dark matter is

$$Q_{\text{max}} = \frac{2m_N v^2}{(1 + m_N/m_\chi)^2} , \quad (\text{B.4})$$

where m_χ and m_N are the masses of the dark matter and the nucleus, respectively. For all but the heaviest nuclei, $v^2 m_N^2 R_0^2$ is small enough that $F^2(Q) \approx 1$ is a good approximation.

In the heavy-squark limit, the effective nucleon couplings f_p and f_n are approximately equal and are given by [146]

$$\frac{f_{p,n}}{m_{p,n}} = \sum_{q=u,d,s} \frac{f_{Tq} f_q}{m_q} + \frac{2}{27} f_{TG} \sum_{q=c,b,t} \frac{f_q}{m_q} , \quad (\text{B.5})$$

where $f_{Tq} = \langle n | m_q \bar{q} q | n \rangle / m_p$ and $f_{TG} = 1 - \sum_{u,d,s} f_{Tq}$. Values for each f_{Tq} are shown in Eq. (4.41).

The neutralino interaction strength is encoded in the parameters

$$f_q = \sum_{i=h,H} \frac{g T_{i11} h_{iqq}}{2m_i^2} - \frac{1}{4} \sum_{\tilde{q}_j} \frac{X'_{qj1} W'_{qj1}}{m_{\tilde{q}_j}^2 - (m_\chi + m_q)^2} . \quad (\text{B.6})$$

The first term of Eq. (B.6) represents the t -channel Higgs exchange diagrams. The effective

Higgs couplings are [218]

$$\begin{aligned}
T_{h11} &= \sin \alpha Q''_{11} + \cos \alpha S''_{11}, & T_{H11} &= -\cos \alpha Q''_{11} + \sin \alpha S''_{11}, \\
Q''_{11} &= N_{31}(N_{21} - N_{11} \tan \theta_W), & S''_{11} &= N_{41}(N_{21} - N_{11} \tan \theta_W), \\
h_{h_u u} &= -\frac{g m_u \cos \alpha}{2 m_W \sin \beta}, & h_{H_u u} &= -\frac{g m_u \sin \alpha}{2 m_W \sin \beta}, \\
h_{h_d d} &= +\frac{g m_d \sin \alpha}{2 m_W \cos \beta}, & h_{H_d d} &= -\frac{g m_d \cos \alpha}{2 m_W \cos \beta}, \\
\sin 2\alpha &= -\sin 2\beta \left(\frac{m_H^2 + m_h^2}{m_H^2 - m_h^2} \right), & \cos 2\alpha &= -\cos 2\beta \left(\frac{m_A^2 - m_Z^2}{m_H^2 - m_h^2} \right).
\end{aligned} \tag{B.7}$$

Here m_A is the CP-odd Higgs masses, θ_W is the weak mixing angle, and N_{j1} are entries in the matrix N that diagonalizes the neutralino mass matrix, given below in Eq. (B.11).

The second term in Eq. (B.6) represents the s -channel squark exchange processes. For the SI amplitude, this requires left–right squark mixings, which we assume are negligible. In particular, for the third and fourth generations we take them to be zero by tuning A -parameters. As a result, tree-level squark exchange contributes only to the SD amplitude, and the SI amplitude is dominated by the Higgs-mediated scattering.

In the case where $m_H, m_A \gg m_h$, we may also neglect the heavy Higgs diagram. In this limit $\alpha \simeq \beta - \pi/2$, so that $\sin \alpha \simeq \cos \beta$ and $\cos \alpha \simeq \sin \beta$. We consider models with $5 < \tan \beta < 50$, so $\sin \beta \simeq \cos \alpha \simeq 1$ and $\cos \beta \simeq \sin \alpha \simeq 0$. With these approximations,

$$T_{h11} \rightarrow N_{41}(N_{21} - N_{11} \tan \theta_W), \quad \frac{h_{h_u u}}{m_u} \rightarrow -\frac{g}{2 m_W}, \quad \frac{h_{h_d d}}{m_d} \rightarrow \frac{g}{2 m_W}. \tag{B.8}$$

The effective couplings $f_{p,n}$ can then be expressed very simply as

$$\frac{f_{p,n}}{m_{p,n}} = N_{41} [N_{21} - N_{11} \tan \theta_W] \frac{g^2}{4 m_W m_h^2} \left[f_{T_d} - f_{T_u} + f_{T_s} - \frac{2}{27} f_{T_G} \right] + \mathcal{O}(m_{H^0}^{-2}, m_{\tilde{q}}^{-2}). \tag{B.9}$$

To further simplify the expression, we can determine the neutralino mixing matrix factors

in terms of the underlying SUSY parameters. The lightest neutralino χ can be written in the gauge basis $\{\tilde{B}, \tilde{W}^3, \tilde{H}_d^0, \tilde{H}_u^0\}$ as

$$\chi = N_{11}^* \tilde{B} + N_{21}^* \tilde{W}^3 + N_{31}^* \tilde{H}_d^0 + N_{41}^* \tilde{H}_u^0, \quad (\text{B.10})$$

where the matrix N diagonalizes the neutralino mass matrix

$$M_\chi = \begin{pmatrix} M_1 & 0 & -m_Z c_\beta s_W & m_Z s_\beta s_W \\ 0 & M_2 & m_Z c_\beta c_W & -m_Z s_\beta c_W \\ -m_Z c_\beta s_W & m_Z c_\beta c_W & 0 & -\mu \\ m_Z s_\beta s_W & -m_Z s_\beta c_W & -\mu & 0 \end{pmatrix}. \quad (\text{B.11})$$

For $|\mu| > M_1$, the lightest neutralino is primarily Bino with a small Higgsino fraction. Given the gaugino mass unification relation $M_2 = 2M_1$, the \tilde{W} fraction $|N_{21}|^2$ is negligible compared to the \tilde{H} fractions, as can be seen in Fig. 4.4. We may then diagonalize the mass matrix in the limit that the \tilde{W} decouples from the lightest neutralino and $\tan \beta$ is large. In this case we may expand in the small parameter

$$x = \frac{s_W^2 m_Z^2}{\mu^2 - M_1^2 + m_Z^2 s_W^2}, \quad (\text{B.12})$$

and find that, to leading order in x ,

$$N_{41} \approx -x \frac{M_1}{m_Z s_W}, \quad (\text{B.13})$$

and the neutralino mass is

$$m_\chi \approx M_1 \left(\frac{\mu^2 - M_1^2}{\mu^2 - M_1^2 + m_Z^2 \sin^2 \theta_W} \right). \quad (\text{B.14})$$

For $|\mu| = 250$ GeV and $M_1 = 200$ GeV, Eq. (B.14) is accurate to 8%. The approximation

becomes poorer for smaller values of $\mu^2 - M_1^2$.

The effective neutralino–nucleon couplings $f_{p,n}$ can now be written explicitly in terms of SM and SUSY parameters as

$$\begin{aligned} \frac{f_{p,n}}{m_{p,n}} &= \frac{M_1 x}{m_Z \cos \theta_W} \left(\frac{g^2}{4m_W m_h^2} \right) \left[f_{Td} - f_{Tu} + f_{Ts} - \frac{2}{27} f_{TG} \right] + \mathcal{O}(x^2, m_H^{-2}, m_{\tilde{q}}^{-2}) \\ &\approx \frac{M_1 m_Z \tan \theta_W \sin \theta_W}{\mu^2 - M_1^2 + m_Z^2 \sin^2 \theta_W} \left(\frac{g^2}{4m_W m_h^2} \right) \left[f_{Td} - f_{Tu} + f_{Ts} - \frac{2}{27} f_{TG} \right]. \end{aligned} \quad (\text{B.15})$$

Equation (B.15) provides a simple analytic expression for the effective scalar neutralino–nucleon couplings when the squarks are effectively decoupled, $m_A \gg m_{h^0}$, $\tan \beta$ is moderate or large, and the neutralino dark matter is Bino-like.

Appendix C

Monte Carlo simulation of vector-like leptons at the LHC

This Appendix describes our Monte Carlo simulation of searches for vector-like leptons at the 14 TeV LHC. We focus on vector-like leptons that mix with electrons or muons; the Run 2 prospects for τ -mixed vector-like leptons are studied in Ref. [143].

C.1 Analysis procedure

SM background events are estimated with the Snowmass background set for 14 TeV pp colliders [219–221]. Signal events are generated with the same procedure that generated the background, i.e., the hard processes are calculated with MADGRAPH5_AMC@NLO [85], showering and hadronization are performed with PYTHIA 6 [172] with the PYTHIA-PGS interface, and the detector is simulated with DELPHES tuned by the Snowmass Collaboration based on DELPHES 3.0.9 [173], with FASTJET [174, 175] utilized for jet reconstruction. In the detector simulation, electrons, muons, and jets are reconstructed and identified based on

the same procedure and efficiency as the Snowmass background set. The lepton identification efficiency is 98% (99%) for electrons (muons) with $P_T > 10$ GeV and $|\eta| < 1.5$, and jets are reconstructed by the anti- k_T algorithm [222] with $R = 0.5$. The objects are required to be separated from each other by the procedures in Ref. [223], and electrons and muons forming same-flavor opposite-sign (SFOS) pairs with $m_{\text{SFOS}} < 12$ GeV are removed.

We do not include further efficiency factors for lepton identification, reconstruction and isolation, even though the results of our analysis, which focuses on events with multi-leptons, are sensitive to these efficiencies. This is because these efficiencies are determined only through LHC Run 2 data. In view of this limitation, the production cross section of the leptons are calculated at tree-level without an NLO K -factor, and we refrain from using tau-tagging (therefore taus are classified as jets), despite the fact that taus from Z and W would increase the sensitivity of the searches. For the same reason b -tagging is not utilized; as we will see later, the background from top quark events is small.

Background events from the Snowmass background set and signal events after the DELPHES simulations are then analyzed as follows. Electrons (muons) with $P_T > 20$ GeV and $|\eta| < 2.47$ (2.4) are tagged as “signal” electrons (muons), which together we call “signal” leptons,¹ and jets with $P_T > 20$ GeV and $|\eta| < 2.5$ are tagged as “signal” jets. These objects are used in the analysis described below.

Events with $N_\ell \geq 3$ are selected, where N_ℓ is the number of signal leptons. The leading (sub-leading) lepton must have $P_T > 120$ GeV ($P_T > 60$ GeV). We define five categories, as described in Table C.1. Each category is then divided into several signal regions (SRs) as follows:

- i The $WZ(j)$ category is designed for the signature $\tau_4^+ \tau_4^- \rightarrow (W\nu)(Z\ell) \rightarrow (jj\nu)(\ell\ell)$. This category is divided into two SRs according to the number of Z -like lepton pairs $N_{Z(\ell\ell)}$,

¹In this Appendix, ℓ denotes electrons and muons, but not taus.

where a lepton pair is tagged as Z -like if it is SFOS and $|m_{\ell\ell} - m_Z| < 10$ GeV:

- a $WZ(j)^-$ for $N_{Z(\ell\ell)} = 0$,
 - b $WZ(j)^Z$ for $N_{Z(\ell\ell)} \geq 1$.
- ii The $WZ(\ell)$ category is designed for the signature $\tau_4^+\tau_4^- \rightarrow (W\nu)(Z\ell) \rightarrow (\ell\nu\nu)(\ell\ell)$. Two SRs are defined by $N_{Z(\ell\ell)}$, but here a Z -like lepton pair must not contain any of the leading two leptons:
- a $WZ(\ell)^-$ for $N_{Z(\ell\ell)} = 0$,
 - b $WZ(\ell)^Z$ for $N_{Z(\ell\ell)} \geq 1$.
- iii The $ZZ(j)$ category focuses on the signature $\tau_4^+\tau_4^- \rightarrow (Z\ell)(Z\ell) \rightarrow (jj\ell)(\ell\ell)$. For this category, three flags are defined: J if the event has a jet pair with $|m_{jj} - m_Z| < 10$ GeV, L if it has Z -like lepton pairs not containing the leading lepton, and Z if the leading lepton does not make a Z -like lepton pair with another lepton. Eight SRs are defined according to whether the flags are on or off. For example, $ZZ(j)^{JLZ}$ requires all the flags be on, $ZZ(j)^Z$ requires only the Z flag, and $ZZ(j)^0$ requires that all the flags are off.
- iv The $ZZ(\ell)$ category is for $\tau_4^+\tau_4^- \rightarrow (Z\ell)(Z\ell) \rightarrow (\ell\ell)(\ell\ell)$. Three inclusive SRs are defined according to the number of jets: $ZZ(\ell)$ for any number of jets, $ZZ(\ell)^{<2}$ for $N_j < 2$, and $ZZ(\ell)^{<1}$ for $N_j < 1$.

C.2 Results

The selection flow for the background events is summarized in Table C.2.² From the expected background contribution, the expected 95% confidence level (CL) upper limit on the number

²According to the categorization of the Snowmass background set, “di-boson” corresponds to the sum of LLB and BB, “tri-boson” to BBB, and “top” is the sum of the categories tB, tj, tt, and ttB.

Table C.1: Definition of signal region (SR) categories. Each category is further divided into SRs, as described in the text. N_ℓ and N_j are the number of signal leptons and signal jets, respectively, and m_{jj} is the invariant mass of the two leading jets. $N_{Z(\ell\ell)}$ is the number of SFOS lepton pairs with $|m_{\ell\ell} - m_Z| < 10$ GeV.

	$WZ(j)$	$WZ(\ell)$	$ZZ(j)$	$ZZ(\ell)$
N_ℓ	≥ 3	≥ 4	≥ 4	≥ 5
N_j	≥ 2	< 2	≥ 2	—
$ m_{jj} - m_W $	< 20 GeV	—	—	—
$ m_{jj} - m_Z $	—	—	< 40 GeV	—
\cancel{E}_T	> 60 GeV	> 100 GeV	—	—
$N_{Z(\ell\ell)}$	—	—	≥ 1	≥ 1

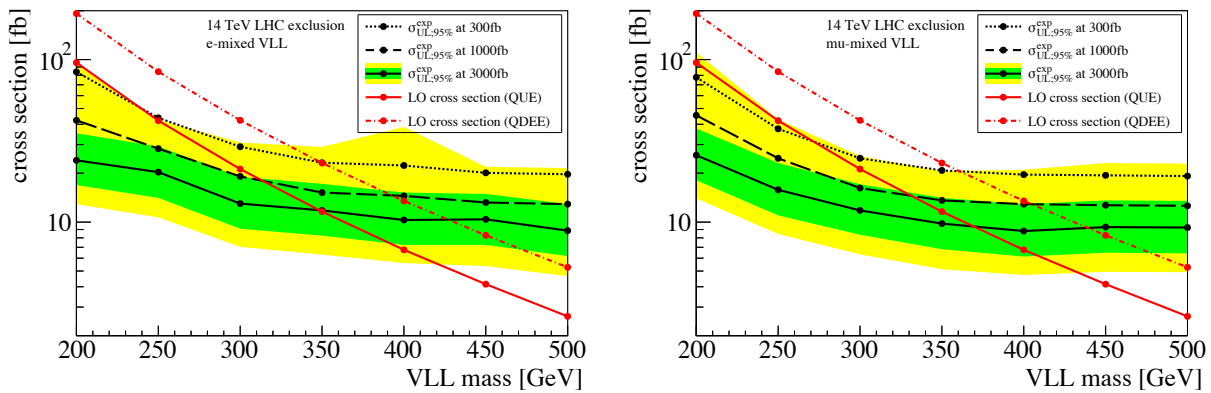


Figure C.1: The 95% CL expected upper limit on the production cross section of $pp \rightarrow \tau_4^+ \tau_4^-$ at the LHC with $\sqrt{s} = 14$ TeV and an integrated luminosity of $\int \mathcal{L} = 300, 1000,$ and 3000 fb^{-1} . In the left (right) plot, τ_4 is assumed to be mixed exclusively with electrons (muons). The uncertainty band is shown only for $\int \mathcal{L} = 3000 \text{ fb}^{-1}$. A systematic uncertainty of 20% is assumed for the background, and statistical uncertainty is included. The signal cross section is calculated at tree level and the theoretical uncertainty on that is not considered.

of events, N_{UL} , is calculated for each signal region with the CL_s method [224], and shown in the table for three values of an integrated luminosity, $\int \mathcal{L} = 300, 1000,$ and 3000 fb^{-1} . Here, we use a systematic uncertainty of 20% for the background contributions.

Seven model points with $m_{\tau_4} = 200\text{--}500$ GeV are defined for both the e -mixed case and the μ -mixed case. The selection flow of the signal events is shown in Table C.3. The values in this table are for the QUE model; for the QDEE model, due to the unified-mass assumptions, all the values in the table are doubled.

Table C.2: Selection flow of the background events in the vector-like lepton search. Upper bounds on the number of events in each SR, N_{UL} , are shown for three values of integrated luminosity, where systematic uncertainty of 20% as well as statistical uncertainty is included.

	background cross section [fb]				N_{UL}		
	di-boson	tri-boson	top	total	300 fb ⁻¹	1000 fb ⁻¹	3000 fb ⁻¹
$N_\ell \geq 3$	222	5.1	13.4	249	—	—	—
$WZ(j)^-$	0.071	0.013	0.082	0.166	25.1	70.4	200
$WZ(j)^Z$	0.643	0.071	0.183	0.898	111	359	1060
$WZ(\ell)^-$	0.014	0.025	0.017	0.056	11.9	27.4	71.1
$WZ(\ell)^Z$	< 0.001	0.005	0.003	0.008	5.1	7.9	14.5
$ZZ(j)^0$	0.194	0.016	0.058	0.268	37.2	111	321
$ZZ(j)^J$	0.064	0.007	0.022	0.093	16.4	41.8	114
$ZZ(j)^L$	0.182	0.012	0.024	0.218	31.2	91.7	263
$ZZ(j)^Z$	0.020	0.004	0.019	0.043	10.2	22.2	55.7
$ZZ(j)^{JL}$	0.060	0.005	0.009	0.075	14.2	35.3	94.3
$ZZ(j)^{JZ}$	0.008	0.001	0.008	0.017	6.7	11.9	25.6
$ZZ(j)^{LZ}$	0.020	0.004	0.019	0.043	10.2	22.2	55.9
$ZZ(j)^{JLZ}$	0.008	0.001	0.008	0.017	6.7	11.9	25.5
$ZZ(\ell)$	< 0.001	0.005	< 0.001	0.005	4.7	6.8	11.5
$ZZ(\ell)^{<2}$	< 0.001	0.003	< 0.001	0.004	4.2	5.8	9.2
$ZZ(\ell)^{<1}$	< 0.001	0.001	< 0.001	0.001	3.6	4.5	6.3

Table C.3: Selection flow of the signal events in searches for the e - or μ -mixed τ_4 in the QUE model, displayed as a signal cross section in fb. SRs marked with *, † and ‡ are the most sensitive for exclusion at $\mathcal{L} = 300, 1000, \text{ and } 3000 \text{ fb}^{-1}$, respectively.

m_τ [GeV], mixing	200, e	200, μ	300, e	300, μ	400, e	400, μ
total	95.7	96.0	21.2	21.2	6.76	6.74
$N_\ell \geq 3$	2.23	2.42	0.634	0.671	0.231	0.230
$WZ(j)^-$	0.018	0.022	0.020	0.024	0.011	0.012
$WZ(j)^Z$	0.049	0.063	0.034	0.036	0.014	0.014
$WZ(\ell)^Z$	0.012	0.014	0.008 [‡]	0.008	0.003	0.004 [‡]
$ZZ(j)^0$	0.066	0.065	0.035	0.044	0.015	0.015
$ZZ(j)^J$	0.035	0.033	0.018	0.023	0.008	0.007
$ZZ(j)^L$	0.045	0.048	0.026	0.031	0.011	0.012
$ZZ(j)^Z$	0.039 [*]	0.042 [*]	0.025 ^{*†}	0.029 [†]	0.010 [*]	0.012 [†]
$ZZ(j)^{JL}$	0.025	0.025	0.013	0.016	0.006	0.006
$ZZ(j)^{JZ}$	0.021	0.022	0.013	0.015 [‡]	0.005	0.006
$ZZ(j)^{LZ}$	0.039	0.042	0.025	0.029 [*]	0.010 [†]	0.012 [*]
$ZZ(j)^{JLZ}$	0.021	0.022	0.013	0.015	0.005	0.006
$ZZ(\ell)$	0.015 ^{†‡}	0.014 ^{†‡}	0.005	0.007	0.003 [‡]	0.002
$ZZ(\ell)^{<2}$	0.010	0.009	0.003	0.004	0.002	0.001
$ZZ(\ell)^{<1}$	0.004	0.003	0.001	0.002	8×10^{-4}	6×10^{-4}

For each model point, the expected 95% CL upper limit on the signal cross section, σ_{UL} , is obtained by the following procedure. First, the upper limit on the signal cross section is calculated for each SR based on N_{UL} and the signal yield. Then, we select the SR that gives the lowest upper limit as the most sensitive. They are indicated in Table C.3. Because the SRs are not mutually exclusive, σ_{UL} for the model point is given by the most sensitive SR.

The obtained σ_{UL} are compared against the signal cross section, $\sigma(pp \rightarrow \tau_{4(5)}^+ \tau_{4(5)}^-)$, as depicted in Fig. C.1. The red solid (dash-dotted) lines are the signal production cross section in the QUE (QDEE) model. They are calculated at the leading order, and theoretical uncertainty is not considered for simplicity. The black lines are the σ_{UL} at the three values of an integrated luminosity.³ For $\int \mathcal{L} = 3000 \text{ fb}^{-1}$, the green and yellow bands indicating the uncertainty of σ_{UL} are also displayed; the observed limits would fall in the green (yellow) band with a probability of 68% (95%). Based on this comparison, the expected upper bound on the vector-like leptons are obtained for each of the four scenarios, i.e., the QUE and QDEE models with the vector-like lepton mixed with electron and muons.

The discovery sensitivity of the 14 TeV LHC is also calculated in terms of CL_b , i.e., p -value of the background-only hypothesis, as shown in Fig. C.2. Solid (dotted) lines are for e -mixed vector-like lepton(s) in the QUE (QDEE) model with three values of the integrated luminosity, $\int \mathcal{L} = 300, 1000$ and 3000 fb^{-1} from top to bottom. Similar sensitivities are obtained for the μ -mixed case.

The results are summarized in Table 4.2 of the main text.

³To be precise, the values of σ_{UL} displayed in the figures are calculated for the QUE model. The upper limits for QDEE model points are slightly better because of our statistical treatment but the difference is negligible.

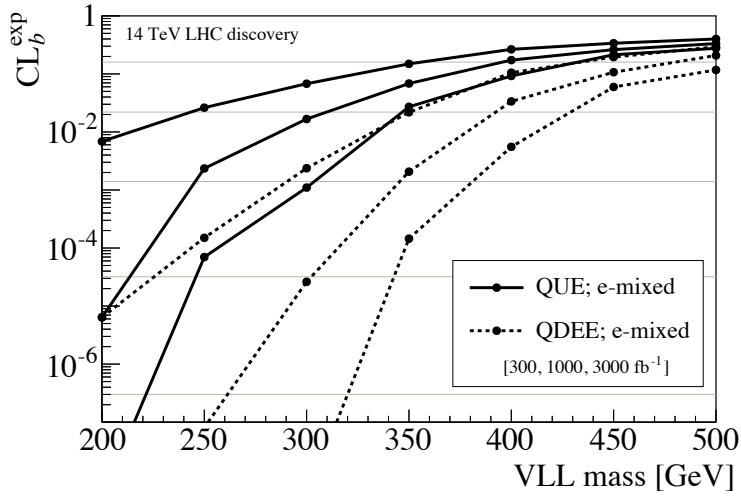


Figure C.2: The expected sensitivity of the 14 TeV LHC to the discovery of vector-like leptons, calculated under the assumption that the background contribution has a systematic uncertainty of 20%. Solid (dashed) lines are for QUE (QDEE) model with e -mixed vector-like leptons, corresponding to the integrated luminosity of 300, 1000, and 3000 fb⁻¹ from top to bottom. Similar sensitivity is expected for μ -mixing cases.